

MINISTRY OF EDUCATION AND SCIENCE OF UKRAINE  
ZAPORIZHZHIA NATIONAL UNIVERSITY

VALERIY MISHCHENKO  
STEPHAN LOSKUTOV

**PHYSICAL AND MECHANICAL  
LAWS OF METALS STRUCTURE  
FORMATION IN THE PROCESSES  
OF TREATMENT  
AND DEFORMATION**  
**Theory, Structuring and Mechanical Properties**

**Monograph**



IZDEVNIECĪBA  
**BALTIJA**  
PUBLISHING

2023

UDC 538.9:539.3:5:620.186.4:669.14  
M75

**Authors:**

**Valeriy Mishchenko**, Doctor of Technical Science,  
Professor of Department of Descriptive Geometry, Engineering  
and Computer Graphics  
**Stephan Loskutov**, Doctor of Physical and Mathematical Sciences,  
Professor Department of Physics

**Reviewers:**

**Sereda Boris Petrovich**, Director of the R&D Center  
of Materials Science and Innovative Technologies, Doctor of Engineering,  
Professor of Dniprovsky State Technical University;  
**Homeniuk Sergey Ivanovich**, Dean of the Faculty of Mathematics  
of Zaporizhzhia National University, Doctor of Engineering

*Recommended for publishing by the Academic Council  
of Zaporizhzhia National University  
(Protocol No. 5 of 22.12.2022)*

M75 **Mishchenko V., Loskutov S.** Physical and mechanical laws  
of metals structure formation in the processes of treatment and  
deformation. Theory, Structuring and Mechanical Properties :  
Monograph. Riga, Latvia : “Baltija Publishing”, 2023. 184 p.

ISBN 978-9934-26-294-4

DOI 10.30525/978-9934-26-294-4

The monograph publishes the latest achievements in physics of metals and applied metallography by academic staff of Zaporizhzhia National University and Zaporizhzhia Polytechnic National University. Some contributions are devoted to the heat treatment of steels, the development of methods of advancing mechanical engineering components and increasing their reliability.

It is intended for research activities of undergraduate and postgraduate students. The monograph will be instrumental in the academic staff's lecture courses and practical classes.

**UDC 538.9:539.3:5:620.186.4:669.14**

# CONTENT

<b>INTRODUCTION.</b>	<b>6</b>
<b>1 GENERAL CHARACTERISTICS OF THE SURFACE</b>	
<b>LAYER OF METALS.</b>	<b>12</b>
1.1 Methods for studying the surface.	12
1.2 Regularities of the material deformation of the surface metals layer.	16
1.3 The dislocations on the surface.	19
1.4 Study of the defect structure of metals by electron microscopy.	21
1.5 The problem of residual stresses.	23
1.6 Macro- and microroughness of a surface.	24
1.7 Development of defective structure near a clean surface.	28
1.8 Influence of the adsorbed substances on the surface on the mechanical properties of metals.	31
1.9 Dependence of work function from the crystal structure of the surface.	34
1.10 Change in work function during tensile test in vacuum.	39
1.11 Work function of electrons depending on the surface processing.	40
1.12 A surface in the field of elastic deformations.	41
1.13 Changing work function of electrons during the contact action on a material of the surface layer.	48
1.14 Electron work function dependence on a deformation speed.	50
1.15 Changes in the metal structure under the influence of ultraviolet and X-ray radiation.	51

<b>2</b>	<b>WORK FUNCTION FOR THE DEFORMED METALS.</b>	<b>53</b>
2.1	Work function for fatigue tested metals.	53
2.2	Work function for the real metal surface.	62
2.3	On structural sensibility of work function.	69
2.4	Formation of energy patterns on metal contact surfaces.	73
<b>3</b>	<b>STRUCTURAL CHANGES DURING DEFORMATION AND HEAT TREATMENT OF METALS.</b>	<b>79</b>
3.1	Parameters control of researched steel carburized layer via differential dilatometer.	79
3.2	Control of carburization and decarburization processes of alloy steels at thermochemical and thermal treatment.	83
3.3	Parameters control of 09Cr3NiMo3VNbr carburizing steel diffusion layer in the process of thermochemical treatment.	90
3.4	Optimization of chemical composition of developed steel 09Cr3NiMo3VNbr.	91
3.5	Determining the thermoplastic deformation mechanism of titanium reduction reactors and recommendations to increase the reactor service life.	95
3.6	Metallurgical aspects of production of chromium – nickel steels with low carbon contents.	107
3.7	Optimization of chemical composition of Lou pearlitic steel of the special setting.	112
3.8	Structural changes of multiphase low-carbon steel in deformation and heat treatment.	121
3.9	Formation of polygonized structures and nuclear recrystallization under controlled rolling of low carbon steels.	124

## INTRODUCTION

3.10	Formation of the grain boundary structure of low-alloyed steels in the process of plastic deformation. . . . .	130
3.11	Structural changes in corrosion-resistant steel. . . . .	139
3.12	Structure and properties of the corrosion-resistant sheet steel 06Kh18ch alloyed with rare-earth metals and calcium. . . . .	145
3.13	Structure formation during recrystallization of cold-rolled sheet steel. . . . .	151
3.14	The effect of plastic deformation on the structure formation of low-alloy steel. . . . .	156
<b>REFERENCES.</b> . . . . .		<b>164</b>

# INTRODUCTION

The main goal of our book is the study of strained metallic surfaces under different conditions. The free surface, being a specific type of flat defect in a crystal, can have a significant effect on its physical and mechanical properties. A real metal surface is a complex structural formation determined by the variety of processes that form it. Thus, the surface, being the interface between the medium and the metal, mediates contact interactions and different types of finishing (hardening) parts.

It is also known that the structure of the surface layers differs from the structure of the inner layers of metals. Therefore, the physical and mechanical properties of the material near the surface should differ from those in the bulk. Therefore, it is obvious that the creation of a physical picture of the deformation of metals involves the development of a theory of the course of deformation processes in the near-surface layers of materials.

The physical nature of the surface influence on the mechanical properties of metals consists of the formation of an ion-electron structure near the surface, which is different from the overall structure. Already in early works, a predominant plastic flow was found in the near-surface layers of crystals in the initial stages of deformation.

Residual stresses are produced by plastic deformations, thermal contractions or can be induced by a production process. The residual mechanical stresses are known to balance in the macroscopic and microscopic areas of materials. The plastic strain of the surface is well-known in the industry as a way to improve the fatigue and strength properties of metallic parts. Shot peening, deep rolling, hammering, treatment by metallic balls in an ultrasonic field, and laser shock peening are the new technological methods used to increase the strength of crucial parts. All these processes induce in one way or another the nanostructures near the surface. The generation of nanostructured surface layers is expected to lead to improved material properties. Structural changes in the

near-surface regions of metals and alloys are of great interest and have not yet been sufficiently studied.

The special material condition of the near-surface layer requires the development of special experimental methods for the study of deformation characteristics. The most important are the methods that allow to establish the relationship between the parameters of microgeometry, residual stresses and surface energy with the mechanical characteristics of elasticity and plasticity, with the resistance to fatigue. The study of the nature of the physical and mechanical properties of the material of the near-surface layer is also necessary to understand the deformation phenomena in polycrystalline materials, at the boundaries of grains and blocks of the crystalline structure.

The electron work function (WF) is of particular and growing interest to scientists and engineers because of its sensitivity to the physical state of the surface. It is known that metals consist of two subsystems. These are the relatively slow crystal lattice of ions and the gas of the fast free electrons. External and residual stresses cause considerable changes in the ionic crystal lattice. The electron emission properties indicate a close interaction between the ionic and electronic subsystems. However, it is essential to emphasize that the relationship between emission properties and elastic and plastic stresses is not yet sufficiently understood. Here we would like to address this lack of data.

We believe that there is a need for a book that serves as a link between the theory and its practical applications. This book is an attempt to bridge the gap between surface physics, solid state physics and technology.

The book consists of three chapters.

A succinct description of the metal surface characteristics is presented in the first chapter. The study of WF changes under various mechanical loading conditions of metals established the sensitivity of the WF to deformation processes. Thus, a new scientific direction was created, during the development of which a link was established between WF changes and specific processes in the crystal structure during deformation. In order to solve this problem, a number of hypotheses have been put forward and physical models

of the formation and evolution of the WF during the deformation of metals have been developed.

The second chapter is devoted to some techniques for experimental studies of deformed metal surfaces. The WF was measured for Al and heat resistant alloy surfaces in fatigue tests. The specimens were also studied using an X-ray method. The position dependence of the WF was observed as a result of fatigue. A decrease in the WF occurred above the future crack. The drop in the WF is related to the breakthrough of dislocations and the emergence of loaded steps on the metal surface. A fatigue process model is considered and some physical values are evaluated from the experimental data.

A method for calculating the WF for a deformed real metal surface is proposed. The method is based on the relationship between the WF and the atomic electro-negativity and takes into account the formation of nanoscale surface defects. The presented calculation results for aluminum and copper are in good agreement with the experimental data.

The work function of metals decreases under the influence of plastic deformation and fatigue tests. The higher the degree of deformation, the greater the drop in the work function. This phenomenon is related to the dislocations moving towards the surface. The creation of loaded steps on a surface is a precursor to crack nucleation.

The WF was measured on the metal surface after wear. A decrease in the WF was observed due to the contact friction interaction. The lower the wear resistance of the hard alloy specimens, the greater the increase in WF and vice versa. The studied method predicts the wear resistance.

The formation of the grain boundary structure of low-carbon steels occurs through the processes of heating, hot deformation, subsequent polygonization, recrystallization, phase transformations, temperature conditions of austenite decomposition, which determine the state of the grain boundaries in the products. Their physical and service properties are the subject of the third chapter.

The object of the research reported in this work is the stress-strain state of the reactors during the production of titanium

sponge by the magnesium thermal method, taking into account the conditions of their operation and the physical and mechanical properties of materials.

The problem considered is the plastic deformation of the reactor in the titanium tetrachloride reduction process. To solve this task, an axisymmetric geometric model of the reactor was built using the CAD module of the Comsol Multiphysics software package. For the calculation, the Nonlinear Structural Materials module was used. Using the finite element method, the critical parameters for the formation of the plastic deformation band of the reactor were determined.

Modeling of the thermoplastic deformation process of the reactor under the conditions of obtaining the titanium sponge allowed to determine the temperature gradient in the upper part of the reactor wall, which leads to local plastic deformation of the wall. The solution to the problem of the continued operation of the reactor would be to prevent the overheating (supercooling) of the reactor wall within the limits of the resulting temperature. The physical and mechanical parameters of the reactor wall material, necessary to prevent the occurrence of an annular band of plastic deformation, were also determined.

This work is devoted to solving the problems related to quality control of machine and scissor steels in the process of product production in mechanical engineering, aviation and shipbuilding industries. A new progressive method for the control of the process of thermochemical and thermal treatment of steels has been proposed and for its implementation the differential dilatometer has been specifically developed.

The operating system of thermochemical treatment allows to ensure obtaining the required parameters of the diffusion layer – the concentration of the saturating element and the gradient of its distribution, the thickness of the layer for high duty products.

The physical and mechanical properties, durability and heat resistance of the developed case-hardened steel are as good as those of chromium-cobalt-nickel-molybdenum steel. For the first time, the differential dilatometer is offered for use in monitoring (and controlling) the thermochemical treatment (TCT) of steel.

The influence of chromium, vanadium and titanium on the mechanical properties is analyzed during the process with the use of the statistical method of planning the active experiment. Conformities to the law of change of mechanical properties are established from the influence of alloying elements and the optimal recommendable chemical composition is chosen appropriately. The most important mechanical properties of the steel depend on the chromium and titanium content of the steel. The influence of the correlation of the amount of chromium and titanium is notable. The presentation of the results of the experiments of the second-degree polynomial type appears justified.

The influence of rolling parameters on structural and phase transformations and on the mechanical properties of steel is analyzed. At a particular combination of temperature, strain and strain rate, a fine-grained austenite structure with a highly developed polygonal substructure can be obtained.

Transmission Electron Microscopy (TEM) allowed studying the effect of variable factors ( $\epsilon$ ,  $\tau$ ,  $t$ ), as well as the relative amount of special low-energy boundaries in ferritic and martensitic components of low-carbon steels in the CSL (Coincidence Site Lattice) concept. The optimal performance of thermoplastic deformation was established, as a result of which the process of polygonization takes place: a change in the configuration of grain boundaries, the formation of low-angle polygonal boundaries, the interaction between them and high-angle and special boundaries. The performance of the developed heat treatment provided an increase in impact hardness of both the base metal and the heat-affected zone of low-carbon steels such as 10ХФТБч steel (a Ukrainian standard). This is due to the appearance of special boundaries – twins, sigma 5 and others, as well as the occurrence of polygonization. It is shown that triple joints are more stable and play an important role in the formation of the final structure of weakly perlitic steels, on the boundary of 120 °C.

This study determines the effect of plastic deformation on the structure formation and the process of phase transformations in low-alloy steel 10ХФТБч (a Ukrainian standard). The deformation temperature was varied from 770 °C to 950 °C, the degree and rate

of deformation remained constant. It was found that the optimal hot deformation mode for low alloy steels exists in the temperature range of 850...950 °C at the deformation rate of  $u=100 \text{ s}^{-1}$  and with the degree of deformation  $\ln \varepsilon=1.2$ . The number of phases is 58–80% ferrite and 20–42% perlite, which significantly increases the strength of the alloy steel, while maintaining sufficient ductility.

This book is intended for undergraduate and graduate students in the subject areas of solid-state physics, surface physics, and materials engineering. It is expected that this book will meet the needs of those concerned with the properties, study and application of modern industrial alloys.

It is hoped that this book will also be useful to materials scientists, engineers, researchers, and practitioners in industries concerned with problems of material properties, surface strengthening, and fatigue resistance.

# 1 GENERAL CHARACTERISTICS OF THE SURFACE LAYER OF METALS

## 1.1 Methods for studying the surface

The development of theoretical concepts and intensification of knowledge about the properties of the surface layers of materials largely depend on the level of experimental studies in this field. The physical methods of surface analysis include, in particular, optical and electron microscopy, X-ray structural analysis, electron diffraction, spectroscopy. non-destructive methods are of particular interest for the study of surfaces.

One of the most common methods for analyzing the chemical composition of the surfaces of solids is a method of Auger-electron spectroscopy [1, 2]. This method provides effective information on the distribution and composition of the elements present on the surface in an amount of more than 0.1%, and allows defining some of the elements in a bound state. Electron spectroscopy methods require the use of high vacuum, which limits their application for studying processes. Fourier and photoelectron spectroscopy are promising to determine the elemental composition of the shallow impurities and their electronic state [3].

A wide range of physical methods of studying the surface layers of metals and alloys is based on the diffraction of X-rays, electrons, and neutrons [4–11]. Electron diffraction method is of interest for decoding structures, especially in the presence of highly dispersed phases, which sometimes cannot be detected by X-ray analysis. Electron diffraction is widely used to study the surface layers of a few nanometers thick, as well as specially prepared thin film. The use of X-ray diffraction methods determines the possibility to identify the interconnection of properties of solids with their structure. X-ray methods make it possible to study the structural changes in metals and alloys under plastic deformation, heat treatment, various power influences. X-ray structural analysis is

widely used for practical purposes in establishing the optimum technological modes of components manufacturing, during their processing and use. An important advantage of the X-ray method of studying the materials is that defined parameters of the structural state are averaged over large volumes and provide a satisfactory correlation with the physical and mechanical properties of the objects studied.

One of the promising methods of nondestructive energy state testing of the surface of solids is an exoelectron emission method (EEE) [12–18]. EEE has a number of regularities that are not typical of other types of emissions. The presence of macro- and microdefects, stress fields, layers of oxides and adsorbates in the surface layer of the materials after machining leads to significant changes in the electronic subsystem of solids, which is reflected in exoelectron properties of the deformed surface. In general, the increased activity of the deformed surface emission is caused by a decrease of the energy barrier for electron yield due to the formation of structural defects. The deformational excitation of the surface layer in metals, gives rise to a chain of processes: the formation of surface defects – the initial drop of WF – adsorption on defect – an additional change in WF. Currently, the EEE methods are used in the nondestructive technique of testing the surface of various materials. However, a single explanation for all manifestations of exoemission does not exist yet. Further development of the EEE method is seen in the way of studying regularities of the electronic states on the deformed metal surface in a variety of environmental influence conditions.

It has been noted that the most important parameter of the electronic subsystem is the work function of electron. Many methods for experimental determination of WF are developed by now: thermionic and photoelectric methods, methods of contact potential difference, surface ionization methods etc. The differences between these methods are conditioned due to the way of energy excitation of electrons [19, 20]. The measurements of WF with the contact potential difference method are attractive due to small perturbations of the state of surface under study, equal suitability for measurements in both high vacuum and

gaseous environment. One of the most accurate and the most often used in practice is a method of vibrating capacitor. In the literature there is a description of a number of devices based on the method of CPD [21–37]. CPD does not depend on the capacity of the condenser, and is determined by the material of plates and measurement conditions. WF values which are obtained with the help of the CPD method are in good agreement with data obtained by other methods. The work [23] describes an apparatus for measuring the CPD with automatic compensation of contact voltage with accuracy up to 1 mV through the use of feedback. Another measurement method is implemented in [24], where the measurement of the CPD in vacuum was carried out by the dynamic capacitor formed by the electrode and the flat thin metal filament of string self-excited oscillator with electrostatic excitation. In [25] it is noted that the effectiveness of the capacitor method can be increased by a joint analysis of the offset voltage and current of the dynamic capacitor, which shape of vibrations allows obtaining additional information about the relaxation oscillations of surface adsorbed charges.

The thermoelectric method and infrared spectroscopy are used in the study of deformation processes on samples and field details. The basis of the thermoelectric method is the measurements of the material temperature using micro thermocouples, fixed on a surface of deformable sample [38–40]. Thermoelectric method has found application in the study of the deformation anisotropy of the yield stress, determining the stresses in an inhomogeneous state of plane stress. The main limitation of this method is the need to implement the conditions of adiabatic flow deformation process. Infrared spectroscopy method is based on the registration of the spectrum of infrared radiation from the surface under the study. Character of change of infrared radiation parameters is depending on the degree of elastic and plastic deformations. Explanations of the experimental dependence of the intensity and the wavelength of the infrared radiation from the strained state of metals have now only a qualitative nature [41].

Integrating basic parameters of the surface metal layer can be considered the surface roughness and residual stresses. They

determine the state of the material, which is formed under processing conditions and regularities of deformation destruction during operation. In its turn, the roughness parameters, the magnitude and distribution of residual stress express physical and mechanical properties of the surface layer material. The most common methods for studying the physical and mechanical properties of the surface layer are tests on the local deformation or indentation. Indentation methods are directly related to the mechanical loading of the metal surface. The fact that they are non-destructive to a certain extent, stimulate the development of research for the indentation parameters to determine the yield strength of the material [42–44]. Another important area is the establishing of the functional relationship between the parameters and characteristics of the indentation stress-strain state in tension [45–55]. When using the continuous pressing method, one can receive information on the deformability of the material on depth of the surface layer. This makes it possible to evaluate not only the elastic and plastic properties of the material, but also the option of strengthening [56–58]. Indentation is primarily a contact interaction of interfaced bodies, as a result of which the actual contact area is formed. In the process of changing the load on the indenter a corresponding change in the metal contact area occurs. Moreover, this area is characteristic of the interaction of bodies already by its very nature. Using the actual contact area as a parameter of deformation and fracture of the interfaced surfaces has not found wide application by now. For continuous determination of the contact area of the interfaced surfaces the most convenient is the method based on the measurement of the contact electrical resistance (CER) [59]. The high sensitivity of the electrical resistance measurement allows studying the kinetics of deformation processes in the surface layer material at loading and unloading of interfaced bodies and revealing the finest features of this process [60]. The informativeness of parameters of the contact electrical resistance in the research of friction and wear phenomena proved in [61, 62]. It is noted that the drop in the contact zone conductivity is related with the formation of oxide insulating films and fretting wear products, leading to fluctuations of the contact

electrical resistance. The papers [63, 64] are dedicated to the study of the contact electrical resistance nature. The basis of experimental and theoretical studies is determination of dependence of the CER on discrete metal contact parameters. The account of the sizes and distribution of the contact points in the most general form, are carried out in the work [59]. Since this work is dedicated to solve electrical engineering problems, it is natural that, dependence of CER on the real contact area received little attention. The real area is an integral characteristic of the totality of conductive points, which takes into account the unevenness of their distribution and mutual influence. It seems promising to use the real area as a parameter of deformability of the rough surface layer on the basis of measurements of the contact electrical resistance.

## **1.2 Regularities of the material deformation of the surface metals layer**

The earliest systematic identification research which concerns the surface role in the process of plastic deformation are works of A. F. Ioffe. The study of the plastic flow kinetics at the initial stage of deformation and explanation the nature of the surface sources are devoted to the study [65–68]. The graph illustrating the influence on the mechanical properties of the surface on metals is represented in Figure 1.1.

In work [69] is found that the surface influence causes profound volumetric regular changes in the crystal. The experiments were conducted on annealed crystals of sodium chloride. During flushing crack by water was observed that it is “grows” as it in depth and in width. For completely flushing was required removing a layer at 10–20 times greater than its depth. As a result of the dissolution of the surface significantly change the picture shifts in the entire thickness of the crystal, observed in polarized light. It can be assumed that the surface influences on the process of plastic flow in volume. Then, the surface plays a permissive role of the process for certain mechanisms of deformation.

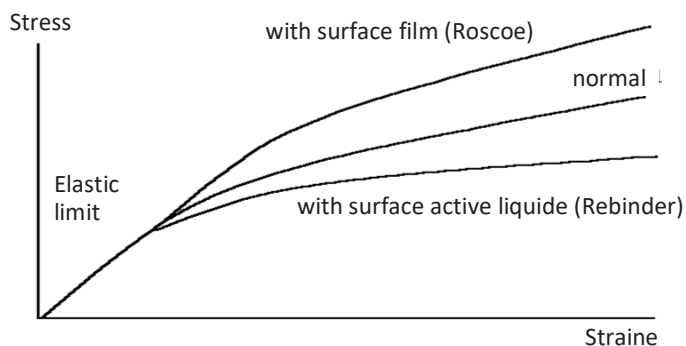


**Figure 1.1** – Surface influence  
on the mechanical properties of the metal

In work [70], a radiographic study of the structural changes in single crystals of tungsten in their four-point bending deformation in the process of electropolishing and without it was conducted. It is found that the flow stress during crystals tungsten at bending varies depending on the rate of metal removal from a surface. It was found that the nature of the structure of the surface layers and in the bulk tungsten crystals deformed by four points bending during electropolishing and without it, it is differed (electropolishing contributes to the phenomenon of mechanical polygonisation in the surface layers of crystals). With increasing current density i. e. with increasing metal removal rate was observed the increase the yield point of tungsten and 50% compared with the deformation without polishing.

The first attempt to obtain separate quantitative information on the characteristics of the plastic flow of surface and inner layers in a number of crystals was the work of Kramer [71–73]. By removing the surface layer of the sample during deformation, Kramer found the extent increasing and decreasing in the slope of curves of the first and second stages of strain hardening. The termination of removing the surface layer increases the coefficient of strain hardening to values observed during deformation without removing it. This is due to the increased a dislocations density in the surface layer, hindering the dislocation occurring during

deformation in the crystal. It is shown that the formation of such a layer does not depend on the presence of the oxide pellicle and the peculiar metals with different types of crystal lattice. It is also established the influence of the surface layer on the activation energy of plastic deformation of metals with face-centered cubic and their activation volume [4]. In work [7] it was found that by removing the surface layer by electropolishing samples of aluminum single crystals flow stress was decreased with repeated loading at all stages of deformation.

In work [74] put forward a point of view according to which the surface layer is characterized by a high density of surface dislocation sources, strength and barrier role in the first stage of strain hardening. It is also noted that, given the trend toward relaxation of the dislocation structure near the free surface, the second stage of strain hardening the surface layer has a lower dislocation density and the dislocation cells larger than the inner layers of the deformed metal. Direct measurement of dislocation density near the surface and in the volume of materials with face-centered cubic it was found that after the deformation in the surface layers of the dislocation density is higher than inside the crystal. It is also established the presence of the dislocation density gradient from the surface into the crystal.

A detailed examination of the physical regulations of microplastic deformation of the surface layers of solids is given by V. P. Alekhine [75–81]. The complexity and diversity of the influence of the surface layer on the nature of the deformation of materials is largely determined by the interaction of the surface with the volume. It was in the course of this interaction is the formation of a surface layer with special properties and further its influence on the general character of the deformation. In work [82], on basis of the various structural methods analyzes the character of the distribution of dislocations wrought by the cross section of the samples studied the impact of surface micro deformations features totaling kinetics of strain hardening. Also the basic physical reasons and factors responsible for the anomaly micro deformations near the free surface were reviewed. It is shown, for example, that the development of the effect of Haasen – Kelly responsible the events

in the surface layer, as a result of the relaxation of redistribution and more rigid fixing dislocations in the surface layer in the process of unloading and the actual barrier effect. There is also notes a mechanism for undersaturated crystal openings during the unloading of the sample, by which they are “absorbed” from the free surface and cause the climb of dislocations [78].

The specific surface energy of the interface metal-environment can be changed due to the adsorption of surfactant components from the gas phase. Electrically charged metal surface changes the surface energy  $\gamma$  in accordance with the thermodynamic relation

$$d\gamma / d\phi = -q, \quad (1.1)$$

where  $\phi$  – potential,  $q$  – the surface charge density.

The impact of electric charging surface of lead in the electrolyte solution is considered in work [83]. Also, in Rebinders works, it was found that the speed of creep is independent of the sign of the charge. The possible impact of the environment on the process of deformation can be explained by the contribution of grain boundary sliding in the deformation. This is due to segregation at grain boundaries impurities diffusing from the environment, as well as the formation of oxide and adsorption pellicles. Grain boundary sliding is the result of slip dislocations in the grain boundaries, and the sliding speed is determined by the non-conservative movement of the edge components. The latter process is controlled by the speed of diffusion of point defects supplying the thresholds on the lines of dislocations.

### 1.3 The dislocations on the surface

Experimental facts suggest that the dislocations are formed on the surface of crystals, in places where there aren't irregularities in the scale absolute of not only light, but electron microscopes. For the formation of dislocations on the crystal surface in terms of the atomic geometry of the latter structure, there are auspicious opportunities due to the presence of monatomic steps, located along the densely packed crystallographic directions. In the work [84]

it was shown that the presence on the surface of crystal ledge with a radius of curvature of the edges of the atomic size (regardless of the height of the ledge) creates, by means of the surface forces, the local concentration of shear stresses about the theoretical strength. While these stresses are concentrated in a very narrow place of the crystal along the ledge, but in the presence of a suitably oriented slip planes it will be enough for a shift to a depth of a few interatomic distances. The gradual decrease in the curvature of the ledge with its movement into the crystal in the quality of dislocations will lead to the stress reduction. The formation of dislocations should be facilitated even more during the replacement of free surface to the medium with a large shear modulus (for example, in the case of the metal-oxide interface).

In the work [85] the formation and accumulation growth of straight dislocations in the flat surface of the crystal are analyzed. It was shown that in a crystal with a random field of internal stresses, generated by grown-in dislocations, the intensity of the dislocations multiplication by surface sources is substantially greater than by the internal (by times). The average dislocation density in external stress  $\tau$  is determined by

$$\rho(\tau) = \rho_0 + \frac{2h}{L} \alpha_s d_s \exp(\tau/\tau_s) + \alpha_i d_i \exp(\tau/\tau_i), \quad (1.2)$$

where  $h$  is the width around the surface zone, in which top-surface sources are located;  $L$  is the characteristic linear dimension of the crystal:  $\alpha_s = P_s \langle n_s(0) \rangle$ ,  $\alpha_i = 2P_i \langle n_i(0) \rangle$ ,  $P_s = 0,37$ ,  $P_i = 0,27$  – the probability of inclusion respectively the surface and internal sources.

If the smooth surface of the polycrystalline sample before applying the scratch receives the significant deformation, the process of “healing” that occurs at high temperature, the mark profile will remain smooth, just as it was in the case of “healing” of the marks to the amorphous body surface [86]. The mark, inflicted on the surface of the sample, that has preliminary long-term annealing, can be hardly healed, but it only changes the profile in accordance with the grain orientation relatively to the plane of the section, and on the distorted surfaces the speed of mark smoothing increases with the degree of distorted surface. The

surface layer, subjected to the deformation, is a complex of finely-divided disoriented microcrystals or blocks that have arisen as a result of polygonization of the near- surface layer. The stability of the structure of the near-surface layer is proved to a possible dissociation of individual elements of the structure, i. e. the presence of a grid of discontinuities, preventing accumulative recrystallization. In case when a polycrystalline surface was subjected to grinding and polishing, it's necessary to distinguish the surface diffusion, which consists in the atoms replacement on the surface of the crystal-vacuum boundary and the "near-surface" diffusion, which occurs in the near-surface layer of a certain thickness, permeated by a variety of interfaces and dislocation lines. The coefficient of surface diffusion must be the material constant, depending only on the temperature, while the coefficient in the near-surface layer is structurally sensitive, and therefore it depends on the nature of the surface treatment. The preservation of a smooth profile in the process of scratches healing on polycrystalline copper samples can be the result of a small anisotropy of the coefficient of surface tension and the presence of mutual disoriented elements of the dispersed structure in the near-surface layer.

#### **1.4 Study of the defect structure of metals by electron microscopy**

A significant number of works are devoted to the study of the process of the plastic deformation in metals by means of electron microscopy [87, 88]. It was found that the sliding tracks in aluminum, copper, silver, nickel, stannum, etc., observed in the light microscope as separate lines, actually have a complex structure. They consist of a few fine lines. The structure of the sliding tracks on the surface of the aluminum alloy was investigated in the works [87, 89]. It was found that the deformation is localized not only in the visible sliding tracks, but also between them. The slide on a pack of atomic planes corresponds to each sliding track. Moreover, the shift on these planes is distributed irregularly. It was shown

that the structure of deformed metal surface reflects the process of deformation in volume.

In the work [90] it was experimentally shown that shift lines at small degrees of plastic deformation can be detected only with the full removal of residual stresses from the surface. The study of the height irregularities on the sample surface of steel 10, shown in uniaxial tension, showed that the height of steps reaches 0.15 microns. The slip bands on the yield line are relatively far from each other (about 7 microns), and the entire volume of the metal between the bands is virtually untouched. It indicates that here the major deformation is concentrated on the slip bands. With increasing of deformation degree, the relief accuracy and the height of the steps increase markedly. The measurement of the micro-hardness along the line, which crosses the boundary between the elastic and plastic deformations, showed that the micro-hardness value increases step-like in the area of plastically deformable metal. During the deformation on the yield line at the border section of elastic and plastic deformation in the deformed part of the sample, if not all, but the vast number of grains join the plastic deformation. The formation of movable dislocations leads to a hard change of the elastic properties of the alloy, the linear relationship between stress and deformation breaks.

In the work [91] the results of direct observation of electromigration of single dislocations in ultra-pure copper monocrystal were presented. The electromigration is carried out directly in the column of the high-voltage electron microscope JEM-1000. At a current density above the threshold value of  $10^7$  A/cm<sup>2</sup>, at first unmovable dislocations started to move generally to the sample surface. Speed of dislocations movement was about 1 mm/s. Upon reaching the current threshold, the worst enshrined dislocations, lying close to the surface, quickly removed. More enshrined dislocations, which can't be pushed by the current to the surface, came on their place from the depth of the sample. In order to remove these dislocations a new increase in the current was needed. The influence of directional flow of electrons resulted in buckling of unmovable dislocations in the direction of the current electromechanical force.

## 1.5 The problem of residual stresses

Mechanical characteristics of metals are determined by microscopic researches that allow determine parameters such as hardness limit of plasticity, work hardening coefficient, fatigue limit, etc. These parameters are directly connected with microstructural state of the material, determined by the chemical composition, direction and distribution of the grains, the density of impurity atoms and dislocations. It is also necessary to bear in mind that mechanical properties of the surface layer differ from those properties of a volume, i. e. the definition of physical and mechanical properties is connected with material volume, overtaken by the measurements. Microstructural changes in the surface layers often lead to plastic deformation of these layers. The continuity of the material between surface and volume causes the residual macro stresses. The latter play a significant role in the process of deformation as they change the values of the stresses, experienced by the material near the surface. Apparently, it is necessary to distinguish the influence of residual stresses and properly microstructure on physical and mechanical properties of metals. At various stages of deformation, and also depending on the loading conditions, variable state parameters of the material structure have a decisive role.

In case when the plastic deformation due to some reasons is impossible or impeded, the residual stresses have a significant impact on the process of destruction. The effect of residual stresses on the fatigue strength is most full studied [92–94].

The presence of compressive residual stresses in the surface layer of the detail increases the fatigue strength [95–97], especially in the places of stresses concentration. It was experimentally established that compressive residual stresses in the surface layer, resulting from the hardening treatment, play a significant role in enhancing the durability of workpieces, working in bending and twisting [98]. It was noticed, that the residual stresses are largely reduced in the surface layers, which by their physical nature, are less robust. With the increase of the amplitude of the diagram cycle the residual stresses are considerably changed, especially in the surface layers [99].

## 1.6 Macro- and microroughness of a surface

The surface of a solid body is wavy and rough. The roughest metal surfaces have roughness's of 0.05–0.1 micron high. The roughest metal surfaces which are found in mechanical engineering have ledges of 100–200 micron high which usually settle down on some wavy surface. The step of this wave changes within 1,000–10,000 micron and its height, respectively from several to 40 microns. Interfaced metal surfaces always have separate small spots of the contact, and owing to a waviness these spots of the contact are located in certain areas. The number of contacts depends both on loading and on a roughness of surfaces. The pressure on contacts is distributed depending on their configuration [100]. Besides, structural changes occur owing to physical and chemical interaction with environment. For example, as a result of “Rehbinder’s effect” and diffusive saturation of elements from the environment and from a counter body, during the process of the chemical interaction with the atmosphere.

A process of friction is determined by periodically repeating local loadings. A material destruction in the conditions of cyclic contact interactions is generally defined by fatigue processes [101–103]. Therefore, studying of characteristics of a surface layer and mechanisms of surface hardening has the defining value in this case too. The technology factors which influence distribution, the size and residual stresses (RS) sign, at the same time influence a surface profile. Special boundary conditions on a surface lead to high-quality change of all near-surface layer condition. Really, at the very surface RS create the forces operating strictly parallel to tangents to a surface to the planes, but with a material depth, according to Saint-Venant’s principle the influence of a surface form has to decrease. Thereby presence of a stressed state in a sample with not ideally smooth surface inevitably entails heterogeneity of this stressed state. As the relief is a set of incidentally and (or) periodically located hollows and ledges the stressed state on a metal surface is non-uniform along the surface. Ledges in relation to the average operating tension are unloaded, hollows

serve as concentrators of tension according to the theory of elasticity [104, 105].

Thus, in the course of receiving and processing of a product a certain microgeometry and stress-deformed condition of a surface layer material are formed. Herewith geometrical and physical-mechanical characteristics are interconnected in many respects. The main way of the processing of metal details is direct mechanical impact on a surface. Operation of details is also followed by mechanical loading of the surface layer material. Therefore, researches of physical mechanical properties of surface layer of details for the purpose of processing optimization and receiving a layer of material with the set properties are actual.

The superficial gradient of dislocations density created at an initial stage of deformation serves as a barrier to the dislocations leaving a volume on a free surface of a crystal [82]. Three main cases of such barrier influence are distinguished:

1. The barrier effect of an atomically clean surface is caused by that the dislocations surface outgoing should have an additional energy spent for work connected with the increasing of the general superficial energy of a crystal during of a step formation of  $nb$  height, where  $n$  – is a number of dislocations in a congestion,  $b$  – Burger's vector.

2. The barrier effect of the real surface covered with oxides and other firm membranes and coverings.

3. The barrier effect connected with a formation of some density gradient of dislocations at a surface and arising owing to realization of the facilitated deformation conditions.

Really these three effects are imposed at each other. In ordinary cases of macroscopic samples deformation, the effect 3 is the most essential. To come to a free surface of a crystal, the dislocation has to form a step of  $b$  height [111]. For this purpose, it is necessary to spend additional energy

$$W = \gamma b, \tag{1.3}$$

length unit of a dislocation, where  $\gamma$  – is a superficial energy. To dislocation could come to a surface, its energy has to be higher than this value. Sliding strips in a cross-section form steps on a sample surface. Height of a step is equal to, at least, a constant

lattice, in this case the step is a trace of the elementary act of plastic deformation. However, lines of sliding from several hundred high to many thousands of a constant lattice are observed most often. It is possible to accept that the average width of the line of sliding has an order of 100, and step height – 1,000 constants of a lattice. This height, obviously, depends on a corner between the directions of sliding in the active (already operating) sliding plane and the observed surface of metal. In aluminum distances between strips of sliding reach 1–2 micron, and between lines of elementary structure – about 30 nanometers. Height of the last ones reaches 2–5 nanometers [106].

In recent years nuclear steps on a surface of a solid body were intensively studied both experimentally, and theoretically, and at experimental studying emphasis generally was on the equipment resolution increasing. So, by means of reflective electronic microscopy in Bragg's position, the contrast formed by the superficial steps having height of one atom was researched [107]. For supervision of mononuclear steps on a surface with sensitivity of 0.01 nanometers in work [108] the method of reflective electronic holography was used. Results of the surface topography research Au and Pt were researched by means of the scanning electronic microscope, are presented in the work [109]. In the survey work [110] it is noted that among the methods allowing nuclear steps (NS) studying on a surface, methods of the translucent electronic microscopy (TEM), diffraction of low energies electrons (DLEE), scanning tunnel microscopy (STM), dispersion of He atoms, dispersion of X-rays have special value. By means of these methods the existence the NS on a material surface is registered, their form, density and distribution on a surface are studied.

In the series of theoretical works [111–114] power aspects of a problem and also interaction between steps of various configuration are in detail considered. The interaction between mononuclear steps investigated in the work [115] showed that the attraction between them is caused by the relaxation of superficial tensions and at distances  $R=3-5$  constant lattices fall down as  $r^{-2}$ . The superficial steps configuration and kinetics of their migration is also considered in the work [116]. In the work [117] by means of the

modified model of dot ions step profiles for eight fcc and bcc crystals surfaces are predicted. Existence of step structures with various degree of an atomic roughness is established, the tendency to the step edge smoothing is noted. The data provided in work will be agreed well with the results of experiments on aluminum and iron.

In work [118] elastic fields on a surface with periodic steps in the form of not isosceles triangle, which one side is a step, and another is a terrace were investigated. Elastic near-surface fields are connected with a deficiency of electrons on the surface. If the surface has a step, then atoms migrate from step edges deep into a surface that leads to its relaxation. In the considered model of elastic medium with a periodic lattice of linear forces with the period equal to the period of steps, it appeared that fields of deformations and tension quickly fade deep into a surface as  $Y \times e^{-\gamma}$ , where  $Y$  is rated distance from the surface, and superficial energy is defined, mainly, by energy of tops and terraces.

The sub microroughness characterizes a thin structure of a real surface and has submicronic scale, having impact on formation of a so-called physical relief. Its emergence is connected with the internal structure of solid bodies and crystallographic imperfections which is tensely deformed by a condition of thin surface layers and an influence of a working environment in a contact zone when processing. Owing to heterogeneity of material structure, the equilibrium condition of a surface determined by a minimum of its free energy usually can't be combined with its initial smoothness, as causes one of reasons for crystal surfaces rejection from ideal and emergence of a natural roughness. It significantly surpasses an atomic roughness in scale. The sub microroughness shows as occasional arrangement of crystallographic surfaces, surfaces of grains, insular membrane of the oxide and adsorptive nature, formed at impact on a surface by streams and particles. It can also appear that the reduction of a surface will be exactly that process which generally will provide the reduction of free superficial energy. This tendency is shown in processes of surface defects smoothing [89].

The research is devoted to a question of influence of a polishing class at a size of a true metal surface. It was established that

roughnesses of a profile within 0.01–2 microns cause increase in a geometrical surface no more than for 3%. Experiments on adsorbed ions quantity measurement on metals show that the true surface of metals, irrespective of a type of polishing, is 2.5 times bigger than the geometrical. Authors [119] draw a conclusion that difference of a geometrical surface of metals from the true is caused by the roughness's lying outside the most high-class processing of metals.

The work is devoted to clarification of extent of machining influence at a size of a true surface [120]. The surfaces of samples of Mg, Al, steel St-3, St-45, bronze and cast iron received when turning and planning, milling and grinding to various classes of purity were studied. Roughness's of a surface were presented in the form of the separate tetrahedral pyramids adjoining one another. A height of these pyramids is defined by a processing class. The measured surface represents the size of side surfaces of pyramids, and geometrical is the sum of the areas of the bases. Change of a roughness of 0.1–2.5 microns and distinction in ways of processing don't influence the size of the measured area. The method of sedimentation of ions also confirms an independence of a true surface of a metal's roughness degree.

## **1.7 Development of defective structure near a clean surface**

A number of theoretical works [121–123] is devoted to the analysis of different aspects of power interaction of dislocations with a surface of a crystal and to influence of forces of the image on the movement of dislocations in near-surface layers. Influence of a surface is shown also in features of elastic interaction of spot and linear defects with a free surface of a crystal. Spot and linear defects near a surface are affected by the field of distortions caused by the relaxation phenomenon. The conclusion is drawn that impurity of implementation and interstitial atoms are attracted to a surface, and vacancies are taken away in depth of metal.

Formation of vacancies is followed by reorganization of a grid around it. Such reorganization has generally electronic character.

In metals electrons of conductivity get in vacancy due to “tunnel” effect. As a result, effective surface energy of vacancy decreases and distributed more evenly on defect volume. Surface tension causes vacancy compression.

The dislocation which has appeared under the influence of image forces about a surface for continuation of sliding has to increase the vector of Burger’s, that is energy. And it causes emergence of force interfering a dislocation exit to a surface. This effect amplifies “spreading” of a kernel of dislocation near a surface. Apparently it needs to be considered at research of processes of adsorption and absorption, influence of external environment on mechanical properties of crystals. When studying interaction of dislocations with a free surface use a method of images [124]. Dislocation is attracted to a free surface with a force

$$F = -\mu b^2 / 4\pi l, \quad (1.4)$$

where  $\mu$  – the shift module;  $b$  – Burger’s vector;  $l$  – distance from dislocation to a surface.

Existence of a layer of oxide on a surface interferes with an exit from metal of the dislocations which are formed at deformation. It is considered that the free surface of a crystal is the most preferable area of heterogeneous origin of dislocations [125, 126].

The ready easily operating sources of dislocations the surface of a crystal can have oxide films, scratches and cracks, upper cuts of a sample, a particle of allocations, surface micro ledges and steps of a chip, an etching pit, area of the appendix of the concentrated electric field, prints from the indenter, etc. The surface of a crystal can also works as a source of dislocations. The specific role of a surface in reproduction of dislocations is also that it, being a powerful source and a drain of vacancies, intensifies recrawling processes. It in turn leads to formation of surface sources at which activation there is both a sliding and recrawling of the dislocation line. The most widespread scheme of heterogeneous origin of dislocations this education them near surface steps.

Steps of different signs A and B turn at crystal stretching into dislocations in different systems of sliding 1 and 11. The mononuclear step on a surface is capable to form not only single

dislocation, but also under certain conditions can work as a source of a set of dislocations on two systems of sliding.

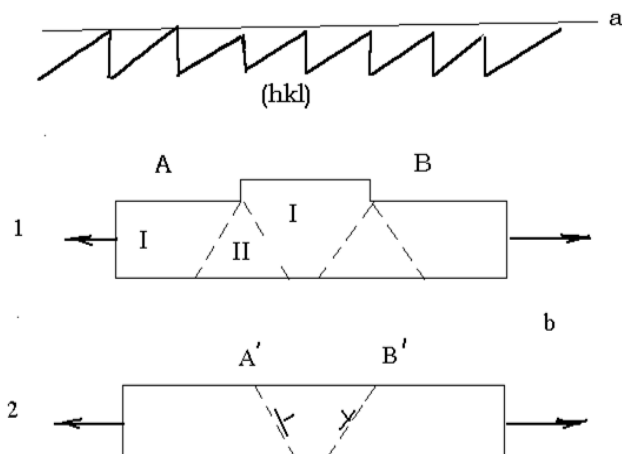


**Figure 1.2** – Scheme of heterogeneous origin of dislocations

Reorganization of dislocation structure in the course of deformation of metals is often carried out is heterogeneous. In work [127] periodic changes of dislocation structure at deformation of aluminum in the conditions of active loading are investigated. Change of a form and width of diffraction lines (200) and (400) was accepted to criterion of existence of reorganizations in structure of material. Periodic changes of dispersion of elastic deformation are found, and the number of fluctuations of dispersion before destruction of material is continuous for this material. For an explanation of results of experiment the model based on effect of rotational instability of ensemble of dislocations is offered. It is supposed that each material maintains quite certain number of fluctuations of defective structure corresponding to number of the possible active rotational systems which are carrying out a dynamic relaxation before destruction.

In work [128] the stationary solution of the kinetic equations for density of dislocations near an exterior surface of the deformed semi-infinite crystal is received. The microscopic mechanisms

which are the cornerstone of interaction of atoms or molecules of external environment with mechanically activated surface of crystal materials still are up to the end not clear. The explanation of influence of the environment on mechanical properties is possible on the basis of the phenomenon of the dislocation dynamic diffusion (DDD) – penetration of atoms or molecules of the environment into a surface layer of a crystal on moving dislocations. Local change of density of dislocations in a surface layer depending on depth of their bedding is unambiguously connected with influence of external environment. And depending on type of the environment in which the crystal is deformed the surface layer either is strengthened, or hardening and softening.

Density of screw dislocations near a surface of the crystal deformed in vacuum decreases at approach to a surface. This results from the fact that forces of the image increase the speed of dislocations to a surface. Falling of density of screw dislocations near a surface of the crystal deformed in vacuum is connected with simultaneous influence of two factors: reproduction of dislocations in volume of a crystal and an attraction of dislocations to its surface at the expense of image forces. Influence of external environment on screw dislocations leads to disappearance of regional effect. It has a talk interaction of the negative dislocations moving from volume with atoms of impurity of external environment which get into the near-surface layer at the expense of DDD which has passed at earlier stage of deformation. Force aims to enlarge the images the speed of dislocations and by that to reduce their density near a surface. Atoms of impurity slow down dislocations and increase their density.

## **1.8 Influence of the adsorbed substances on the surface on the mechanical properties of metals**

It's known about an effect of adsorption strain relief when the adsorption agent, reducing the surface energy of a rigid body, contributes to the emergence of flow shears and development of defects variety in the surface layer under the application mechanical

loading. The effect of surface-active agents (surfactants) on the deformation of a number of metals was studied in the work [129]. The dependence of the adsorption effect from the orientation of the acting sliding elements was found for single crystals of tin and zinc, expressed in the fact that the reproducible values of the effect are obtained only for the samples with the same orientation of slip planes to the axis of the single crystal. It is also observed that the concentration of the surfactant, which is corresponding to the maximum effect of single crystals, is the same as that for the polycrystals of tin, lead, copper, and corresponds to the equilibrium saturation concentration of the adsorbed layer. The increasing of surface hardening of polycrystalline metals (zinc and copper) with periodic deformation is found out. It's a running with roller or ball in adsorption-active medium (increasing of microhardness). The effect of the surfactant depends on the deformation rate and has maximum. The value of the adsorption effect is determined with deformation mode and can be observed in certain, although quite wide range of deformation rates. The boundary of this area depends on temperature. The adsorption effect increases with increasing heterogeneity of the stress state (with decreasing in the ratio of the stretched crystal to its diameter). Adsorbed substances under the influence of an already hardened crystal can reduce hardening coefficient during further deformation to a value nearly corresponding to non-hardened metal. Surfactant affects mainly grains situated in the surface layer while adsorbing on the outer surface of the metal. The higher the fineness of grains, the metal is the less susceptible to the effects of surfactant during creep. "Adsorption fatigue" both at very small and very large ( $10,000 \text{ min}^{-1}$ ) frequencies stops operating practically and is the maximum in the range  $1,500\text{--}3,000 \text{ min}^{-1}$ .

Plasticizing effect is the most common effect of action in surface-active media, and it is always a case of metals deformation in any surface-active medium. The essence of the positive impact of the surface layers plasticizing of metals at the initial moment of the cyclic deformation is to remove local normal stress arising at the head of dislocations accumulation at the surface of the metal, which can be a significant barrier for moving dislocations under

ordinary conditions [130]. In the work [131] there is an attempt to evaluate the impact of air, vacuum (133 MPa and 1.33 MPa) on the principle of change long-term strength and structure of the nickel alloy ЭИ868 in the range (700...900) °C. The material was studied in a position of supply (hardening from 1,150 °C with delay of 1 hour). The specimens with working part size of  $1 \times 3 \times 9$  mm<sup>3</sup> were tested and manufactured by stamping from a sheet of 1 mm thick, followed by filing and polishing of the surface. The phase composition of the alloy after treatment in various media was determined using DRON-3 in copper K<sub>β</sub>-radiation (30 kV, 15 mA). The value of the nickel lattice parameter was determined from the integrated intensity of the line (111). It was found that the influence of the environment on the alloy at a temperature of 700 °C is significant on base of 10<sup>3</sup> minutes – test or more. During the interaction of EI868 (Ukraine) nickel alloy with a medium containing oxygen in the range (700...900) °C oxides of chromium and molybdenum are formed, isolated as separate particles along the grain boundaries (133 MPa), or in the form of a continuous film (in the air). This continuous film has a strengthening effect on the alloy. When the temperature changes from 700 °C to 800 °C strengthening effect of the oxide film is weakened due to the formation of less dense oxide Cr<sub>2</sub>O<sub>3</sub>. The alloy without any precipitates (1.33 MPa) has the greatest deformation capacity at the same temperature and failure stress value and alloy with oxide precipitates along the grain boundaries (133 MPa) has lowest deformation capacity.

Using of unsymmetrical X-ray reflection lets to analyze the surface layers of metal with thickness comparable with the set one. In the work [132] radiography was made through direct sliding beam of alloys АД0 (Ukraine) and АМч6 (Ukraine) in different environments in the air, in a vacuum (10<sup>-2</sup> Pa), vacuum grease and films coated with TiN of different thicknesses. During the study a reversible change in the interplanar distances in the surface layer thickness of 15–20 microns was found. It occurs during pumping and puffing in the chamber with sample of air. In the samples coated with a surface lubricant, the interplanar distance value in comparison with pure samples in the air changed even more significantly than in a vacuum. It was also found that the durability

of the samples the more increases under vacuum, the smaller the amplitude of the load. Whereas samples durability with surface lubrication is significantly reduced and the change in air pressure (in contrast to the objects with a clean surface) has no effect on it. The nature of the durability changes after coating depends on the layer thickness – its growth to the critical value thickness (<1 micron) goes into decline at supercritical thicknesses. The authors of [133] believe that the fatigue durability is determined by the adsorption-desorption mechanism of the environment influence. In the work [134] WF change during adsorption was calculated using the formula

$$\Delta\varphi = -4\pi x_0 e^2 \frac{c}{S} q_{ad}, \quad (1.5)$$

where  $x_0$  is the distance from the nucleus of an adatom to the metal surface;  $c$  is the degree of filling of the adsorbate lattice under consideration;  $S$  is the area of the unit cell of the lattice;  $q$  is the charge of the adatom.

Also, the authors analyze the dependence of WF on the degree of the surface coverage by adatoms. An approximate dependence has the form

$$\Delta\varphi = -0,23\theta^{1,33}, \text{ eV}. \quad (1.6)$$

## 1.9 Dependence of work function from the crystal structure of the surface

Consider the question about the bond of the electrons work function with the electronic structure of metals. The work function of electrons, as one of the fundamental solid's characteristics correlated with the atomic volume, compressibility factor, the crystal lattice energy, surface tension, atomic radius [135]. This shows that electrons work function reflects to some extent the power of the interatomic bond. Physical constants by which WF is expressed, determined by spatial directions of the not paired  $d$ - and

*p*-electrons, and extreme values of these characteristics correspond to the density extreme values of the not paired electrons in the outer *d*- and *p*-levels. The nature of WF reduce with the appearance defects in the crystal structure due to the plastic deformation has been investigated in the works of L. Andreev and Palige, V. S. Kortow, R. I. Mintz et all. Even the early work suggests that the WF change is due to the advent as on the metal surface and as in volume during the deformation of a significant defects number of the crystal structure, leading to local dilatation of the crystal lattice. Dilated phenomena in lattice leads to a change the average by volume sizes of the unit cell and to significant local changes of the unit cell parameters. These changes, in turn, are the cause of changes in the distribution of the electron states density due to the Fermi energy level of bias. The Fermi energy increase causes a WF decrease. The integral effect of these defects occurs at the Fermi level when structure crystal defects is appeared in the metal volume, which leads to uniform WF reduction for the entire metal surface (retaining crystallographic anisotropy). This decrease is the backdrop for local WF reduction in the immediate vicinity of the formed defects on the surface and in the subsurface. V. S. Kortov informs [136] about the discovery the greatest WF decrease in alloys with low stacking fault energy. Experiments were performed on a polycrystalline zinc of commercial purity after annealing in a furnace with an inert atmosphere at 160 °C. Metallographic studies showed that such samples the twinning is the most main mechanism of deformation in tension at a rate of 1.0–2.5 mm/min. doubles formation occurred in an avalanche that was fixed by voltage jump, corresponding to the instantaneous disordering of the sample material. Power jumps were accompanied by a sharp WF decrease.

Another mechanism of the WF change on the deformed metal surface is considered in work [137]. It is assumed that the non-uniformity of plastic deformation may be the cause between neighboring areas of the crystal lattice, spaced at the distance about 10 angstroms, contact potential difference is to 0.1–0.4 V. This will lead to the emergence of the electric field density of about  $10^6$  V/cm.

The WF surface distribution of the germanium and silicon samples was investigated in work [138]. It was assumed that the

grain boundaries consist of clusters of edge dislocations and due to the existence of dislocations in dangling bonds, they must act as acceptors. And the minima on WF curve distribution were observed only after three hours of the samples processing in a vacuum  $\geq 10^{-6}$  torr at 700 °C. Yield slip planes on the surface was determined by a chemical etching in the solutions in 30% HF + 70% HNO<sub>3</sub> for *n* – Ge; 40% HF + 30% HNO<sub>3</sub> + 30% CH<sub>3</sub>COOH for the *p* – Si.

The author assumes that all the broken bonds of dislocations are found near the surface. Therefore, the region near the dislocation is positively charged. The positive surface charge and negative charge of the dislocation changes dipole moment on the surface and as a result WF decreases. Changes are possible in the power states of the oxide layer. The linear WF increase was noticed from the middle to the sample's edges, which could be explained by the distribution gradient of impurities and dislocations caused by the heat treatment.

One way to measure WF changes is the determination of the energetic position of the onset of the secondary electron energy distribution. The WF measurements ionic sputtering (Ar) of the set-multilayer surface Ni – Cr was noticed in the work [139]. Authors obtain periodic relief of the WF changes according to the thickness of sputtered Ni or Cr layer. Has been shown that the sensitivity of the WF changes with depth not less than 30 angstroms. Based on these data one can assume that the WF formation is determined by subsurface layer with thickness of <30 angstroms.

The influence of mechanical stress on the contact potential difference of several metals Al, Cu, Au, steel, brass was investigated by Kelvin method in the work [140]. It is shown that the load application leads to displacement of the surface charge in a positive direction. The comparison electrode was made of brass, the vibrating electrode oscillation frequency was 150 Hz. The stresses applied to the samples were limited to a few percent of the elastic yield limit. Before the measurements the samples were washed in alcohol. Loading and unloading of samples was carried out in the range of 65.5–131 kg/cm<sup>2</sup> using a press through a lead gasket.

In the work [141] WF measurements were carried out depending on number of atomic steps on the surfaces (111) for Pt and Au, and also on the surface (110) for W. In all cases there was a WF linear

decrease with increasing density of the atomic steps, and also it has been revealed that WF depend on the orientation of the stairs. The authors suggested that the observed WF change is due to surface electric dipoles. Samples of Pt and Au were prepared by MRC monocrystal 6 mm in diameter (zone melting). Cylindrical spark samples were prepared by cutting. Samples with different density of atomic steps were prepared in different crystallographic directions.

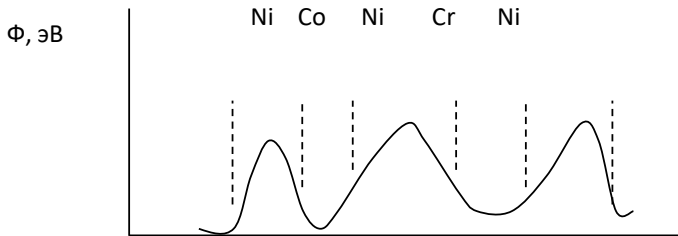


**Figure 1.3** – Periodic relief of changes in WF depending on the thickness of the deposited film

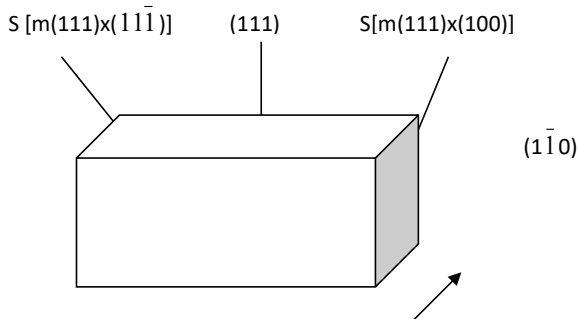


**Figure 1.4** – Samples with different density of atomic steps in different crystallographic directions

And the radius of the cylindrical surface is approximately 20 mm. Samples were annealed to remove carbon in an oxygen atmosphere at 5.10 Pa, 900 °C for Pt and 700 °C for Au during 10 hours. Surface cleaning was carried out by ion bombardment of Ar. Local surface WF changes were obtained from the corresponding changes in the low-energy secondary electrons boundaries. It is shown that the

density of monatomic steps depends on the cut angle of the single crystal relative to considered crystal plane.

Since the terraces divided by monoatomic steps, the terraces width decreases with the increase of the slope cut angle and the density steps is increased accordingly. It has been shown that the density of atomic steps ranges from zero to  $3.5 \times 10^6 \text{ cm}^{-1}$ . Terrace considered as dangling atomic planes, like an analog of dislocations to the surface. In the case where the polycrystal deformation is explored you must keep in mind the deformation of the individual single-crystal grains and grain boundaries form. One of the main results of is that a different WF dependence on the density of steps for different metals and different crystallographic orientations of the same metal (changing the angle of inclination of the graph).

Another important result is the discovery of a WF linear dependence on the density of atomic steps. To change the WF on the unit length you can obtain by:

$$\Delta\varphi = 300 \times 10^{-8} 4\pi\mu, \quad (1.7)$$

where  $n$  is a number of steps to 1 cm;  $\mu$  is a dipole moment of 1 cm (Debye).

It is known that the redistribution of charge at the metal-medium caused by adsorption depends essentially on the orientation of the metallic edges. In [142, 143] the framework of the microscopic approach a quantitative assessment of the impact of adsorption from the gas phase on the orientation dependence of the surface energy and the electron work function are carried out.

It is shown that the adsorbate leads to a noticeable anisotropy smoothing of the surface energy and a change in the orientation dependence of WF. The most dramatic change of the surface energy and WF in the presence of the adsorbate appear on loose edges.

## 1.10 Change in work function during tensile test in vacuum

Regularity of WF change by plastic deformation of metals studied in [144, 145]. The value of these investigations consists in carrying out of the contact potential difference measurements during the deformation of metals at ultrahigh vacuum ( $10^{-10}$  millimeters of mercury).

The study was exposed to molybdenum and tantalum filament. Before a tap device was subjected to a long workout at 400...450 °C in a vacuum  $10^{-5}$ – $10^{-6}$  millimeters of mercury, the samples were outgassed by direct current heating or electron bombardment. During the tapping the sample was in the heated state.

In the process of producing ultra-vacuum the sample was periodically heated by electric current to 2,100...2,200 °C. It was found that the sample was heated to 2,200 °C in the first hours of the pumping after the tap led to the loss of vacuum in the 1–1.5 and about one-temporarily observed decrease WF to 1,000 mV. After stopping the heating of the sample WF is increased, asymptotically approaching some constant value for 1 hour. As the pump and increase the number of periodic vacuum annealing, and reduce the effects of WF changes were reduced to nothing.

The authors suggest that the observed phenomenon is due to the adsorption and absorption of residual gases. Tensile tests have shown that under the deformation 3–5% WF decrease is occurred on 15–20 mV.

The work [146] is devoted to study the intensity of emission and exoemission from deformation of the commercially pure metals Cu and Al. On the samples after annealing exoemission measurement and WF were performed at the same time under tension of the samples in a vacuum  $2 \times 10^{-6}$  millimeters of mercury or better. Art. community nature of the process is indicated at a strain rate of 2.5 mm/min: the growth of emission current corresponds to a WF decrease. After deformation the curves are extreme points and there is a reverse process: the emission current decreases and WF increases. Extreme points for Cu are shifted relative to the end of the deformation in the direction of the big times and have no Al. Moreover, deformation and relaxation times measured value is several minutes.

## 1.11 Work function of electrons depending on the surface processing

Considerable experimental material about metal deformation influence on WF is presented in the work [136]. In the work [147] WF measurements on samples of pure aluminum (99.999%), titanium, and tungsten are done. Measurements were made from surface of pre-deformed samples in air, and places in the vacuum camera. Measurements results are evidence of WF increasing in pre-deformed samples. Heating influence on WF changing of aluminum samples is discussed in the work [148]. After aluminum deformation in vacuum samples were heated to 400 °C. WF increased up to 270 °C and then decreased, but more slowly. The sample before deformation was annealed in vacuum on 450 °C. WF spreading on certain surfaces areas was studied. It was shown that the degree of heterogeneity is maximal when sample deformation in vacuum and it decreases when annealing. Air deformation reduces the degree of heterogeneity because of oxidation of deformed surface. Complicated WF changing when heating in a range from 20 to 450 °C of copper monocrystal is discussed in [16]. Sample surface under consideration had misalignment [110] no more than 7°. Deformation was made by rolling in the direction [112]. It was developed that in a range from 40 °C to 120 °C WF is increasing, reaches maximum, then decreases dramatically and reached minimum when 180...250 °C. With temperature increase, WF is increasing slowly too. When reheating described kinetics is less expressed. Slight decrease of WF goes after low temperature maximum, its value than stabilizes on the same level. With deformation decrease parametric characteristics of the curve of WF thermal dependence – starting value when room temperature and minimal value. Both parameters decrease with deformation growth. It was also shown that for copper monocrystals deformed on 37% a thermal interval of process connected with structural rebuilding is 180...200 °C. Thus, WF changing while annealing of deformed copper monocrystals considerably depends on structural transformations. It's possible that on first stages of recrystallization characterized by initiation

of grain boundaries and increasing of their mobility, WF decreases, and as recrystallization is finishing, it increasing. The first WF growth while heating is apparently connected with desorption processes, water desorption, in general.

## 1.12 A surface in the field of elastic deformations

Heterogeneity of distribution of tension with elastic anisotropy in materials creates premises for effects of origin of destructions. In pilot studies of elastic properties of metals, it must be kept in mind that Hooke's law is only the first approach at the description of physical properties of real materials at an initial stage of their loading. Actually deviations from Hooke's law which are found in property of imperfect elasticity [190] take place. Properties of imperfect elasticity are shown in a number of the phenomena arising when loading crystalline solids to an elasticity limit. These phenomena are manifestation of a relaxation which decides by a deviation from internal balance when loading a body on final speed. One of manifestations of imperfect elasticity is the elastic after-effect of metals which is shown over time in additional deformation of a body under the influence of tension.

Residual (irreversible) deformations of solids are found at very small tension in the field of the deformations  $10^{-6}$  which are traditionally referred in literature to elastic [149]. Inelastic deformations are shown in this area at all types of the solids (mono- and polycrystals of flexible and fragile materials, amorphous solids) which are strongly differing by the nature and physic mechanical properties. These deformations can be referred to a special type of inelastic deformations – quasimicroplastic, and effect of quasimicroplasticity – to fundamental property of solids.

Research of WF change in the field of elastic deformation of metals devoted not so much work. In work [150] described an experiment in which was found a small radial potential difference in the rapidly rotating rotor made of titanium, aluminum and stainless steel in air at a pressure of between  $133.3 \times 10^{-4}$  and

$133.3 \times 10^{-6}$  Pa. The cross-shaped rotor has a diameter of 15 cm and 2 cm in thickness. Width of bands was 2 cm. It was found that the electric potential at a point on the surface of the rotor with the radius remains constant for a long time at constant rotor speed and temperature. If the rotor speed is increased, the electric potential at the periphery becomes positive compared to the area close to the axis. After returning to the original speed, it was restored such as the corresponding speed of the surface potential. Radial volume potential was approximately proportional to the square of the speed of the rotor. In some experiments with the plastic deformation of the rotor was observed the change of the potential at the direction positive change. To analyze this experiment in terms of changes in the work function of electrons is difficult. First of all, it is causing some confusion circuit potential measurements shown in Figure 1.5.

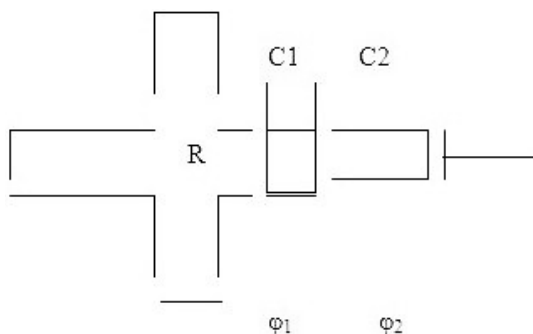


**Figure 1.5** – Scheme of measurement potentials on a rotating rotor

Capacitor C2 fixed the change in potential from the end of the working part of the rotor, i. e. which operated from the surface with compressive stress. Secondly the authors [151] do not discuss and probably do not take into account changes in value of the clearance between the plates of the capacitor C2 at rotation of the rotor. If still trust the experimental data of, the observed potential shift in a positive direction indicates the WF decrease in the action of compressive stresses on the surface of the metal.

The ability to use the changes of electric potential for the registration of deformation of metals is considered in [152]. The

authors measured the potential difference between the uniaxially stretchable sample of aluminum D16AT ( $20 \times 8 \times 150 \text{ mm}^3$ ) and the copper probe (diameter – 20 mm, height – 5 mm). The thickness of the dielectric laying equal to 0.02 mm. In Figure 1.6 shows a diagram of the experiment and received data. Registration begins immediately after the loading of sample, as voltmeter readings fell within a few minutes. It was found that with increasing tensile stress the potential of the sample is increasing (area of the elastic deformation). It was noted that the evidences are fixed for a few minutes. Apparently, the latter due to the existence of the contact potential difference between the sample and the standard.

For relaxation of the electron subsystem of the metal must be a certain time to equalize the chemical potential. In the considered experimental system Figure 1.6, a sample from aluminum to copper on attitude positively charged. Therefore, when calibrating the author filed in the sample received a negative potential and a linear dependence of the potential of the sample from the probe potential. Then in a test specimen in tension it has been found that the mechanical stress applied analogously occurrence of a negative charge on the sample. Thus, we can conclude that the tensile stress in the elastic region of deformation lead to a shift in the negative potential of the sample area or increase WF. The measurements were performed using an electrometer voltmeter VK2-16. It was found that the registration of the results immediately after loading the sample and in a few minutes later, giving different potential values. If the unloading of the sample was carried out after the establishment of indications of the voltmeter, the probe potential is much more positive. This experiment suggests that the potential of the sample increases with increasing tensile stress. Since the negative probe potential is obvious that with increasing tensile stress, the sample becomes more and more positively charged. Apparently, this indicates the occurrence of plastic deformation in the metal surface layer.

In work [139] studied the intensity of EEE, micro hardness and intensity of infrared radiation from the elastic stresses during deformation alloys VT-9 and 30HGSNL. A linear dependence of

these parameters on the elastic stress. Also, there was an increase in tension and WF decrease in compression.

The review [153] is devoted to the study of the formation of a potential gradient on the surface of metals under the action of a self-weight on the metal.

First calculations performed Schiff and Barnhill shown that in a metal pipe by its own weight occurs electrostatic field equal  $mg/e$ . Moreover, it is directed down to the ground surface. It is known that in a metal the electrons occupy all the energy levels up to the Fermi energy. The deformation of the metal changes the value Fermi energy, if there is a deformation gradient, there is a gradient of the Fermi energy. The electrons flow from a region of higher to lower energy Fermi. A consequence of this process is the formation of an electric field which reduces the electron current generated by the deformation compensates the effect of the gradient. In [154] reviewed a possible mechanism for the change in the Fermi energy by deformation.

It uses the simplest model in which the metal is a degenerate electron gas in a uniform field of positive charge. Since the relative change in volume during deformation is equal

$$\frac{dV}{V} = -\frac{dn}{n}, \quad (1.8)$$

the derivative of the Fermi energy of deformation is equal to

$$\frac{d\mu}{dV/V} = -\frac{2}{3}\mu. \quad (1.9)$$

There is  $n$  – electron concentration. In general, the Fermi energy changes by changing the crystal field in the deformation. If we denote by  $u_{ik}$  the strain tensor, then the derivative

$$\overline{\lambda}_{ik} = \frac{\partial\mu}{\partial u_{ik}} \quad (1.10)$$

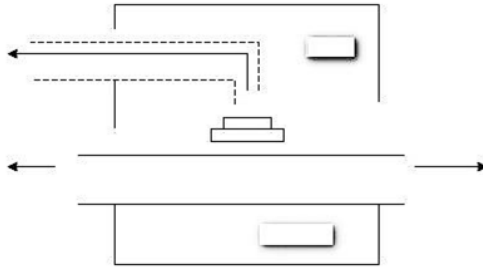
in absolute value of the order of the Fermi energy,  $\lambda_{ik}$  – deformation potential, averaged over the Fermi surface.

In conditions of thermodynamic equilibrium throughout the metal has to be constant, the electrochemical potential of electrons

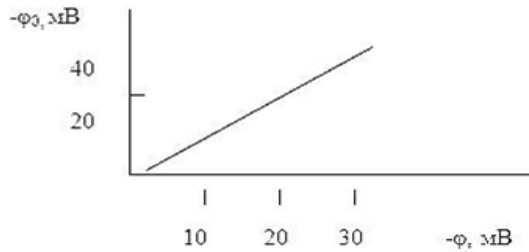
equal to the sum of the chemical potential and the potential energy in the electric and gravitational fields

$$\mu(\vec{r}) - e\varphi_i(\vec{r}) - m\vec{g}\vec{r} = const. \quad (1.11)$$

Screen



Calibration supply potential on the sample



Measurement

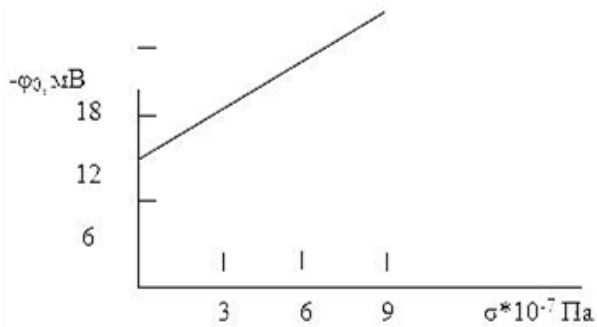


**Figure 1.6** – Scheme of the experiment and the results of measurements

Here  $\phi$  – the potential of a macroscopic electric field within the metal. From the equilibrium condition it follows that the field inside the metal is equal to

$$E_i = -grad\phi_i = \frac{1}{2}(mg - grad\mu). \quad (1.12)$$

Direct the  $OZ$  axis opposite compressive force of gravity, then the field produced by the same strain

$$-\frac{1}{e} \frac{d\mu}{dz} = -\frac{1}{e} \overline{\lambda_{ik}} \frac{\partial \mu}{\partial z} ik. \quad (1.13)$$

In the elastic isotropic metal in the gravity field

$$\frac{\partial u_{zz}}{\partial z} = \frac{\rho g}{E_y}, \quad \frac{\partial u_{xx}}{\partial z} = \frac{\partial u_{yy}}{\partial z} = -\frac{\sigma}{E_y} \rho g, \quad (1.14)$$

where  $\rho$  – density;  $E_y$  – Young’s modulus;  $\sigma$  – Poisson’s ratio.

Let’s move on to finding the electric field outside the metal. Let the potential of the electric field is outside the metal. The difference  $\phi_e - \phi_i$  – equal to the potential jump on the surface of the double layer. This potential jump can be changed by adsorption of molecules, changing the filling of surface electronic states.

If the density of the double layer was constant, the change in the work function  $\Delta W$  would be equal to the change of the Fermi energy with opposite sign. In general

$$\Delta W = -\Delta\mu - e\Delta(\phi_e - \phi_i). \quad (1.15)$$

In a state of thermodynamic equilibrium along the metal surface must be constant and the work function of the amount of the negative of the potential energy of the electron:

$$W + e\phi_e(\vec{r}) + m\vec{g}\vec{r} = const. \quad (1.16)$$

Then the field without metal is equal to

$$\vec{E}_e = -grad\phi_e = \frac{m\vec{g}}{e} + \frac{1}{e} gradW. \quad (1.17)$$

To assess the field  $grad W/e$  metal is necessary to know how the deformation at the surface dipole moment. It is known that the

contact fields near the interfaces between the various bodies close to the edges of the crystals whose faces have different WF, typically compensated fields of adsorbed ions, the redistribution of electrons in the surface states.

By dynamic capacitor is measured by the work function of metals and alloys at a uniform tension and compression. In all cases, the elastic range WF reduced compressive and tensile growing by about  $(10^{-6}-10^{-5})$  eV per  $\text{kg}/\text{cm}^2$ . This means that WF change of the same order as the change in the Fermi energy in the volume of metal.

In work [155] studied the effect of the deformation curve at WF (the method of Anderson), the Si (111) doped with Al. It is shown that the application of mechanical stress to  $310^8$  Pa causes an increase WF 0.52 eV, and after unloading WF remains at 0.12 eV higher than in the initial state. The change in the interplanar spacing at the surface reaches 2%.

The author of work [156] argues that the character of the WF on the degree of deformation for all metals is the same: there is a slight increase in the WF in the elastic region, and then there is a rapid decrease in WF at a stage of strong hardening, and when approaching a stage of dynamic recovery rate of change of WF decreases.

As a result of experimental studies of the effect of uniaxial stretching of metals and alloys WF in work [157], it was found that the strain variation WF near the elastic deformation region is positive and negative in the plastic. Effect of elastic stress appears to change the Fermi energy, and as a consequence of a change in WF. Lowering the electrochemical potential due to dilatation of the sample leads to the growth of WF. Interestingly, the growth of WF was also observed in the process of martensitic transformations that occur with a change in volume. The magnitude of growth WF near the elastic deformation region varies between 1–5 mV.

### **1.13 Changing work function of electrons during the contact action on a material of the surface layer**

Processes of metal details producing and processing are considerably connected with a surface layer influence on a material. That is why contact action of metals and alloys laws studying is of both science and practical interest.

A factual form of the hard phase subsurface field depends on the real crystal structure defined by lattice defects. In its turn, defect structure of conjugate crystal lattices while friction depends on surface energy value on the phase division border. Energy changes that occur simultaneously with pressure of electron gases on the metals division border from each side can be valued. It is said in the work that in the metal with smaller chemical potential, the effect of surface layer plasticizing should be expressed stronger.

The character of surface contact interaction is connected with their energetic state. A force field of metals spreads over the surface on the distance less than 1 mkm and can be fully pictured by the boundary lubricant layer. It is important to take into account a kish effect. Screening electromagnetic fields beamed by solid bodies, oxide films reduce the noncontact adhesion and have a lubrication function in such a way. Compering with forces of small action radius on real contact areas, noncontact adhesion forces are long-distance and characterize condensed phases attraction on the surface areas belonged to difference of nominal and factual contact surfaces. The same oxides can turn out to be semiconductors with the bigger number of surface conditions. Besides, they can be of such a type that the film contact adhesion with a metal (or film) will be complicated enough.

In the metal with smaller WF, surface layer plasticization is exercised easiest. Surface energy decrease results in dislocation mobility increase that causes plastic flow acceleration in the surface layer. It is discovered that a sample material is protected from fretting corrosion if it contacts with a material that has more negative electric potential than it has.

Electrostatic condition of contact zone areas is continuously changing (while friction). Surfaces, free energy of which increased

as a result of interaction, will wish returning to the state of the biggest passivity. Both, friction factors and relation between them depend on how quickly friction mechanical activation can be taken off and what the character of physical-chemical processes run during this. The formula used for estimating the surface energy is

$$\sigma = \frac{\varphi z}{1.885 \times R^2 \times 10^{-3}}, \quad (1.18)$$

where  $z$  – number of free electrons per atom,  $R$  – atomic radius, angstrom. WF is defined on the base of contact potential difference (CPD) measurements relative to the metal-sample.

It was found that surface conditioning of a set of metals (brass, aluminum, steel) with flint paper and friction with no lubrication lead to evanescence of WF. WF restoration comes in 10–15 days. In boundary lubrication conditions while friction (friction stripe) in process of time WF increases and overtops the base value before the friction test. It is possible to explain such an effect of WF growth by formation in condition of friction with lubrication the surface strongly active to environment. Due to lubrication more regular plastic deformation (covers more surface atoms) and the oxidation process suitable to the new surface condition occur. In this case, density of oxidized atoms increases.

The contact interaction mechanism is considerably defined by presence of crystal lattice defects [158]. For seizure films on surfaces of the frictional metals should be damaged by plastic flow, and juvenile surfaces formed should be brought together on the distance of interatomic forces action. Under outer load in the contact zone dislocation centers occur necessarily, and intensive increase of vacancy concentration and embedded atoms happens. In active centers zones by the vacancy mechanism, diffusion between contact metals with metal connections forming is realized. In this case, the completion of electron levels of atoms of seized metals in energy profitable correlation.

The work [159] is devoted to studying of physical-chemical facts in the micro- surface layer of metals. The least surface wear of details in contact with liquid lubrication between them is obtained if linked materials have small transmission of nonlocalized electrons

from one element to another, and have big static weight of atoms with stable configurations. If two details have metallic contact, the least surface wear should be obtained by forming “electron lubrication” between details in contact because of using materials with enhanced donor strength (the layer of repelling electrons).

### 1.14 Electron work function dependence on a deformation speed

The measurements, made on different extension rates: 6.3; 2.5; 1.01 mm/min show that increasing of the deformation rate goes with a great rate of WF changing. Authors make a conclusion about the defining influence of structural changes in the surface layer of the malformed metal on the WF quantity, because numerous experiments are indicative of WF interconnection with the degree and character of the deformation made on different conditions, including an ultra-high vacuum [160]. The blocks and grains borders, micro cracks, dislocations and other defects contain the definite charges. It is known that a charge presence changes the surface tension and significantly influence on mechanical properties [161, 162]. A charge cluster should define the connection of cloud of dirt with dislocation, diffusion on short circuit lines, processes of nucleation during new phase crystallization, and influence on an adsorption process. Simple calculation of WF dimensional dependence [163] leads to the formula

$$\Delta\Phi = \frac{\sigma}{\rho} \left( \frac{3}{\pi} \right)^{1/3}, \quad (1.19)$$

where  $\sigma$  – surface tension;  $r$  – radius of a sphere with a similar ratio of surface and volume increment ( $a=2r$ ,  $a$  – a cube edge);  $\rho$  – density of electrons. Using a formula for surface energy like this

$$\sigma = \frac{h^2 \pi b^4}{128m} \rho^{4/9}; \quad (b = \left(\frac{3}{\pi}\right)^{1/3}), \quad (1.20)$$

we can get

$$\Delta\Phi = -\frac{e^2}{r} \left( \frac{3.7}{\Delta} - 0.5 \right), \quad (1.21)$$

where  $\Delta$  – the relation of a lattice period to the radius of the first Bohr orbit. WF measurement subject to deformation of monocrystalline molybdenic fibers with a 1 mm/min speed and vacuum  $(5-2) \times 10^{-8}$  millimeters of mercury show that a plastic deformation cause decreasing of WF samples. The authors [164] note that analogical WF dependence on the deformation also happen in a low vacuum ( $10^{-4}-10^{-5}$ ) millimeters of mercury, and for oxidized samples. It is important that aside of a vacuum, WF changing value corresponded to the definite achieved deformation maintains constant for two and more hours after the deformation is done. It is noted that in addition to a dimensional effect of WF changing, films properties changing, influence of surface imperfection on a surface potential jump value, caused by smearing of electrons wave function out of a metal, and changing the conditions of gas molecules adsorption connected with surface micro cracks and an asperities appearance.

### 1.15 Changes in the metal structure under the influence of ultraviolet and X-ray radiation

The work [165] is devoted to the study of the energetic effect on metals. The effect of the emission of hydrogen or argon tubes was studied – the vacuum ultraviolet with a flux density of  $10^{17} \text{ cm}^{-2} \times \text{s}^{-1}$ , and an energy of about 10 eV. When metal is radiated with vacuum ultraviolet, defects appearing in a thin surface oxide layer on subthreshold mechanism can penetrate even at room temperature at a sufficiently great depth, causing a change in the metal structure of submicron and micron thick. Similarly, during the growth of the oxide film on the metal surface subtraction loops are formed in its volume, growing at the expense of vacancies coming from the section “oxide – metal”. At the initial stage the growth of the oxide film is accompanied by the formation of the Fresnel pairs. Own shifted atoms in the electrostatic potential field migrate to the

surface, and the vacancies along the dislocation lines – inside the sample, causing a climb of dislocations and forming dislocation subtraction loops.

In the work [166] for epitaxial film of Al and Ti was discovered the effect of changes in the lattice parameters and defect structure under the influence of long-term (250 hours) X-ray radiation of copper cathode. Tube mode:  $U=20$  kV,  $I=20$  mA, the flux density of quanta –  $10^{13}$   $\text{cm}^{-2} \times \text{c}^{-1}$ . The stimulated radiation annealing of structural defects was observed. The authors suggest that the decreasing in the period of lattice has vacancy nature. Whereas, the formation of vacancies occurs in the impurities and dislocation defects on the mechanism similar to alkali halide crystals.

Assuming that the boundary field strength depends only on the concentration of chemisorbed particles, and that the structural and electrostatic members virtually don't change, we obtain for the WF difference on the free and occupied by a chemisorbed particle surface

$$\Delta\varphi = \varphi_a - \varphi_0 = \frac{kT}{e} \ln \frac{n^{(R)}}{n^{(0)}} - aE, \quad (1.22)$$

after substitution we obtain

$$\Delta\varphi = -\frac{2\pi e}{\varepsilon} \left( \frac{n^{(\sigma)}}{n^{(0)}} \right)^2 + 2an^{(\sigma)}. \quad (1.23)$$

The corresponding formula for the  $p$ -type oxide can be obtained by assuming that the number of electrons removed from the surface of the oxide, are equivalent to the formation of holes on the surface

$$\Delta\varphi = a \frac{4\pi e}{\varepsilon} n^{(\sigma)} - \frac{kT}{e} \ln \left[ \frac{2\pi e}{\varepsilon} \frac{(n^{(\sigma)})^2}{n^{(0)}} \frac{1}{V} \right], \quad (1.24)$$

$V$  is chemisorbed volume. WF must grow, if the electron is transferred to the chemisorbed gas during the chemisorption. In case of  $n$ -type adsorbent, increasing of WF is described by a quadratic and in the case of  $p$ -type adsorbent – by complex linear-logarithmic dependence on the surface concentration of the chemisorbed gas.

## 2 WORK FUNCTION FOR THE DEFORMED METALS

### 2.1 Work function for fatigue tested metals

For metals two subsystems are known to be typical. One of them is the ionic lattice and the other consists of the gas of free electrons. The first subsystem is considered to be relatively massive and slow and the second one is regarded as light and fast. Interactions between these two subsystems under an effect of plastic strain are of great interest.

The work function of metals is defined as a difference between the electron barrier height on the metal-vacuum interface and the Fermi energy. Thus, WF is related to properties of the electron gas. Stresses applied to materials have an effect on ionic lattice. Interaction between the electronic and ionic subsystems of metals results in a change of WF [167–169]. In previous works it was discovered that WF actually depends upon plastic strain as well as upon cyclic stresses [170–173].

Fatigue of materials is known to be a very dangerous type of fracture. Any methods which allow to forecast the fatigue cracks formation are important. On the other hand, the plastic deformation events are known to precede the fatigue fracture.

Our aim was to investigate the effect of the fatigue tests on the work function of metals. This paper describes data of nondestructive measurements as a study of processes which had been developed before the fatigue crack origination.

Materials under investigation were aluminum and two heat-resistant iron-based steels. The first steel denoted as A contained (weight %) 0.15 C; 16.0 Cr; 2.0 Ni; 1.5 Mo; 0.7 W; 0.3 Nb; 0.2 V; 0.03 N. Composition of steel B was 0.15 C; 15.8 Cr; 2.1 Ni; 1.0 Mo; 0.07 N.

The work function was measured by Kelvin dynamic capacitor method [174]. As it is known the surface of specimen and an oscillating electrode form the capacitor of alternating voltage.

Investigator should compensate the signal of unbalance. The voltage of compensation is equal to the contact voltage difference between the specimen and material of the standard electrode. As the WF of the standard material is known the WF of the specimen can be calculated proceed from this data. In our work this method was improved and automated. Details of improvement will be reported elsewhere.

Fig. 2.1 represents the functional scheme of the experimental set-up. It includes a portable piezoelectrical source of mechanical vibrations BQ1 and set of measuring equipment. A computer D1 is used for the process control and for the data work-up. The specimen 2 was fastened in a cantilever geometry and was subjected to the forced mechanical oscillations. Flat specimens shaped as single shovel with narrow working part were used. The examined surface formed the capacitor with the electrode 3. It was made as a golden probe whose diameter was equal to 1.4 mm. The amplitude of oscillations of the specimen was measured with the aid of microscope 1. An equipotential electrical screen 8 was used to decrease stray capacitance. The specimen was placed between dielectrical plates 7. At the desk 9 of the mechanical vibration source 9 a clamp 5 was fastened. The specimen 2 was fixed with a bolt 6. Fatigue tests were carried out by means of the piezoelectrical source of mechanical oscillations BQ1. The amplitude of the desk was regulated with amplifier G2.

The frequency of oscillations of the standard electrode 3 was set by generator G1 and was controlled by the frequency measure device. The signal of decompensation passed through the amplifier A4, which switched the electrometer A4.1, the synchronous detector U3, the integrator A4.2 and the analog-digital converter U4. The analog-digital converter U4 was controlled by the personal computer and formed the signal of compensation.

Flat specimens of  $3.0 \times 11.5 \times 101.0$  mm<sup>3</sup> dimensions with a selected working part were used. The test frequency was equal to 5,881 rad/s for Al and 2,338 rad/s for steels.

The WF was measured between bending cycles, i. e. before, during and after fatigue tests. No less than 15 specimens of steels and 10 specimens of Al were tested. The measurements were made

along 6 longitudinal lines, which were parallel to the specimen axis. The experimental points were located every other 1 mm. Thus 40 measurement points were situated at the distance of 40 mm on the working part of the specimen. Three measurements per position were performed. The average result was used. The fluctuations, which were caused with accidental errors, were less than 5 meV. The WF curves as the plot of distance as well as the plot of the cycle number were repeatable. The variation of the WF before the fatigue testing was no more than 5 meV. The accuracy of the WF measurement was  $\pm 2.0$  meV.

In a number of cases an ultraviolet radiation of specimens was applied in order to avoid gas adsorption. A source of radiation EL1 (Fig. 2.1) was used. We have investigated preliminary an influence of surface irradiation upon the adsorption – desorption equilibrium [175, 176]. It was shown that the ultraviolet rays seem to create more high energetic surface levels and the effect of adsorption on WF measuring decreases. Oxidation and gas adsorption have an influence on the WF quantity. However, it is necessary to take into account that our measurements were relative. We mean that the measurements of the WF difference were performed before fatigue and after fatigue. There are all the grounds to be convinced that the observed changes of WF were due to effects of deformations and owing to structure alternations. According to our experience a varying state of oxidation can only move curves of WF along OY as a whole. A difference in WF because of strain was the same.

Specimens after fatigue tests were investigated with X-ray method. The  $K_{\beta}$  – radiation from tube with Co-cathode was used. Harmonic analysis of the X-ray reflections was applied [177]. Reflexes of (200) and (400) for Al were recorded and dependences of intensity  $I(2\theta)$  were obtained ( $2\theta$  is Bragg's angle). An annealed specimen was used as a standard. Every curve was divided in 50 intervals and was expanded into Fourier series. Coefficients of Fourier were calculated. The internal stresses  $\epsilon$  and the sub grain dimensions  $D$  of materials under investigation were measured. Proceed from these data the dislocation density  $\rho$  was calculated in conformity with equation [178]

$$\rho = 4 \times \pi^2 \times \varepsilon^2 / b^2 n, \quad (2.1)$$

where  $b$  is Burger's vector;  $n$  is number of dislocations in pile-up;  $n \approx 100$  was assumed.

During the fatigue tests visible changes of the surface potential relief came about. The work function was found to decrease at the very place of the specimen where the crack would be formed, long before its origination. For example, WF started falling only in 5–10% of the common service life of Al specimens.

In Fig. 2.2 the typical increment of WF on surface of the heat-resistant steel A is plotted against the number of cycles. The decrease of WF occurs directly above the future crack. Obviously the observed falling of WF reflects some structural changes of the specimen during stress cycling, especially nearby the surface.

In early stages of fatigue tests the increment of WF was found to have cyclic variations with  $N$  (Fig. 2.3), as if it was reversible. Intervals in tests were done between measurements at every point. One can see that every subsequent maximum of WF is some less than the former one. There are grounds to suppose that up to certain time defects accumulation in crystal lattice and relaxation change each other.

The typical WF distribution on the steel B surface is shown in Fig. 2.4. WF decreased at the same areas where applied stresses were larger. The cross-section of the specimen is minimal at the point of 17 mm. A localization of deformation processes is obvious at the distance of 16–27 mm from the left.

The method of WF measurements was shown to have prognosis possibilities as to fatigue cracks origination. This method can be applied to study the fatigue phenomena.

The results that have been obtained make it possible to assume the existence of two stages of structural changes in fatigue-tested metals:

1. Stage of reversible structural alternations when WF at a given point of specimen decreases and increases periodically.
2. Stage of irreversible changes in the surface layer when WF decreases monotonically owing to generation of charged steps. Quantity of  $\Delta\Phi$  depends upon material under investigation.

If a metal specimen is subjected to alternating stresses the generation of dislocations is known to occur. There is a threshold stress for this process to begin

$$\tau_s = \mu_s \times b \times \sqrt{n \times \rho_0} / (2 \times \pi), \quad (2.2)$$

where  $\tau_s$  is the shear modulus;  $b$  is Burgers' vector;  $n$  is the number of dislocations in the pile-up;  $\rho_0$  is an initial dislocation density.

Dislocations, which have been generated, move along the intersected slip planes. Generation of dislocations nearby surface, as well as their breaking through results in emergence of steps on the surface. These steps are known to have dipole moments [179]. Negative charges are accumulated between surface atoms. Dipoles contribution tends to decrease the work function.

The rate of dislocation multiplication is known to be equal to [180]

$$\frac{d\rho}{dt} = \delta \times \rho \times V, \quad (2.3)$$

where  $\rho$  is the dislocation density;  $V$  is the dislocation velocity and  $\delta$  is the coefficient of proportionality (i. e. the factor of the dislocation multiplication). The authors developed following equation for the dislocation density increment during fatigue tests:

$$\ln \frac{\rho}{\rho_0} = \delta \times V_0 \exp\left(-\frac{U_0 + b^3 \times \tau_s}{k \times T}\right) \times \int_{t_{so}}^{t_{sf}} \exp\left(\frac{b^3 \times \tau_m \times \sin(\omega \times t)}{k \times T}\right) \times dt, \quad (2.4)$$

where  $V_0$  is a pre-exponential multiplier;  $U_0$  is the activation energy for dislocation motion;  $\tau_m \times \sin(\omega \times t)$  is alternating stress;  $t_{so}$  and  $t_{sf}$  are the start and the final times of the dislocation motion within the half-cycle accordingly;  $k$  is Boltzmann constant;  $T$  is temperature.

Equation (2.4) was solved numerically. The dislocation density in a surface layer was calculated for every cycle. Initial dislocation density in Al was equal to  $\rho_0 = 3.75 \times 10^7 \text{ cm}^{-2}$ . The rate of the dislocation multiplication was chosen to be equal to  $d\rho/dN = 37.5 \text{ cm}^{-2} \times \text{cycle}^{-1}$ . Criteria for choice of these figures were experimental data [181] and the agreement between our experimental and calculated data of  $\rho(N)$ . If these values were available there was no need to know constants  $\sigma$ ,

$V_0$  and  $U_0$ . The following reasonable values of other constants were chosen (Al):  $\tau_s=2.70 \times 10^4$  MPa;  $b=2.86 \times 10^{-10}$  m;  $\tau_m=82$  MPa;  $\omega=5.88 \times 10^3$  rad/s;  $T=300$  °K.

The results of calculations of dislocation density in Al are shown in Fig. 2.5. The fit between experimental points and calculated curve is satisfactory on condition that parameters given above were assumed. The increase in dislocation density was found to be in agreement with the decrease of WF.

The increment of WF due to increase of the step density is given by,

$$\Delta\Phi = -A \times \mu \times n, \quad (2.5)$$

where  $\Phi$  in eV;  $A$  is constant which is equal to  $3.77 \times 10^{-15}$  eV  $\times$  cm<sup>2</sup>/D;  $\mu$  is the dipole momentum divided by interatomic distance in D/cm;  $n$  is the step density in cm<sup>-1</sup>.

From (2.5) we can obtain

$$d\Phi/dN = -A \times \mu \times dn/dN. \quad (2.6)$$

On the other hand, the breaking through dislocations to surface causes the origination of steps. Equation of conservation of the crystal lattice defects can be written as

$$\sqrt{\rho} \times L \times V \times dt = dn \times \bar{h} \times L, \quad (2.7)$$

where  $L$  is size of the crystal;  $Vdt$  is the mean free path of dislocations to surface;  $\rho$  is the mobile dislocation density, cm<sup>-2</sup>;  $dn$  is the increment of the steps density, cm<sup>-1</sup>;  $\bar{h}$  is a mean height of steps. Thus, the rate of steps formation is related to dislocation density and to velocity of their motion

$$dn/dt = \sqrt{\rho} \times V / \bar{h}. \quad (2.8)$$

As  $dt=2\pi \times dN/\omega$ , substituting formula (2.8) into equation (2.6) we can obtain

$$d\Phi/dN = -2 \times \pi \times A \times \mu \times \rho \times V / (\omega \times \bar{h}). \quad (2.9)$$

For aluminum value of  $d\Phi/dN=-1.67 \times 10^{-7}$  eV/cycle from graphs was estimated. Now we can evaluate some quantities proceeding

from experimental data. However, we should make a certain reasonable supposition because some values are unknown.  $\mu = e \times b / (b \times 3.34 \times 10^{-28}) = 4.79 \times 10^8 \text{ D/cm}$ . Assume that  $\bar{h} \approx b$ . Then according to (2.8) velocity of dislocations equals to  $4.04 \times 10^{-10} \text{ cm/s}$ . Now from (2.2) we can determine the factor of the dislocation multiplication  $\delta = 2.48 \times 10^{-3} \text{ cm}$ . From (2.7) we obtain  $dn/dt = 86.5 \text{ steps} \times \text{cm}^{-1} \times \text{s}^{-1}$ . E. g. it makes for  $N = 2 \times 10^6$  cycles total  $1.85 \times 10^5 \text{ steps/cm}$ . It coordinates with quantities that have been obtained by direct microscopic method. K. Besocke, B. Krahl-Urban and H. Wagner for Au and Pt single crystals have evaluated of  $(2 \div 4) \times 10^5 \text{ steps/cm}$  and corresponding drop of WF of order 300 meV.

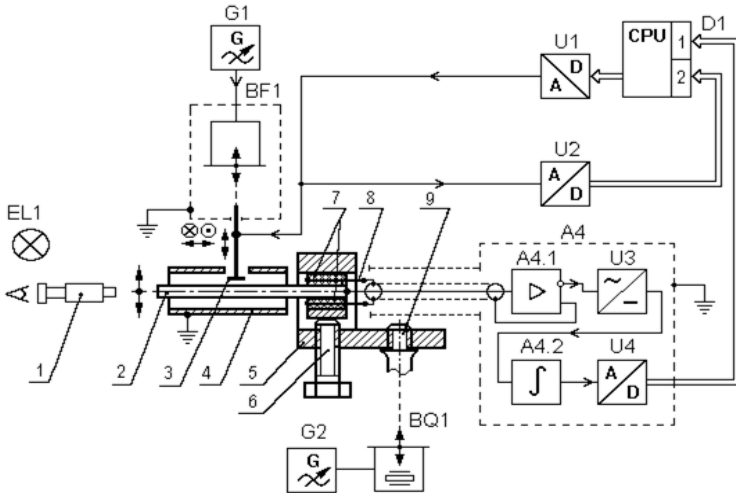


**Figure 2.1** – Experimental set-up for the work function measurements during fatigue tests:

- 1 – microscope; 2 – specimen; 3 – electrode; 4 – screen; 5 – clamp;
- 6 – bolt; 7 – dielectrical plates; 8 – equipotential screen;
- 9 – support of the source of mechanical vibrations

Thus, WF measurements enable of order – of magnitude evaluation of physical values. The work function of aluminum and heat-resistant steels was measured under the effect of fatigue tests.

A decrease of the WF occurred long before a crack started to form. The decrease in WF observed is related to the creation of charged steps on the metal surface because of dislocations breaking through. The method of WF measurement was shown to have prognosis possibilities as to the fatigue cracks origination.

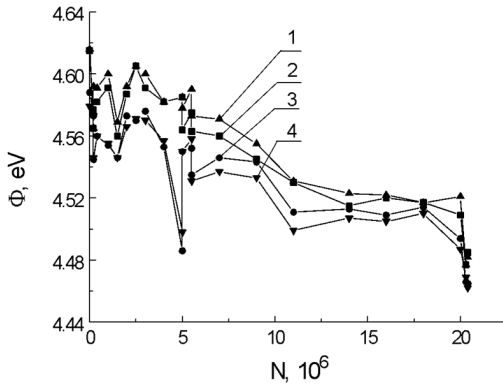


**Figure 2.2** – Work function versus number of cycles for the heat-resistant steel A:  
1–4 – four different points at the area of the future crack

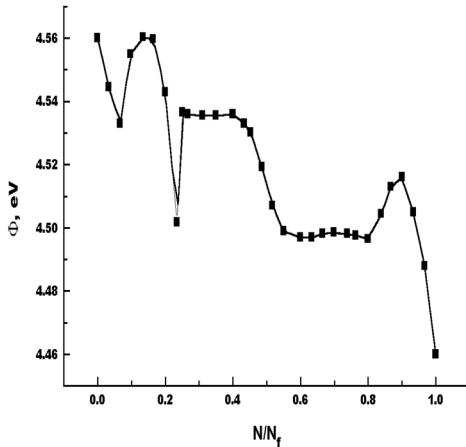


**Figure 2.3** – The effect of fatigue tests upon the work function for steel B

SECTION 2  
Work function for the deformed metals

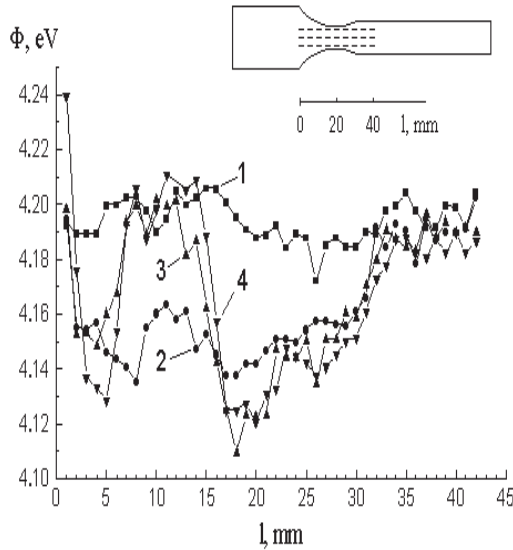
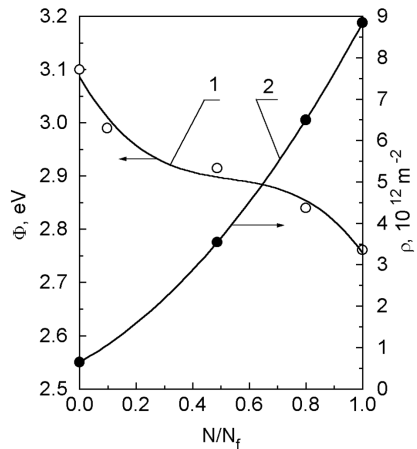


**Figure 2.4** – Distribution of WF over the surface of steel B during testing: 1 –  $N=0$ ; 2 –  $N=28 \times 10^6$ ; 3 –  $N=85 \times 10^6$ ; 4 –  $N=97 \times 10^6$  cycles

**Figure 2.5** – The effect of fatigue tests upon the WF and the dislocation density in Al:  
1 – the WF versus  $N/N_f$ , where  $N_f$  is the number of cycles till fracture;  
2 – computed curve of the dislocation density according to the equation (2);  
• – experimental data of X-ray measurements  $\rho(N/N_f)$ ,  
 $\tau_m = 52$  MPa;  $\omega = 5,881$  rad/s;  
 $\tau_m = 535$  MPa;  $\omega = 2,338$  rad/s



In insertion is shown scheme of lines, along which the WF measurements were carried out. The largest stresses correspond to distance of 17 mm from the left.

## 2.2 Work function for the real metal surface

Work function of metals has been studied experimentally under various conditions of strained state [182, 183]. It was found out that elastic strain increases WF up to several meV. WF of the plastic deformed metals decreases by tens and hundreds meV.

In paper [184] a stabilized jellium model within the self-consistent Kohn-Sham calculation method is considered; stabilization energy and consequently work function, surface energy etc. as function of electron density and deformation are derived. However, a physical model, which would be able to explain changes of WF for surfaces with crystals defects, has not been worked out as yet. Calculations of WF for real metal surfaces based on quantum mechanics are too complicated.

The authors [185, 186] have proposed a method of WF calculations for a non-ideal surface. This method is based on the semi-empirical theory of the neutral orbital electro-negativity (NOE). The general idea is that work function can be represented as the orbital electro-negativity localized close to atom on the surface. The surface constituent of WF is changed with strain considerably as the surface potential changes abruptly. In their turn these changes depend upon the surface microgeometry and upon the coordination of atoms on it. The determination of the surface atomic coordination has become possible due to the last achievements in the scanning tunnel microscopy [187, 188].

The ground for the work was the fact that till today there is no calculation scheme for determining WF of real metallic surfaces. The quantum mechanics methods solve the problems for metal surfaces with regular structure [189, 190] and with indirect deformation consideration [191]. The proposed scheme of calculation does not worse other semiempirical methods [192]. At the same time, it has some advantages. Due to the experimental data of scanning

tunneling electron microscopy, information about nanometric geometry of surface at metal's deformation can be obtained [193], and it is possible to calculate WF of any surface unit in the accordance with the known atom distribution over the surface.

Aim of this work is to develop method of WF calculation for the strained real metal surface. Connection between work function and atomic electro-negativity taking into consideration formation of surface defects is used in this work.

The numbers of disrupted interatomic bonds with the nearest and with the distant neighbours,  $i$ ,  $j$ , respectively, are used for the characteristic of the surface imperfection. Dependence of WF on  $i$  and  $j$  may be expressed as [185]

$$\Phi_{ij} = x_{ij} = 0.98 \frac{(V_n - i)n_a + (V_{nn} - j)n_b + 1}{r_a} + 1.57 \text{ eV}, \quad (2.10)$$

where  $x_{ij}$  is the orbital electro-negativity of an external atom on the surface;  $V_n$  and  $V_{nn}$  are numbers of the nearest and the next neighbors of atoms in volume, respectively; these numbers are dependent upon the type of crystal lattice;  $(V_n - i)$  and  $(V_{nn} - j)$  are the numbers of bonds of the external atom with the nearest and the next neighbors;  $n_a$  and  $n_b$  are the numbers of electrons taking part in bond of the surface atom with the nearest and the distant neighbors, referred to one atom;  $r_a$ , Å., is the atomic radius of the element according to Pauling. The formula (2.10) is semiempirical; the detailed substantiation of the constants is in article [186].

Formula (2.10) well describes the experimental data on work function of monocrystal planes of metals. Calculations of WF of some metals were executed on the basis of the theory of neutral orbital electro-negativity. The results of these calculations are in accord with the experimental data.

It is shown on the fig. 2.6, constructed on the basis of the data taken from the work [194]. WF of the non-ideal surface of metal can be considered as the average value of electro-negativity of external atoms of metal. On close-packed monocrystal metal surface all external atoms are identical, therefore their total contribution is identical too in any point outside the surface. Close to non-ideal surface or inside of a part covered with adsorbed particles surface

the total contribution of external atoms is spatially dependent. Close to such surface gradient of potential takes place. In model of NOE the following assumption is used: superficial atoms of metal keep to some extent individual character. Wave functions, describing the state of electrons on the surface, are approximated in immediate proximity from superficial atom by wave function of isolated atom. Hence, on a surface there are some atom orbitals or their combinations. Such representation takes into account asymmetry of an environment of atoms and corresponds to the certain superficial atom of metal. Using of the idea gives a possibility to interpret electronic emission as transition of an electron from the located electronic configuration of metal atom to the free state and to consider neutral orbital electro-negativity equal to WF as the activation energy. For non-ideal surface WF is the average value:

$$\bar{\Phi} = \sum S_{ij} \Phi_{ij}, \quad (2.11)$$

where  $S_{ij}$  is the fraction of surface that is occupied with the spot of  $\Phi_{ij}$ .

In works [187, 188] it has been shown, that deformation processes on a surface are determined by formation and evolution of nano defects. These are nanometric defects having the form of prisms of various sizes which sides are formed due to dislocations output to the surface over the planes of easy sliding. Formation of dislocation steps on surfaces changes the electrostatic superficial barrier and accordingly work function.

Dislocations output to the surface of metal under stress, and nano defects of the first rank are formed on it (the length of sides of nano defects of the first rank makes ~80 nanometers for copper, they are formed at emission of ~300 dislocations by clusters of sources of the first rank). Concentration of nano defects of the first rank grows until it reaches thermodynamically optimum value when the entropy of nanodefects and atoms of the crystal lattice has the maximal value. Then one part of these nano defects resolves, and the other part forms ensemble of nano defects of the second rank. Concentration of nano defects of the second rank grows, reaches about 5% and then one part of them resolves and the other part transforms into nano defects of the third rank, etc. The influence of load on the sample results in rising of new portions of nano defects

of the first rank and then transformation of the part of them into nano defects of the second rank, then the nano defects of the first rank are accumulated again and the process cyclically repeats. It is experimentally established, that the nanodefects on the surface of the loaded copper form four ensembles, and the energy of their formation in each of the next ensembles is 3 times less, and the size is 3 times larger, than in the previous [188].

Formation of nano defects is directly connected with the value of plastic deformation of the sample. Each nano defect is characterized by its geometrical size. At constant speed of deformation, the number of dislocations outputted to the surface, which formed a certain nano defect, is calculated. Plastic deformation of sample is determined by the area of projections of all the nano defects on a free surface of the sample. And, knowing the kinetics of formation and development of nano defect structure according to tunnel scanning microscopy, it is possible to determine size of deformation with the increment of the area of the free surface of the sample. Formation of new sites of free surface determines deformation, and difference in coordination of atoms of these surfaces influences the change of WF of the free surface. The method of NOE allows calculating changes of WF caused by change of coordination of an atom on surface of deformed metal owing to evolution of nano defect ensembles.

The average value of  $\Phi$  is calculated as follows. The arrangement of atoms on free surface of metal is computed at any moment of deformation. The strain is determined as the function of the free surface increment. WF is calculated at the change of the surface atomic order.

Distances between the nearest and the next neighbors,  $R_1$  and  $R_2$ , respectively, are changed as the result of elastic deformation. These values exert the influence on the quantities of  $n_a$  and  $n_b$ .

WF is calculated at plastic strain for each  $i$  and  $j$  in addition to elastic deformation. Calculations are performed for different crystal planes of copper and aluminum single crystals.

For face-centered cubic lattice in [100] direction

$$R_1(\varepsilon) = a \frac{\sqrt{2 + \varepsilon^2 + 2\varepsilon - 2\nu\varepsilon + \nu^2\varepsilon^2}}{3} + a \frac{1 - \nu\varepsilon}{3\sqrt{2}}, \quad (2.12)$$

$$R_2(\varepsilon) = \frac{2a(1 - \nu\varepsilon) + a(1 + \varepsilon)}{3}, \quad (2.13)$$

where  $a$  is the lattice parameter;  $\nu$  is the Poisson coefficient;  $\varepsilon$  is the strain.

The number of electrons that bind the surface atom with the nearest neighbors is given by

$$n_a(\varepsilon) = \frac{\nu}{V_n + V_{nn} \times \exp\left(\frac{R_1(\varepsilon) - R_2(\varepsilon)}{0.26}\right)}. \quad (2.14)$$

The number of electrons connecting the surface atom with the next neighbors can be expressed as

$$n_b(\varepsilon) = n_a(\varepsilon) \times \exp\left(\frac{R_1(\varepsilon) - R_2(\varepsilon)}{0.26}\right). \quad (2.15)$$

Elastic deformation of metal electrodes results in a change of potential on their surface. Let's assume that the double electric layer on the metal surface is the layer of dipoles. Then the elastic strain leads to redistribution of electrical charge. Electrostatic surface barrier and work function change accordingly. Taking into account the correction due to the charge, redistribution formula (2.11) should be rewritten as follows:

$$\Phi_{ij} = (0.98 \times \frac{(V_n - i) \times n_a + (V_{nn} - j) \times n_b + 1}{r_a} + 1.57) \times (1 + \frac{\delta(\varepsilon) - \delta(0)}{\delta(0)}). \quad (2.16)$$

Here

$$\delta(\varepsilon) = \frac{1}{\pi} \times \left( \operatorname{arctg} \frac{\rho + R_1(\varepsilon) / 2}{\lambda} - \operatorname{arctg} \frac{\rho - R_1(\varepsilon) / 2}{\lambda} \right), \quad (2.17)$$

where  $\lambda$  is thickness of the double electric layer;  $\rho$  is effective length [185].

Let's assume the reasonable quantities of  $\lambda=0.05$  nm,  $\rho=0.05$  nm. Varying the values of  $i, j$  we can calculate the work function in conformity with equation [188] for different crystal planes.

Time-dependent oscillation of nano defects concentration (in accordance with the experimental data received in work [188]) was

included into the program of calculations. Relation of the frequency of the first rank defects formation to the velocities of the relative deformation was approximately 3.6 for all the three considered velocities of deformation. It was observed that WF fall under plastic deformation is mainly defined by forming of surface defects of first rank. Oscillates character of surface defects evolution and experimentally observed output on plateau of WF change under limiting plastic deformation causes need to take into account the influence defect of 2, 3 and 4 ranks. The influence of the last on WF appears in WF growth compensation, caused by the decrease of first rank defects amount. For explanation of WF growth under reversal load an assumption was proposed about reversible nature of the surface defects formation. For development of the physical picture of fatigue it is interesting to research the nanometric structure of metal surfaces after different number of cycles of fatigue loading.

We have calculated the dependence of WF from plastic deformation of copper. Three elongation rates were examined. Kinetic of the nano-metric defects generation was taken into account. An oscillation of these defects was considered, too. In Fig. 2.7 the data obtained is presented. One can state the satisfactory fitness between the calculated data and the experimental results [195]. The elastic strain causes increase of WF (Fig. 2.8). As it is seen from Fig. 2.8 the experimental and the computed dependences of WF at deformation are similar. The close-packed atomic plane (111) has the larger quantity of WF than (100) and (110) planes have.

On the basis of the presented in the given work results it is possible to draw a conclusion about the advantage of using the shown model of electronegativity in the calculations of WF dependences in different schemes of mechanical metal loading. The correlation of the change of WF with the number of surface defects of all ranks should be observed experimentally for the further development of the offered scheme.

Model of the atomic electro-negativity allows calculation of work function of strained real metal surface. The fitness between the experimental results and the computed data for copper and aluminum is satisfactory.

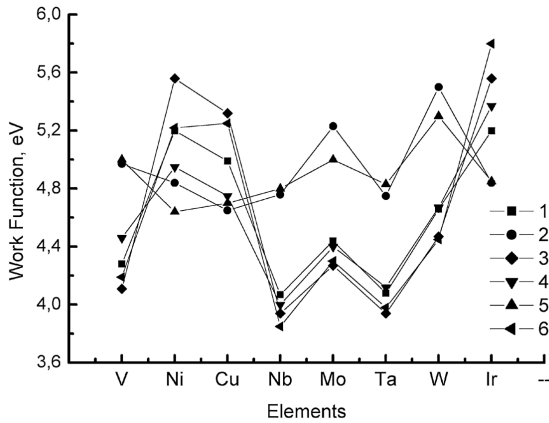


**Figure 2.6** – Values of work function of electrons for monocrystals of different elements. Calculation by the method of neutral orbital electro-negativity for planes 1 – (100), 2 – (110), 3 – (111).

Experiment (the method of contact potential difference (CPD)) or the method of thermo-ionic emission (TE)) for planes 4 – (100), 5 – (110), 6 – (111)

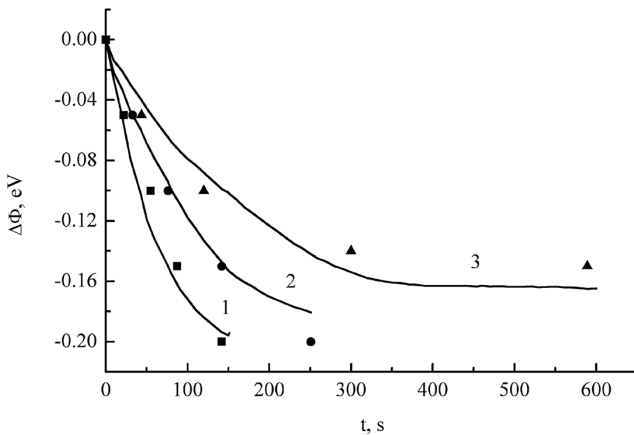


**Figure 2.7** – Comparison of the WF calculation results (solid lines) with the experimental data [8] (markers) for the plastic strain of copper. Rate of the specimen tension:

1 – 6.3; 2 – 2.5; 3 – 1.0 mm/min

SECTION 2  
Work function for the deformed metals

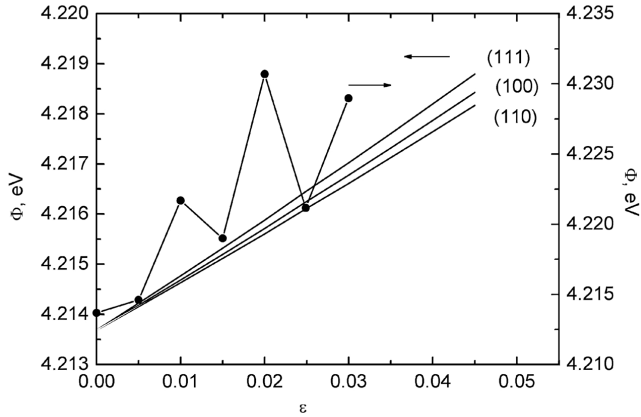


**Figure 2.8** – Comparison of the WF calculation results (solid lines) with the experimental data (markers) for elastic deformation of

### 2.3 On structural sensibility of work function

Stresses applied to metals have an effect on ionic lattice as well as on the free electron gas. It was discovered that the work function of metals changes as a result of strain [168, 172, 183, 196]. However, the structural sensibility of WF has not been sufficiently studied.

The aim of this work was the investigation of the work function dependence upon plastic strain and upon fatigue tests of metals and alloys.

Materials under investigation were Al, heat-resistant steel and Ti-based alloy. Specimens and blades of gas-turbine engine were objects of study. Heat-resistant Fe-based steel contained (weight %) 0.15 C, 15.8 Cr, 2.1 Ni, 1.0 Mo and 0.07 N. Ti-based alloy contained 6.1 Al and 3.3 Mo.

Dumbbell specimens with gauge dimensions of  $20 \times 10 \times 0.2 \text{ mm}^3$  were cut from aluminum foil. These specimens were used for investigation consisted in straining at a constant rate and in measuring the WF at selected points on the surface. Tensile strain rate was of  $5.67 \times 10^{-2} \text{ } \mu\text{m/s}$ . At various stages of

deformations straining was stopped and the distribution in WF was measured along selected lines of the surface of the specimen. WF was measured in steps of 1 mm along three or six longitudinal lines, which were parallel to the specimen axis.

Flat specimens of Al and heat-resistant steel of dimensions  $101 \times 11.5 \times 3 \text{ mm}^3$  were used for fatigue tests. These specimens had the shape of a single shovel. The test frequency was equal to 5,881 rad/s for Al and 2,338 rad/s for steel.

Contact potential difference was measured by Kelvin capacitor method [174]. As it is known, the surface of specimen and an oscillating electrode form the capacitor of alternating voltage. The signal of unbalance should be compensated. Quantities of WF were calculated proceeding from these data. Experimental set-up includes a portable piezoelectrical source of mechanical vibrations and set of measuring equipment. Details of experimental techniques have been reported [197]. Standard electrode was made of gold. Diameter of electrode was equal to 1.4 mm. The accuracy of WF measurement was  $\pm 2.0 \text{ meV}$ .

Real gas-turbine compressor blades of Ti-alloy were examined. The length of blades under investigation was 80 mm. Several blades were annealed at 923 K in three hours. Strengthening treatment of blades was carried out by means of special installation with steel balls as a working tool. Balls were put in motion by chamber walls vibrating under ultrasonic field with the frequency of 17.2 kHz and the amplitude of  $45 \text{ }\mu\text{m}$  [198]. WF was measured along the back and along edges of blades. Experimental points were located every other 1 mm.

In Figure 2.9 the typical dependences of stresses and WF upon strain are presented. The region of elastic strain is limited to  $\varepsilon=0.005$ . In the region of plastic deformation, WF drops sharply, decreasing of 180 meV. It is important to note the existence of a limiting value of the WF. Starting from a certain elongation ( $\varepsilon=0.055$ ) no significant decrease in WF is observed. However, after unloading WF increases. Evidently, that is caused by a relaxation process. There occurs a rapid rise of WF (by about 20 meV) without loading and then slow relaxations, which is realized in 12–15 hours.

The transition to the stage of plastic strain at  $\varepsilon=0.005$  causes a characteristic decrease in WF along lines of measuring. The

greater the degree of strain in the gauge part of the specimen, the greater the decrease in WF.

WF distribution for heat-resistant steel after fatigue tests is presented in Figure 2.10. Before fatigue tests, in the initial state, a scattering of WF quantities along specimens is observed (Figure 2.10, *a*). The scattering of points is equal to about 30 meV.

Area of 10 mm length of the specimen is located near a clamp of the vibration source. One should compare WF quantities in the loaded area (15–25 mm from the left) and WF in unloaded part (more than 25 mm). The largest level of applied cycling stresses is located at 17 mm from the left edge of the specimen. In Figure 2.10, *b* one can see that a minimum of WF appears after 50% of the specimen durability. At this place the WF drop equals to 75 meV. It is two times more than the scattering of points. During subsequent fatigue tests, the minimum erodes. The difference in WF between unloaded and loaded areas of specimen achieves 100 meV.

Thus, WF was found to decrease at the very place of the specimen where the fatigue crack would be formed, long before its origination. Observed falling of WF reflects some structural changes during stress cycling, especially nearby the surface of the specimen.

WF that has been measured along the blade axis drops extremely owing to strengthening with steel balls, which are vibrating in ultrasonic field (Figure 2.11). There is a great difference in WF between annealed and strengthen blades. The increment of  $\Delta\Phi$  is equal to 400 meV. Evidently, the surface deformation as well as the appearance of residual stresses result in the decrease of WF. The variation in WF between strengthen blades is equal to about 100 meV.

If a metal specimen is subjected to stresses, the generation of dislocations is known to occur. There exists a threshold stress for this process to begin. Dislocations, which have been generated, move along intersected slip planes. Generation of dislocations nearby a surface, as well as their breaking through, results in the occurrence of steps on the surface. These steps are known to have electric dipole moments [179]. Negative charges are accumulated between surface atoms. Dipoles contribution tends to decrease the work function.

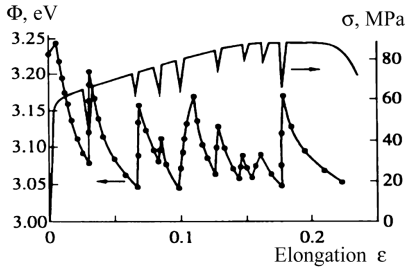


**Figure 2.9 –**  
Dependences  
of WF and stress  
upon strain for  
aluminum

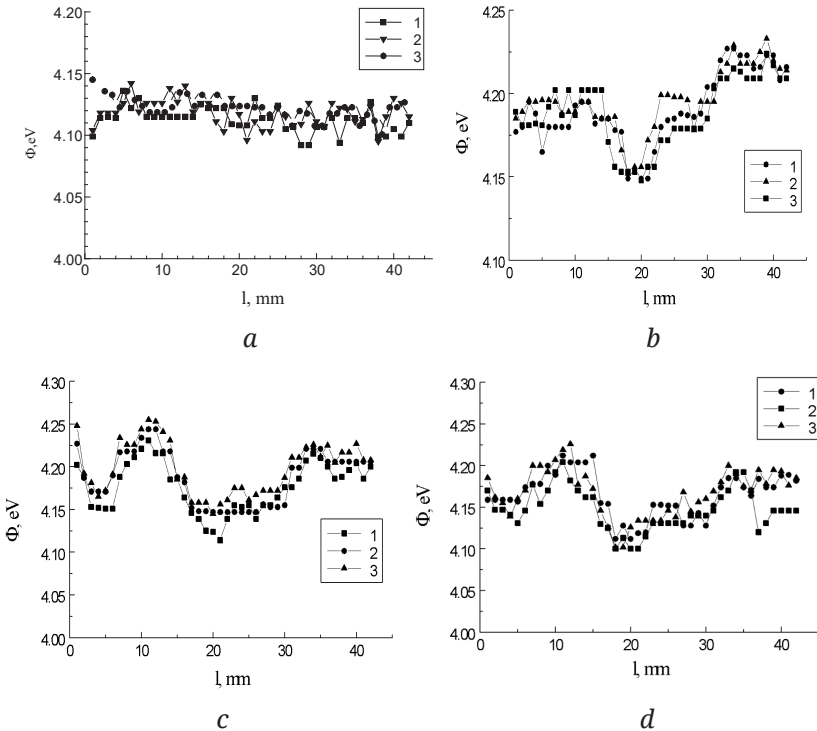


**Figure 2.10 –** Distribution of WF along fatigue tested specimens of heat-resistant steel: (a) initial quantities (number of cycles  $N=0$ ); three kinds of points conform to various series of measures; (b) curves from 1 to 3:  $N$  was changed from  $52$  to  $69 \times 10^6$  cycles; (c) curves from 1 to 3:  $N$  was changed from  $72$  to  $84 \times 10^6$  cycles; (d) curves from 1 to 3:  $N$  was changed from  $89$  to  $97 \times 10^6$  cycles

Stepped surfaces of Au and Pt single crystals have been studied with the direct microscopic method [179]. Steps were made by spark erosion machining the surfaces. Authors discovered WF drop of 300 meV and the corresponding step density of  $10^5$ – $10^6$  steps/cm. WF decreased linearly with increasing step densities. Our results of  $\Delta\Phi$  measurements are of the same order of magnitude.

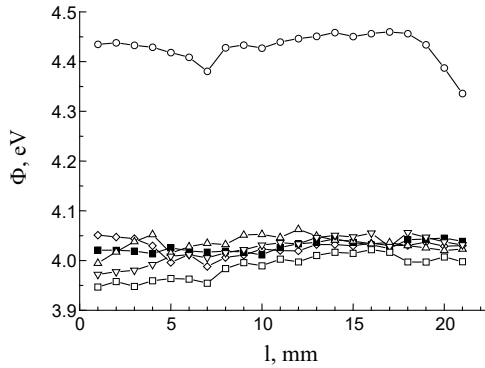


**Figure 2.11** – Distribution of WF along the blade backs:  
o, annealed blade; five kinds of other points conform  
to five blades after strengthening

## 2.4 Formation of energy patterns on metal contact surfaces

Actual metal surface is a complicated structural formation which serves as a mediator in contact interactions between connected machine elements. Deformation processes in metals depend to a considerable extent upon a development of dislocation structure. An increment of free surface takes place owing to going out of the dislocations and formation of surface crystal lattice defects. It results in a redistribution of electrons over the surface.

The electronic work function is known to be one of the main energy characteristics of metals. WF is defined as a difference between the height of the electron barrier on the metal-vacuum surface and the Fermi energy. The value of WF can be determined by

the measurements of the contact potential difference (CPD) between two metals. This method gives a chance to observe the changes in electron distributions [173, 199] and affords an opportunity to visualize the pattern of the strain energy on the surface. The data on measuring WF under different strain conditions have been published in papers [170–172].

Measurements of the absolute work function should be carried out in vacuum conditions. However, for industrial purposes it is not expedient to perform tests in vacuum. Methods which can be made in gas atmospheres are useful generally in order to compare the work functions of two surfaces. These methods are based on the fact that there is CPD between the surfaces of two conducting materials which are electrically connected. For this application, the contact potential difference is defined as the difference between the external potentials (beyond the image charge region) of two electrically connected materials. The outer potentials are themselves related to WF of the specimen surface. This work function depends both on the material itself, and the condition of the surface being examined.

The aim of present work was to investigate the evolution of contact metal surfaces in the course of friction and wear by means of WF measurements.

Materials under investigation were hard-facing alloys of Fe-C-Cr-B system, titanium and aluminum. Contents of elements in alloys are presented in Table. Structure of alloys consists of austenite-martensite matrix in which chromium carbides and carbo-borides are distributed uniformly. Specimens of  $35 \times 20 \times 4$  mm<sup>3</sup> were manufactured.

Tests of alloys for abrasive wear were carried out by means of a laboratory installation of the pneumatics type. As an abrasive the quartz sand of 160–250 μm fraction was used. The specimens were worn by the flow of abrasive particles falling at an angle of 24 degrees with the surface. Velocity of the flow was equal to 200 m/s. 6 kg of the abrasive were passed through the nozzle in the time of one test. No less than 7 specimens of the same chemical composition were tested simultaneously. Two series of experiments including 5 tests in each were performed. Loss of the specimen weight was measured and the average figure was used.

An installation for friction wear tests has been developed. The flat specimen rotated in horizontal plane. To apply a constant normal load to it a spherical contact indenter was used and a ring friction track was made on the specimen surface. Indentor of the 6.25 mm radius made of ball-bearing steel was employed for testing aluminium specimens. For hard alloys the spherical indenter of 3 mm radius manufactured of a super-hard alloy was applied. Tests of aluminum and titanium were carried out at a speed of 0.006 m/s and under the load of 1.5 N. In the case of hard alloys the relative specimen velocity was equal to 0.011 m/s and the load was of 1.5 N.

The work function was measured by Kelvin dynamic capacitor method [174]. As it is known the surface of specimen under investigation and an oscillating electrode form a capacitor of alternating voltage. Signal of unbalance should be compensated. The voltage of compensation is equal to  $CDP_{me-st}$  between the specimen and material of the standard electrode. As WF of the standard material is known  $WF_{me}$  of the specimen can be calculated proceeding from these data. The standard golden electrode was of 1.4 mm diameter. Unknown quantity of WF is determined by

$$WF_{me} = 4,300 - CDP_{me-st} \text{ (eV)}, \quad (2.18)$$

where WF of gold is equal to 4,300 eV. Accuracy of WF measurement was 1,0 meV.

In a number of cases an ultraviolet radiation of specimens was applied in order to avoid gas adsorption. Oxidation and gas adsorption have an influence on the WF quantity. However, it is necessary to take into account that our measurements were relative. We mean that the measurements of the WF difference were performed before contact deformation and after it. There are all the grounds to be convinced that observed changes of WF were due to effect of wear and owing to structure alternations. According to our experience a varying state of oxidation can only move curves of WF along *OY* as a whole. A difference in WF because of strain was the same.

Data on the abrasive wear of hard-facing alloys as well as WF increments are presented in Table 2.1. The weight loss of 0.244 mg per 1 kg of abrasive particles was assumed as a relative unit of wear.

The more the wear of specimen the larger the increment of WF. Alloy 1 which contains 2,0 C + 18,0 Cr + 2,0 B has discovered the largest resistance against abrasive wear. Weak alloying of specimen 8 results in wear resistance that is 1.41 times less. The correlation coefficient between WF and wear was found to be equal to 0.845. Thus, there is a high degree of correspondence between these two values.

Typical curves of WF distribution across the friction tracks are shown in Fig. 2.12. Fall in WF is observed along the friction path for three materials under examination. For soft aluminum the drop is the largest.

WF versus test time of aluminum is presented in Fig. 2.13. In the initial period WF considerably decreases. However, after a time WF does not change.

WF plotted against distance from center of specimens for four alloys is presented in Fig. 2.14. Dependences correspond to data of Table. Except two minimums which have been pointed out one can see that curves have a different inclination with respect to distance. For instance, this inclination is about 50 meV for specimen 8, however it is about 80 meV for specimen 1 and about 100 meV for specimen 3.

If the surface of the metal specimen is subjected to contact stress a lattice strain occurs and a generation of slip dislocation is known to take place. Origination of dislocations nearby the surface as well as their breaking through it results in emergence of steps on the surface. These steps are known to have a dipole moment [179]. Thus, the drop of WF observed (Fig. 2.12–2.14) was due to influence of charged microscopic steps which have been formed on the surface in the process of contact friction. Evidently the higher degree of plastic strain in the material having a low resistance to wear the larger WF drop occurs.

As for different inclination of curves in Fig. 2.14 the following supposition can be made. When colliding with the specimen the abrasive particles hit the hardening phase and transmit a part of its kinetic energy to it. The mechanical hardening of matrix is possible at its deformation in virtue of carbides and carbon-borides particles. Multiple process of colliding results in the plastic deformation in nearby layer. Probably for well hardened materials the wear process

is characterized by fatigue (e. g. alloy 1, Fig. 2.14). For weaker alloys the micro cutting takes place (e. g. alloy 8).

The work functions of aluminum and hard-facing alloys were measured after frictions tests. The work function was found to be sensitive to wear process. Its value decreased as a result of contact friction. The decrease of WF observed from the creation of microscopic charged steps on the friction surface. The method of work function measurements was shown to forecast the wear resistance.

**Table 2.1** – Correlation between the abrasive wear of hard-facing alloys and WF changes

Number of specimens	Content of elements, %			Specific wear, relative units	Average WF change, meV
	C	Cr	B		
1	2.0	18.0	2.0	1.00	38
2	0.5	18.0	2.0	1.21	50
3	2.0	7.0	2.0	1.11	47
4	0.5	7.0	2.0	1.19	48
5	2.0	18.0	0.5	1.36	53
6	0.5	18.0	0.5	1.27	65
7	2.0	7.0	0.5	1.19	47
8	0.5	7.0	0.5	1.41	83
9	1.25	12.5	1.25	1.12	39

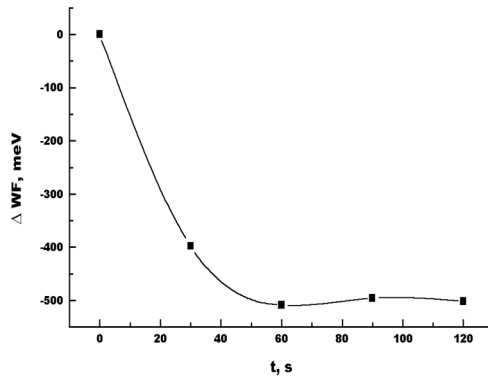


**Figure 2.12** – Increment of WF across of the friction track in aluminum versus the wear time

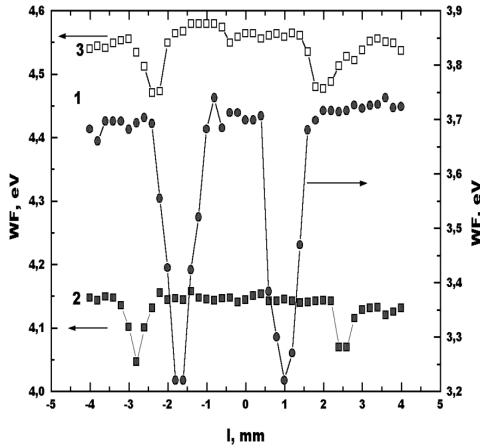


**Figure 2.13** – Distribution of WF across the friction track for materials under investigation: 1 – aluminium, test of 120 s; 2 – Fe-C-Cr-B alloy, 1,800 s; 3 – titanium, 1,800 s

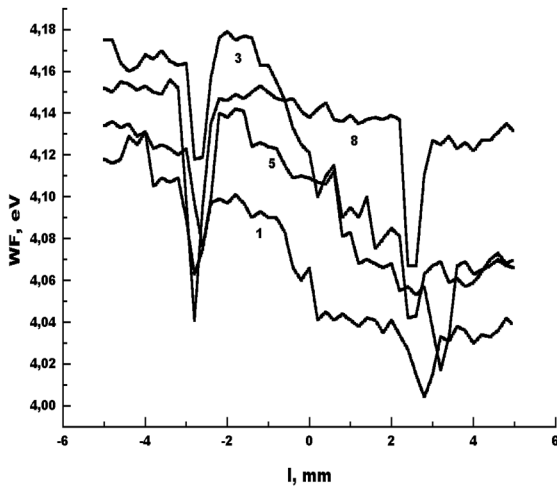


**Figure 2.14** – Dependence of WF upon the distance for four hard-facing alloys after gas-abrasive tests and following wear tests. Curves correspond to number of alloys in the Table.

# 3 STRUCTURAL CHANGES DURING DEFORMATION AND HEAT TREATMENT OF METALS

## 3.1 Parameters control of researched steel carburized layer via differential dilatometer

This work shows the possibility of using a differential dilatometer method and its application to control parameters of the diffusion layer of researched carburized steel.

The method allows registering the beginning and the ending of the saturation, tracing the process of decarbonization (denitrogenation) directly during the TCT process, and also adjusting saturation environment activity to achieve guaranteed diffusion layer parameters. Rods 1 and 2 must not be affected by carbonization environment and undergo phase transformations when operating (rods are made of X20H80 alloy, Standard of Ukraine). Reference 5 and tubular sample 9 are made of the same steel grade as details that undergo the TCT (Fig. 3.1). Registration precision of the diffusion saturation beginning can be improved by using hollow reference 5 (wall thickness 1.5 mm) instead of solid one, due to faster heating when coming to TCT temperature (Fig. 3.1) [200–202].

After reaching the TCT temperature, difference between rods 1 and 2 lengths, which is caused by temperature gradient during heating, vanishes. At the saturation temperature (1,030 °C) sample has austenitic polycrystalline structure (face-centered cubic structure). The coefficient of linear expansion of the austenite has identical values for all crystallographic directions ([010], [100], [001]). In the hollow sample austenite polycrystals averagely disoriented relatively to each other. Therefore, it can be assumed that linear dimensions of the sample change equally in all directions directly proportional to austenite lattice parameters changes. During the TCT (with saturation environment temperature remaining

constant), sample 9 lengthens due to carbon concentration increase, what is associated with an austenite lattice parameters increase.

During diffuse saturation of hollow sample, reference 5 retains its dimensions, as it is protected from carbon diffusion by a special layer (e. g. a 0.1 mm thick nickel layer). It provides an opportunity to measure sample lengthen  $\Delta l$  with high precision via watch indicator 11. Diffusion layer parameters directly at the moment of TCT process can be determined by  $\Delta l$  values on calibration graphs. Calibration graphs of dependence of layer thickness  $B$  and concentration on a surface  $C$  on elongation  $\Delta l$  are built based on chemical, metallographic and durametric tests.

Carburization of experimental steel was implemented in a laboratory shaft furnace, at temperature  $1,030 \pm 10^\circ\text{C}$  in solid carburizer (Fig. 3.2).

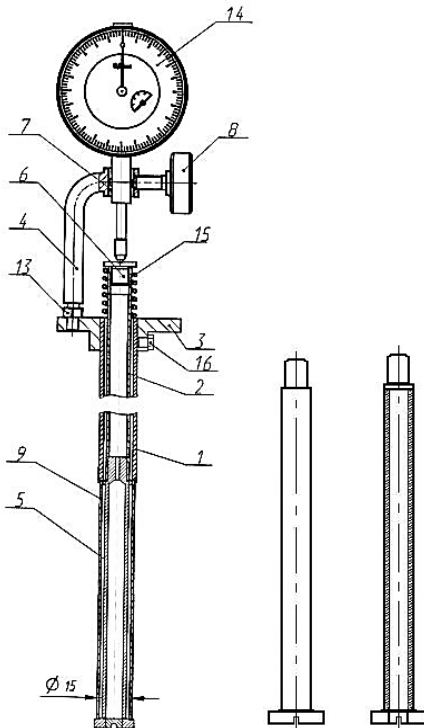


**Figure 3.1** – Differential dilatometer and references:  
*a* – differential dilatometer  
 (1 – external pusher,  
 2 – internal pusher,  
 3 – flange, 4 – bracket,  
 5 – reference, 6 – plate,  
 7 – bushing, 8 – screw,  
 9 – sample, 10 – nut,  
 11 – watch indicator,  
 12 – spring);  
*b* – solid reference;  
*c* – hollow reference

Reaching of the furnace temperature to carburization temperature (1,030 °C) was fixed. It took 1,740 s after loading of the container with dilatometer into the furnace to reach it (Fig. 3.3, *a*, point *a*). After reaching the point *a* the temperature in the container (1,030 °C) remained constant throughout the following aging. Therefore, point *a* is selected as the reference point of the length of the diffusion saturation.

Use of hollow reference with a wall thickness of 1.5 mm (see Fig. 3.1, *b*) can significantly improve the fixing accuracy of the diffusion saturation beginning (see Fig. 3.3, *a*, ver. II, curve 3) as compared with the case of use of a solid reference (Fig. 3.1, *b*; Fig. 3.3, *a*, ver. III, curve 2). The gradual increase of  $\Delta l$  starts after the reference and the sample temperature equalizing from the 1,460 s for version II and 1,860 s for version III.

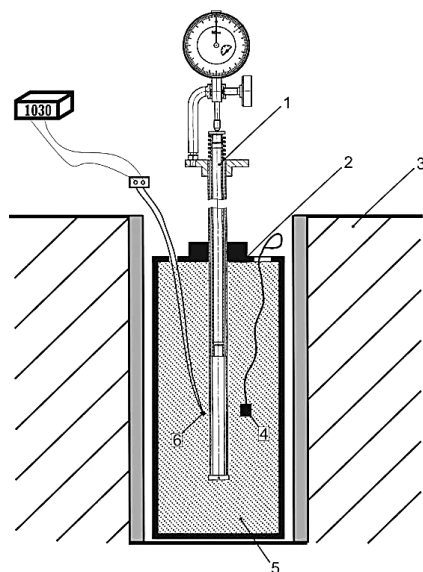


**Figure 3.2** – Diagram of dilatometer installation in the shaft electric furnace during the carburizing of experimental steel:

- 1 – dilatometer; 2 – container; 3 – electric furnace;
- 4 – witness sample; 5 – carburizer; 6 – thermocouple

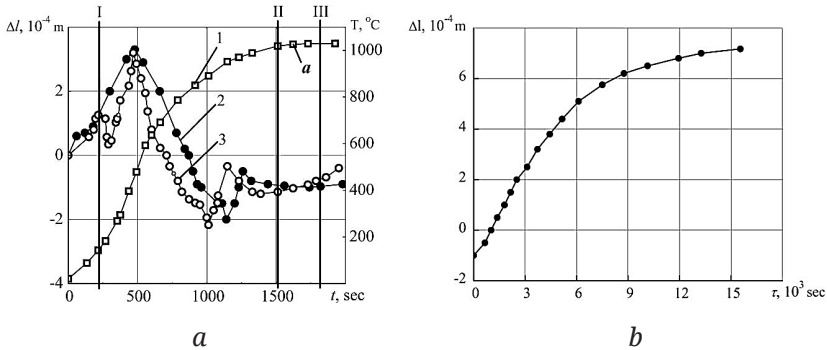


**Figure 3.3** – *a*: 1 – temperature dependence from aging duration in the container; 2, 3 – dependence of the elongation  $\Delta l$  of tubular sample from the heating time  $\tau$  to the carburizing temperature of experimental steel with use of solid and hollow reference accordingly; *b* – dependence of the elongation  $\Delta l$  of tubular sample from diffusion saturation duration  $\tau$  during the process of steel carburizing

Thus, with solid reference the beginning of increase of  $\Delta l$  (see Fig. 3.3, *a*, ver. III) takes place after the temperature 1,030 °C (see Fig. 3.3, *a*, point *a*). Moreover, in this case a less sharp (in comparison with the case of hollow reference) increase of  $\Delta l$  values after reaching the indicated temperature is observed (see Fig. 3.2, ver. II). These features can be explained by sustained heating of the solid reference in comparison to the hollow reference. It is accompanied by a decrease in measurement accuracy during the reaching of carburization temperature range of furnace.

The heating of experimental steel in carburizer without pre-drying was accompanied by some reduction of  $\Delta l$  of tubular sample in the temperature range of 450...550 °C (Fig. 3.3, *a*, curve 3, ver. I). It can be described by process of oxidation due to use of carburizer that contains water in initial state. Use of dried solid carburizer increases the oxidation resistance (Fig. 3.3, *a*, curve 2). After reaching the carburizing temperature (1,030 °C) the only thing that effects on tubular sample dimensions  $\Delta l$  is the quantity of diffused carbon in it.

It is established that for production of heavy-loaded aircraft reducers gears complex alloy steel 09X3HM3ФБч with high operation properties is appropriate to be applied.

The advantages of TCT for the secondary hardness of developed steel are shown.

Use of differential dilatometer to control diffusion saturation process will provide the stable obtaining of parameters of carburized (nitrocarburized) layer of aeronautics and shipbuilding reducers' gears teeth that will provide an opportunity to significantly increase their reliability and durability.

### **3.2 Control of carburization and decarburization processes of alloy steels at thermochemical and thermal treatment**

Dynamic development of such Ukraine industries as aircraft industry, mechanical engineering, and shipbuilding requires the development of new perspective materials and technologies of their processing for obtaining of competitive production. Increase of reliability and durability of products, which are affected by temperature, alternating loads during operation and operate under the conditions of friction and corrosion or abrasive media, is relevant task up to date.

The thermochemical treatment (TT) was widely used for surface hardening of details and tool. In order to obtain high-quality products, it is necessary to control TT processes (in particular, carbonizing, nitrocarburizing), which can be carried out in the gaseous or liquid media with the use of vacuum glow discharge, electrolytic and plasma treatment, etc. Constructional alloyed steels undergo carbonizing (diffusive surface carburization) and nitrocarburizing (saturation by carbon and nitrogen). For example, for production of tooth gears or reducers of aviation engines, the steel of the increased and high heat resistance: 14HGSN2MA, 13H3NVM2F, 16H3NVFM B, M50NiL, etc. is used [203–206]. TT of these steel grades is conducted at high temperature (1,220...1,300 °K) in the carbon and/or nitrogen-containing media.

Quality of the workpieces can be significantly reduced due to termination of saturation while holding during TT, and to such processes as decarburization, denitration, and also excess of carbon (nitrogen) concentration on a surface.

Quality of TT is determined by formation of such diffusive layer parameters, which allow guaranteed obtaining of optimum physicomachanical and operational properties of a product. Parameters of a diffusive layer are the following: concentration of the saturated element C, a gradient of its distribution with layer depth, and also thickness of a layer V. The structural condition and properties of steel surface layer after finishing operations of TT depend on concentration of carbon on surfaces and its distributions with layer depth.

When long-term high-temperature holding during the steel heat treatment (HT) (thermohardening, annealing), there can be decarburization and the subsequent oxidation of process material surface. In particular, such processes appear most strongly when processing of cemented and high carbon steels (ShH15, ShH15SG, U8, etc.) and lead to non-collectable scrap of steel in the form of scale, and also to decrease in mechanical properties of decarburized material layer, which is the closest to the surface.

Thus, it is necessary to control the value of parameters of diffusive layer directly within TT process for obtaining of optimum properties of products. During heat treatment, it is necessary to avoid decarburization, which precedes oxidation, and therefore, losses of metal and decrease in its properties.

The objective of work is system testing, which makes it possible to control the processes of TT and HT of special steels. In the paper, it is shown that the tasks can be solved successfully by use of specially designed device – differential dilatometer [200–202, 207].

The steel grades I 4HGSN2MA and ShH15SG-V were selected as materials for researches (Table 3.1. Steel of I 4HGSN2MA grade is used on “Zaporozhye machine-building design bureau “Progress” state enterprise named after academician A. G. Ivchenko” for production of tooth gears, which undergo gas carbonizing. Steel of ShH15SG-V grade is produced by PJSC “Dneprospetsstal” in Zaporizhia in the form of high-quality section iron. Heat treatment

(high-temperature annealing) of section iron is necessary technological operation for production of finished products.

**Table 3.1** – Chemical composition of steels under investigated

Steel grade	The containing of alloying elements in steel, % of mas.									
	C	Mn	Si	P	S	Cr	Ni	W	Mo	V
ShKh15SG-V	0.98	1.08	0.51	0.014	0.006	1.49	0.16	0.02	0.03	0.01
14KhGSN2MA	0.13	0.9	0.6	0.019	0.012	1.5	1.7	—	0.35	0.04

Chemical composition of steel under investigation determined by spectrometer Spectromax, and the content of carbon in the cemented layer of steel 14HGSN2MA by gas analyzer LECO-CS-230. Distribution of microhardness determined by depth of decarbonized layer of steel ShH15SG-V was determined by microhardness tester PMT-3. Research of kinetics of cementation processes of steel 14HGSN2MA and annealing of steel ShH15SG-V was carried out on the designed differential dilatometer. The differential dilatometer was tested at carburization of steel 14HGSN2MA and annealing of steel ShH15SG-V.

Carburization was carried out in the laboratory electric furnace SShOL 11.6/12-M3 with the use of solid carburizing material (GOST 2407-83) at a temperature of  $1,300 \pm 10$  °K (Fig. 3.4). For studying of saturating medium influence on diffusive layer parameters, the following compositions of carburizing material are selected: 1) 100% of fresh carburizing material; 2) 50% of fresh and 50% of sampled carburizing material (by volume). It took 29 minutes from the moment of loading of the container with dilatometer in the furnace to increase the temperature in the container to 1,300 °K, and then the temperature in container was invariable during the whole isothermal time. When holding, the value  $\Delta l$  was affected only by carbon concentration in a sample for the selected composition of carburizing material; as the value of reference standard remained fixed (Fig. 3.5).

Parameters of curves 1 and 2 for selected mode of carburizing are determined on Fig. 3.5 by composition of the saturating media (carburizing material). In spite of the fact that the fresh carburizing material (100%) must be more active, lower values of  $\Delta l$  (see also

curve 2 in Fig. 3.5) are observed, in comparison with were the case when using of mix of fresh and sampled carburizing (see curve I in Fig. 3.5). It can be explained by the fact that during isothermal holding when carburizing, shrinkage of carburizing material took place. As a result of the last the content of  $\text{CO}_2$ , increased, that is the ratio  $\text{CO}-\text{CO}_2$ , gases in the container changed, which in turn, caused the decrease of the carburizing material activity.

By means of a gas analyzer LECO-CS-230, it was established that after carburizing with the use of fresh (100%) carburizing material, the content of carbon in tubular sample (at the depth up to 300 microns from a surface) was 1.15–1.32% of mas.

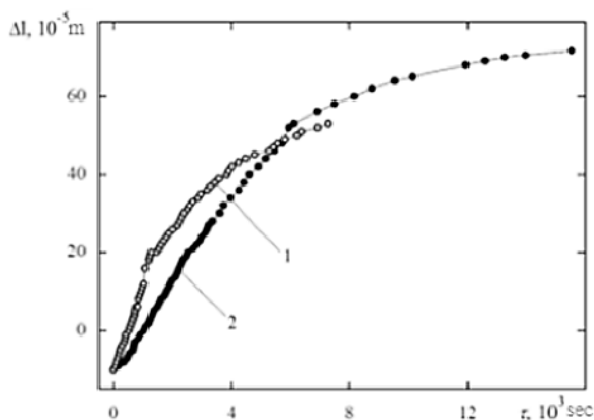


**Figure 3.4** – Dependence of elongation  $\Delta l$  of sample on time  $\tau$  during isothermal holding when carburizing of steel 14HGSN2MA for carburizing material of such composition: 1) 50% of fresh, 50% sampled (by volume); 2) 100% of fresh

For use of the dilatometer during TT, it is also necessary to construct the calibration curves of dependences of the maximum carbon concentration in a layer C and thickness of layer B on elongation  $\Delta l$  of sample, where certain distribution of carbon concentration and structural condition with layer depth corresponds to each point of the diagram. Thus, it is possible to control the value of diffusive layer parameters directly during TT if there is

opportunity to change the potential of the saturation atmosphere (gas, vacuum carburizing, etc.).

Annealing of steel ShH15SG-V was carried out in the mine electric furnace SShOL-11.6/12-M3 at a temperature of 1,070 °K for 19 hours in the air atmosphere (Fig. 3.5). The thermal furnace atmosphere, which is not protective (in particular, the air atmosphere), is conducive to decarburization and subsequent oxidation of steel surface [208].

The reference standard and tubular sample of the dilatometer were made of steel ShH15SG-V (see Table 3.1). The external surface of reference standard, and also internal surface and butt end of a tubular sample were covered with a nickel layer of 0.1 mm in thickness for protection against oxidation.

Pilot joints and dilatometer were charged into the furnace after its preliminary warming up to 1,070 °K. The moment of full warming up of a tubular sample up to the annealing temperature (in 720 sec. after loading of the dilatometer) was considered as reference point of time in case of curve construction of dependence of sample shrinkage  $\Delta l$  on time  $t$  while annealing of steel ShH15SG-V in the air. When annealing of steel ShH15SG-V in the electric furnace (in the air atmosphere), the thickness of oxidized layer of pilot joints increased depending on holding duration (Fig. 3.4, 3.5, *a*). The conducted measurements of microhardness of pilot joints surface layer of steel ShH15SG-V after annealing in the air allowed determining of the decarbonized layer value, which did not exceed 0.03 mm throughout the whole process of annealing.

Thus, reduction of length  $\Delta l$  of tubular sample over time  $\tau$  (see Fig. 3.5, curve 2) could take place as a result of simultaneous effect of such factors: reduction of austenite lattice parameters as a result of decarburization and oxidation processes.

The designed dilatometer was also used during research of decarburization process of high-quality section iron made of steel ShH15SG-V (Table 3.1). The device was tested in the chamber furnace of thermal department of PJSC Dneprospetsstal in Zaporizhia.

Annealing of steel ShH15SG-V was carried out according to the following mode: heating of section iron for 5 hours up to the

temperature of 1,070 °K. holding at this temperature was 17 hours (warming-up of heat treatment load – 3 hours, duration of holding of warmed section iron – 14 hours); cooling of the furnace to the temperature of 950 °K for 6 hours, holding at this temperature was 6 hours; cooling to 850 °K for 5 hours: cooling to 290 °K in case of the furnace open door.

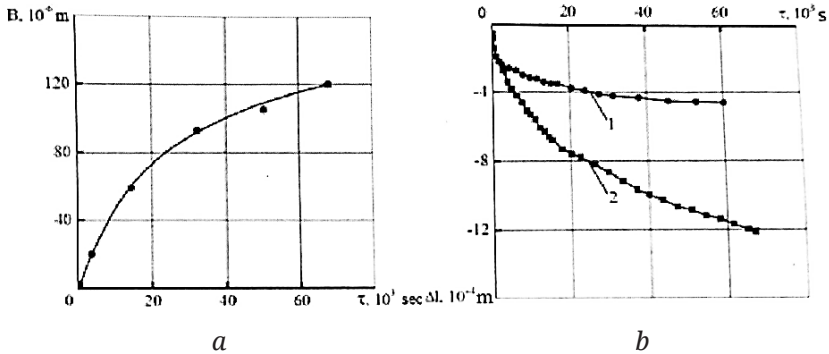


**Figure 3.5** – Dependences of change of samples parameters on duration  $r$  of steel ShH15SG-V annealing: *a* – thickness of oxidized layers  $B$  of pilot joint when annealing in the air; *b* – shrinkage  $\Delta l$  of tubular sample (1 – in the atmosphere of the chamber furnace of PJSC Dneprospetsstal; 2 – in the air)

The dilatometer was arranged in a place of thermocouple 1 in the chamber furnace (Fig. 3.6) at the time of reaching of annealing temperature (1,070 °K). The tubular sample of the differential dilatometer was near the top of heat treatment load.

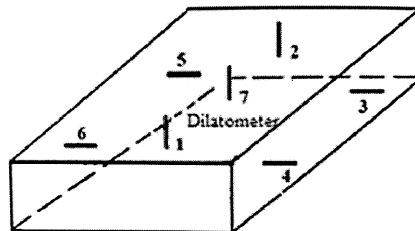


**Figure 3.6** – The pattern of arrangement of thermocouples and dilatometer in working space of the chamber furnace

Depth of the decarbonized layer, which was about 0.6 mm (Fig. 3.7), was determined by metallographic and durometric methods of the analysis. The gradual increase of microhardness from 3,050 to 4,500 MPa in the direction from surface to steel core was observed.

Change of tubular sample dimensions  $\Delta l$  of holding time  $\tau$  when annealing of steel ShH15SG-V in the atmosphere of chamber furnace of thermal department of PJSC Dneprospetstal is presented in Fig. 3.5 (curve 1). The value  $\Delta l$  reduction (reduction of sample) causes the necessity of change of endopotential of the furnace atmosphere for postreduction of sample sizes to the reference value that allows avoiding of further decarburization and oxidation of high-quality section iron.

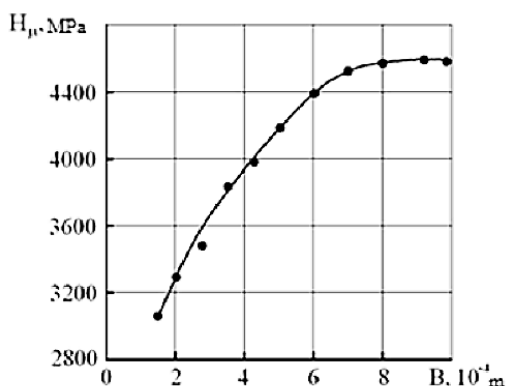


**Figure 3.7** – Dependence of microhardness distribution on depth of the decarbonized layer of steel ShH15SG-V after annealing

By means of the designed differential dilatometer and calibration curves, it is possible to control decarburization degree directly in the course of annealing of both steel ShH15SG-V and other alloys for the purpose of its full prevention by formation of the protective atmosphere in the chamber furnace [209].

1. In the work, the testing results of designed differential dilatometer, by means of which it is possible to control the processes of thermochemical and thermal treatment of steel, are presented.

2. By means of the dilatometer and calibration curves, it is possible to obtain guaranteedly the necessary parameters of diffusive layer by change of activity of endopotential of the saturation atmosphere directly during TT process.

3. The developed device and way of its use allow preventing of undesirable phenomena of decarburization and scale formation directly during annealing of special steels by change of atmosphere potential in the thermal furnace.

4. Testing results of the dilatometer when annealing made it possible to introduce the recommendation on production of high-quality section iron of steels ShH15 and ShH15SG at the electrometallurgical enterprise PJSC Dneprospetsstal in Zaporizhia.

5. The design of the differential dilatometer and way of its application are protected by patents of Ukraine for inventions.

### **3.3 Parameters control of 09Cr3NiMo3VNbr carburizing steel diffusion layer in the process of thermochemical treatment**

Aircraft engines gears work in conditions of high rotation speed and alternating power loads. Engines power increase induces a sharp rise of torque that reducer transmits and increase gears load. Therefore, demands to strength and operating properties are should be higher while gears scale and mass remains the same. This task can be done by increase of the mechanical and operating properties of steel. Known medium-alloy carburized steels 14CrMnSiNi2MoA, 13Cr3NiWMo2V, 16Cr3NiWVMoNb (Standard of Ukraine) and M50 NiL are not satisfying modern requirements, that are demanded to materials for heavy-loaded gears. Particularly, steels 14CrMnSiNi2MoA and 16Cr3NiWVMoNb are not heat resistant enough ( $\leq 300$  °C), steels 13Cr3NiWMo2V and M50 NiL are characterized with high core hardness, that makes mechanical treatment more complicated, and all of these have low values of contact durability [204, 210].

Thermochemical treatment (TCT) of gear steels is carried out at high temperatures (850...1,050 °C) in environment, that contains

carbon (or carbon and nitrogen). Quality of treated product can become lower as a result of unexpected (emergency) termination of diffusion saturation during the TCT and can be accompanied with such unwanted processes as decarbonization, denitrogenation etc.

Monitoring and control of the TCT processes (carburizing and nitrocarburizing in particular) that can be carried out in liquid or gaseous environment with use of vacuum glow discharge, electrolytic plasma procession etc. is necessary. The quality of the TCT is determined forming such properties of diffusion layer that allow obtaining optimal physical-mechanical and operating properties of product. The properties of diffusion layer are the concentration of the saturating element C, gradient of its layer's depth distribution and layer thickness B. Structural condition and properties of surface layers of any known steel after the TCT are mainly determined by the carbon concentration on the surface and its layer's depth distribution. In this work possibilities of increase of the aircraft reducer gears operating properties are studied.

On the one hand, achieved results of the mechanical and operating properties of developed steel 09Cr3NiMo3VNbr with optimized chemical composition are shown [211–213]. On the other hand, advantages of the direct control of the carburizing (nitrocarburizing) steel diffusion layer parameters during the TCT with the differential dilatometer are shown. Thus, use of developed complex alloyed carburizing steel 09Cr3NiMo3VNbr and additional quality control of the TCT with the differential dilatometer can guarantee necessary layer structure and ensure trouble-free operation of the gears under high loads and operating temperatures up to 450 °C.

### **3.4 Optimization of chemical composition of developed steel 09Cr3NiMo3VNbr**

Optimization of the composition of steel 09Cr3NiMo3VNbr was carried out with experiment planning by Box-Wilson method [214, 215]. Fractional replica  $2^{6-3}$  was implemented to build

regression equations. Common alloying elements concentration (factors) were varied: carbon, chrome, molybdenum, vanadium, niobium and total content of rare-earth metals (REM) cerium and lanthanum, because these elements cause the greatest impact on structure formation and mechanical properties of the researched steels core (Table 3.2). Factors levels and ranges of variation are shown in Table 3.3.

**Table 3.2** – Chemical composition of the researched steels

Alloy №	C	i	n	Al	Ni	Cr	o	V	Nb	Ce	La
0	0.032	0.08	0.35	0.06	0.96	2.20	1.84	0.45	0.15	0.03	0.01
1	0.060	0.06	0.21	0.09	1.3	1.9	1.71	0.21	0.06	0.002	0.001
2	0.028	0.08	0.14	0.08	1.1	2.85	1.68	0.29	0.13	0.055	0.031
3	0.074	0.09	0.28	0.07	1.2	2.07	2.21	1.21	0.087	0.013	0.0044
4	0.020	0.07	0.1	0.03	1.09	1.99	2.46	0.31	0.22	0.017	0.0045
5	0.050	0.08	0.24	0.1	1.06	2.98	2.29	0.33	0.2	0.054	0.021
6	0.034	0.12	0.31	0.14	1.03	2.17	1.74	0.99	0.37	0.035	0.014
7	0.065	0.13	0.26	0.084	1.01	2.98	1.46	1.06	0.37	0.03	0.0094
8	0.028	0.1	0.18	0.07	1.00	2.59	2.61	0.95	0.13	0.012	0.0031

\*P, S, N content  $\leq 0.025\%$  mass.

**Table 3.3** – Factors levels and ranges of variation

Levels and ranges of variation	Alloy elements content, % mass.					
	C(x <sub>1</sub> )	Cr(x <sub>2</sub> )	Mo(x <sub>3</sub> )	V(x <sub>4</sub> )	Nb(x <sub>4</sub> )	Ce + La(x <sub>6</sub> )
Main level	0.045	2.5	2.0	0.7	0.15	0.045
Range of variation	0.025	0.5	0.5	0.4	0.10	0.035
Upper level (+)	0.070	3.0	2.5	1.1	0.20	0.08
Lower level (-)	0.020	2.0	1.5	0.3	0.05	0.01

Next properties of samples cores after carburizing for secondary hardness were chosen as optimization parameters: ultimate strength  $\sigma_B$ , hardness HRC and impact toughness KCU. To study the ultimate strength, at different test temperatures (20 °C, 150 °C, 300 °C and 450 °C), hardness HRC and impact toughness KCU at 20 °C were used samples with such TCT: industrial oil hardening at  $1,030 \pm 10$  °C and following four tempering at  $530 \pm 5$  °C with 1 hour aging.

The ultimate strength  $\sigma_B$ , of researched steels was determined with testing machine 10 kN, hardness HRC with Rockwell hardness tester HRA-1, impact toughness KCU with pendulum hammer 300 N. Average values of the optimization parameters  $\sigma$  and KCU were obtained after two parallel experiments, HRC – after four parallel experiments.

Matrix approach to regression analysis was used to calculate regression equations coefficients, to determine their significance and to check models adequacy [214, 215]. The results of regression analysis for mechanical properties of the reducers' gears teeth core made from researched steels are shown in Table 3.4. The choose of linear product VC in regression equations was driven by the high resistance of primary vanadium carbides VC to dissolution in solid solution and their impact on mechanical properties of typical steels through the decarbonization of solid solution [216, 217]. Check of regression coefficients' significance by Student's t-test showed that in all regression equations coefficients  $b_i$ , (except  $b_3$ , in equation for impact toughness KCU) are significant (Table 3.4).

**Table 3.4** – The results of the regression analysis

Regression equations in factors' natural values	Fisher criterion, F	
	$F_p$	$F_{theor}$
$\sigma_B^{20} = 624 - 766 \times C + 56Cr + 146Mo - 706 \times V + 476 \times Nb - 1557 \times (Ce + La) + 10407 \times VC$ , MPa	0.069	5.3
$\sigma_B^{150} = 582 + 643 \times C + 56Cr + 106Mo - 575 \times V + 286 \times Nb - 1411 \times (Ce + La) + 8446 \times VC$ , MPa	0.001	
$\sigma_B^{300} = 910 - 1849 \times C + 78Cr - 31Mo - 522 \times V - 54 \times Nb - 2447 \times (Ce + La) + 8714 \times VC$ , MPa	0.002	
$\sigma_B^{300} = 1106 - 3094 \times C + 93Cr - 143Mo - 394 \times V - 5447 \times Nb - 2501 \times (Ce + La) + 7913 \times VC$ , MPa	0.003	
HRC = $32,8 - 171,6 \times C + 5,0Cr + 1,4Mo - 36,7 \times V + 13,8 \times Nb - 109,2 \times (Ce + La) + 499,9 \times VC$	0.066	4.3
KCU = $1,29 + 0,99 \times C - 0,06Cr - 0,28 \times V - 0,29 \times Nb + 2,03 \times (Ce + La) + 2,14 \times VC$ , MJ/m <sup>2</sup>	0.0004	5.3

According to the results of experimental research, hardening in the carburized layer of laboratory alloy 5 is most effectively realized via secondary hardening (Table 3.2). Ultimate strength ( $\sigma_B = 1,005$  MPa) and hardness (33 HRC), achieved for alloy 5, turned

out to be insufficient to satisfy the requirements for gas-turbine engine gears. In order to improve indicated characteristics, while maintaining impact strength KCU values, “gradient” motion was used [214].

The best way to improve strength and hardness of steel as delivered by the manufacturer was chosen – carbon and molybdenum content increase [203, 218]. At the same time, other elements content was held on a chosen alloy (alloy 5, Table 3.2) level. To define optimal chemical composition of developed steel, has been completed a step-by-step calculation of maximum  $\sigma_B$ , HRC and KCU values with content variation of C, Cr, Mo, V, Nb, Ce+La within the limits of values, close to indicated elements content in chosen alloy.

Data analysis allowed a chemical composition correction of developed steel 09X3HM3ФБЧ. Increasing carbon content up to 0.1% of mass and molybdenum up to 3% with REM content of approximately 0.001% of mass allows improving of ultimate strength  $\sigma_B^{20}$  are hardness HRC, and achieving of satisfactory impact strength (Table 3.5).

**Table 3.5** – Mechanical and operating properties  
of carburized steels

Steel grade	Core properties			Carburized steel properties	Contact durability, $\sigma_{Zmax} = 3,200$ MPa	Operating temp. (max.)
	$\sigma_{B20}$ , MPa	HRC	KCU, MJ/m <sup>2</sup>	HRC	N50, 10 <sup>6</sup> cycles	T, °C
Primary hardness TCT						
14XГСН2МА	980–1,050	38–41	0.95–1.05	≥58	20	180
16X3НВФМБ	1,220–1,280	42–44	0.78–0.85	≥62	23	300
Secondary hardness TCT						
M50 NiL	1,300–1,400	42–46	—	60–64	—	400
13X3НВМ2Ф	1,150–1,300	42–44	0.50–0.77	60–62	39	450
09X3HM3ФБЧ	1,282–1,405	38–44	0.85–1.19	61–63	≤101*	450

\*Max contact stress  $\sigma_{Zmax} = 3,500$  MPa

However, it is necessary to restrict overall content of REM between 0.001% and 0.01% mass, because going beyond the upper limit drastically reduces indicated properties (Table 3.2, Table 3.4). It is important to consider, that expected strength ( $\sigma_B$ ) and hardness HRC characteristics lowering in case of REM content excess in researched steels may be caused by ferrite-forming effect of these elements.

### **3.5 Determining the thermoplastic deformation mechanism of titanium reduction reactors and recommendations to increase the reactor service life**

World manufacturers of sponge titanium face a serious problem related to the curvature of reactors in the process of magnesium-thermal production of titanium sponge. This leads to premature damage to reactors and increased production costs [219]. Reactors of the magnesium-thermal process, operating under conditions of sharp heat changes, undergo significant thermal stresses, which prevail over the threshold values of the strength indicators of the material. Solving this problem can significantly increase the efficiency of the metallurgical industry.

Thermal stresses occur at uneven heating or cooling. In technological processes, cooling should be the most uniform. When the reactor is cooled, a temperature gradient occurs in its upper part – the exothermic reaction zone. The stress that occurs in this case depends mainly on the temperature gradient, linear expansion coefficient, and thermal conductivity of the metal. The lower the cooling temperature in the upper part of the retort, as well as the greater the coefficient of linear expansion and the lower the thermal conductivity of the metal, the greater the thermal stress and, correspondingly, the deformation.

Under industrial conditions, the formation of a deformation strip, narrowing of the retort in its upper part are observed, which complicates the unloading of the titanium sponge and shortens the service life of the equipment. In recent years, special attention

has been paid to increasing the productivity of the process of magnesium-thermal production of titanium sponge, by increasing the volume of the reactor [220]. As a result, the stressed-strained state of the material of the reactor walls is significantly complicated. Increased mechanical stresses and significant temperature gradients are technologically difficult to control. This necessitates a theoretical analysis of the deformation processes in the reactor material. Therefore, building a model of thermoplastic deformation of the material in the reaction zone is extremely relevant and in demand to eliminate the warping of the reactor walls during operation.

The main problem in obtaining titanium sponge by the magnesium-thermal method is the warping of the reactor. The reactor is simultaneously affected by a large number of adverse factors. The inner surface is consistently affected by magnesium chloride  $MgCl_2$ , metallic and liquid magnesium, vapor tetrachloride titanium  $TiCl_4$ . The outer surface is exposed to high temperature (1,000...1,200 °C) of the air containing chlorine vapors. The consequence of this effect is the corrosion of the material of the walls of the retort in the oxygen-free oxidizing environment of the furnaces.

Theoretical provisions and causes of deformation of reactors are corrosion in the oxygen-free oxidative medium of reduction and vacuum separation furnaces, which are discussed in [221].

Reactors, as a rule, are made of steel AISI 321 and AISI 304. Steels of this group are analogs of the steel of grade 12X18H10T only when used up to 500...600 °C as they have a different carbon content. In addition, they have an increased content of harmful impurities, such as sulfur and phosphorus, and they also have an increased content of copper. In [221], it is proved that at temperatures above 600 °C, the residual deformation in them increases significantly, which is unacceptable for devices for magnesium-thermal production of sponge titanium operating at 1,000 °C. Steels 04X18H10T and AISI 321, despite the low carbon content, on the lower boundary of chromium and nickel, as well as the presence of titanium, are unstable to the interaction of the aggressive environment and are not corrosive in the full sense. Increasing the heterogeneity of the structure of these steels activates corrosion of the inner surface of

the reactor, which leads to increased contamination of the titanium sponge with nickel [222]. Attempts to use other grades to increase the service life of the reactors did not lead to a positive result.

The process of shape change, which leads to the failure of reactors, is due to factors related to the consistent effect of the melt of magnesium chloride, metallic and liquid magnesium, vapor-forming titanium tetrachloride loaded into the reactor, on the one hand. And on the other hand, the effect of a temperature of 1,000...1,200 °C on the walls of the retort with the simultaneous interaction of the hot air of the furnace containing chlorine vapors. As a result of research [223], it was found that the greatest wear of steel 10X18H10T is observed at the boundary of the gas phase with the melt in the zone of the exothermic reaction of titanium tetrachloride with magnesium.

The temperature change in the outer wall of the reactor occurs during the technological process of reducing titanium tetrachloride with magnesium. At the same time, the high temperature of the outer wall of 920...940 °C ensures complete reduction of titanium tetrachloride [224].

The processes of shape change in such an aggressive environment have not been studied enough (as well as the “handling” of the retort material); another issue is the choice of material for the manufacture of retorts [225, 226]. In addition, the optimal dimensions of the retorts and the influence of operating modes are also poorly understood.

Modern titanium and magnesium production is characterized by a shortage of mineral raw materials and large volumes of waste; loss of valuable components, which reduces the economic efficiency of production.

This suggests that it is expedient to conduct a study aimed at determining the influence of changes in the temperature factor on the warping of the reactor vessel.

The considered problems can be solved by theoretical analysis of deformation processes caused by uneven temperature distribution in the retort reaction zone, and ensuring the minimum temperature of critical overheating of the wall of a 10-ton reactor during the reduction of titanium tetrachloride with magnesium  $\Delta T_{crit} = 60$  °C.

The aim of this work is to determine the deformation mechanisms that lead to a change in the shape of the side wall of reactors under the influence of a heterogeneous temperature field. This will make it possible to find technological solutions for the elimination of thermoplastic deformations.

To accomplish the aim, the following tasks have been set:

- to establish the places and magnitude of the greatest development of mechanical stresses in the reactor vessel;
- to determine the minimum overheating temperature of the reactor walls in the reaction zone, which leads to plastic deformation.

The object of study in this work is the stressed-strained state of the reactors, taking into consideration the conditions of their operation and the physical and mechanical properties of the materials. The main hypothesis of the study assumes that the "behavior" of a real reactor can be described on the basis of the "behavior" of its virtual model, built using a CAD module of the Comsol Multiphysics software package.

The retort load diagram and temperature field distribution are shown in Fig. 3.8.

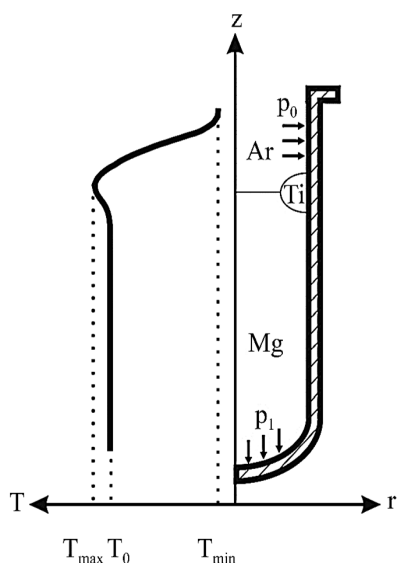


**Figure 3.8** – The scheme of the reactor with the loads acting on it, as well as the distribution of the temperature field on the outer wall. 10-ton reactor with a height of 3.6 m, a diameter of 2.0 m, a wall thickness of 25 mm

A type of reactor model with a temperature field distribution and a temperature gradient are depicted in Fig. 3.9.

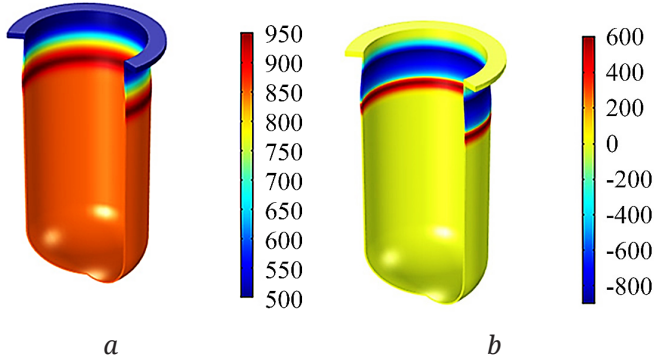


**Figure 3.9** – Reactor CAD model:  
*a* – temperature field distribution  $T(z)$ , °C;  
*b* – temperature gradient distribution  $\partial T/\partial z$ , °C/m

For the calculation, temperature dependences of the reactor material coefficients are used. As a material for the manufacture of retorts, widely used chromium-nickel steel of type AISI 321 was chosen.

The reactor was considered in a cylindrical coordinate system, considering that the displacement vector  $u$  does not depend on the angular coordinate  $\phi$  due to the axial symmetry of the reactor:

$$u(r, z) = u_r e_r + u_z e_z . \quad (3.1)$$

The components of the Cauchy deformation tensor for small movements are determined from the expression:

$$\begin{pmatrix} \varepsilon_{rr} & 0 & \varepsilon_{rz} \\ 0 & \varepsilon_{\phi\phi} & 0 \\ \varepsilon_{rz} & 0 & \varepsilon_{zz} \end{pmatrix} = \begin{pmatrix} \partial u_r / \partial r & 0 & (\partial u_r / \partial z + \partial u_z / \partial r) / 2 \\ 0 & u_r / r & 0 \\ (\partial u_r / \partial z + \partial u_z / \partial r) / 2 & 0 & \partial u_z / \partial z \end{pmatrix} . \quad (3.2)$$

Complete deformation  $\varepsilon$  can be represented as the sum of residual  $\varepsilon^0$ , elastic  $\varepsilon^{el}$ , plastic  $\varepsilon^{pl}$ , and thermal  $\varepsilon^{th}$  deformations:

$$\varepsilon = \varepsilon^0 + \varepsilon^{el} + \varepsilon^{pl} + \varepsilon^{th} . \quad (3.3)$$

The tensor of elastic deformations  $\varepsilon^{pl}$  is related to the tensor of stresses  $\sigma$  via Hooke's law:

$$\sigma_{ij} = C_{ijkl} \times \varepsilon_{kl}^{el}, \quad (3.4)$$

where  $C_{ijkl}$  is an elastic tensor. For an isotropic body, the components of the elasticity tensor can be expressed through the Lamé constants  $\lambda$  and  $\mu$ :

$$C_{ijkl} = \begin{pmatrix} \lambda + 2\mu & \lambda & \lambda & 0 & 0 & 0 \\ \lambda & \lambda + 2\mu & \lambda & 0 & 0 & 0 \\ \lambda & \lambda & \lambda + 2\mu & 0 & 0 & 0 \\ 0 & 0 & 0 & \mu & 0 & 0 \\ 0 & 0 & 0 & 0 & \mu & 0 \\ 0 & 0 & 0 & 0 & 0 & \mu \end{pmatrix}. \quad (3.5)$$

Lamé constants can be written through the Young modulus  $E$  and the Poisson coefficient  $\nu$ :

$$\lambda = \frac{\nu E}{(1 + \nu)(1 - 2\nu)}, \quad \mu = \frac{E}{2(1 + \nu)}. \quad (3.6)$$

In the zone of plastic deformation, the relationship between stresses  $\sigma^{pl}$  and deformations  $\varepsilon^{pl}$  is given by the expression:

$$\sigma^{pl} = \sigma_{0.2} + \frac{E_t}{(1 - E_t / E)} \varepsilon^{pl}, \quad (3.7)$$

where  $E_t$  is the tangential hardening module; for metals,  $E_t = 0.001 \times E$ .

The condition for the transition from elastic deformation to plastic is the Mises criterion:

$$\sigma_{eff} = \sqrt{\frac{(\sigma_{rr} - \sigma_{\varphi\varphi})^2 + (\sigma_{\varphi\varphi} - \sigma_{zz})^2 + (\sigma_{zz} - \sigma_{rr})^2 + 6\sigma_{rz}^2}{2}} \geq \sigma_{0.2}. \quad (3.8)$$

Using standard mathematical transformations, we obtain a system of related partial differential equations to determine the components of the displacement vector:

$$\frac{\partial^2 u_r}{\partial r^2} + \frac{\lambda}{\lambda + 2\mu} \frac{1}{r} \frac{\partial u_r}{\partial r} - \frac{\lambda}{\lambda + 2\mu} \frac{u_r}{r^2} - \frac{\lambda}{\lambda + 2\mu} \frac{\partial^2 u_r}{\partial z^2} = \frac{(3\lambda + 2\mu)\alpha}{\lambda + 2\mu} \frac{\partial T}{\partial r};$$

$$\frac{\partial^2 u_z}{\partial z^2} + \frac{\lambda}{\lambda + 2\mu} \frac{1}{r} \frac{\partial u_r}{\partial z} - \frac{\lambda}{\lambda + 2\mu} \frac{\partial^2 u_z}{\partial r^2} = \frac{(3\lambda + 2\mu)\alpha}{\lambda + 2\mu} \frac{\partial T}{\partial z}. \quad (3.9)$$

For most materials, the Lamé coefficients  $\lambda(T)$  and  $\mu(T)$ , as well as the temperature coefficient of linear expansion  $\alpha(T)$ , are nonlinearly dependent on temperature. To determine the components of the temperature gradient  $\partial T/\partial r$  and  $\partial T/\partial z$  included in [225], the following analytical relationship was proposed for temperature distribution on the outer wall of the reactor:

$$T(z) = \begin{cases} T_0 + (T_{\max} - T_0) \exp\left(-\frac{(z-h)^2}{\delta^2}\right), & -H \leq z \leq h; \\ T_{\max} - (T_{\max} - T_{\min}) \times \\ \times \frac{\xi}{\xi + 1} \left(\frac{z-h}{H-h-h_0}\right)^n, & h \leq z \leq (H-h_0); \\ T_{\min} + \omega(|z-H|)^m, & (H-h_0) \leq z \leq H. \end{cases} \quad (3.10)$$

The exponents of power  $n, m$  lie in the range of  $1.2 \leq (n, m) \leq 2.5$ .  $T_0$  is the temperature of the reaction.  $T_{\max}$  is the maximum temperature in the exothermic reaction zone.  $T_{\min}$  – temperature of the flange cooled by water.  $2H$  – reactor height,  $H-h$  – distance from the flange to the reaction zone.  $h_0$  – distance from the flange to the heaters in the furnace,  $\delta$  is the width of the reaction zone. Smoothness of the dependence  $T(z)$  is provided by the parameters  $\xi$  and  $\omega$ :

$$\xi = \frac{m}{n} \left(\frac{H-h}{h_0} - 1\right), \quad \omega = \frac{1}{h_0^m} \frac{T_{\max} - T_{\min}}{1 + \xi}. \quad (3.11)$$

We solved (9) by the method of finite elements. For this purpose, on the basis of drawings of real retorts, its axisymmetric geometric model was built using the CAD module of the Comsol Multiphysics software package [227–232]. For the calculation, the Nonlinear Structural Materials module was used. It makes

it possible to simulate the behavior of the model during deformation, to determine the zones of elastic and plastic deformation, to predict the destruction of reactors during the process of reduction of spongy titanium. To simulate the behavior of a 10-ton reactor with a height of 3.6 m, a diameter of 2.0 m, a wall thickness of 25 mm during the recovery process, the following parameters were selected:  $T_0=850\text{ }^\circ\text{C}$ ,  $T_{\min}=500\text{ }^\circ\text{C}$ ,  $\delta=0.2\text{ m}$ ,  $h=1.0\text{ m}$ ,  $h_0=0.3\text{ m}$ . The temperature in the reaction zone  $T_{\max}$  ranged from  $850\text{ }^\circ\text{C}$  to  $950\text{ }^\circ\text{C}$ . Value  $\Delta T=T_{\max}-T_0$  determines the local overheating of the outer wall in the reaction zone of the recovery process, which is automatically cooled from the outside by air from the fans.

The temperature distribution over the height of the reactor is shown in Fig. 3.10.

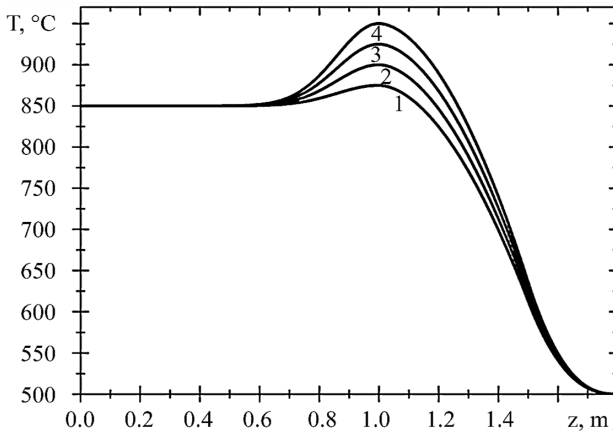


**Figure 3.10** – Temperature distribution in the reaction zone  $T(z)$   
for different overheating temperatures  $\Delta T$ :  
1 –  $\Delta T=25\text{ }^\circ\text{C}$ ; 2 –  $\Delta T=50\text{ }^\circ\text{C}$ ; 3 –  $\Delta T=75\text{ }^\circ\text{C}$ ; 4 –  $\Delta T=100\text{ }^\circ\text{C}$

The dependence of the deformation tensor components is depicted in Fig. 3.11.

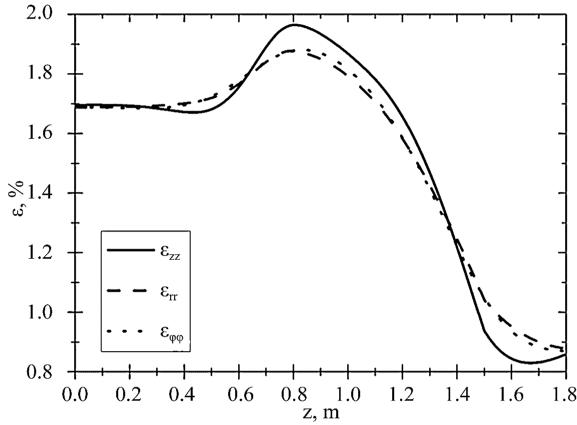


**Figure 3.11** – Distribution profiles of components  $\varepsilon_{rr}(z)$ ,  $\varepsilon_{\phi\phi}(z)$ ,  $\varepsilon_{zz}(z)$  of a complete deformation tensor  $\varepsilon$  calculated at  $\Delta T=100\text{ }^{\circ}\text{C}$

Data analysis in Fig. 3.10, 3.11 shows that the distribution of the main (diagonal) components of the deformation tensor is due to the distribution of the temperature field on the side wall of the retort, that is:

$$\varepsilon(z) \approx \varepsilon^{th}(z) = \alpha(T(z) - T_{\min}). \quad (3.12)$$

Distribution profiles of the stress tensor components in the reaction zone for different temperatures are depicted in Fig. 3.12.

Effective stresses calculated from expression (8) arising in the reduction reaction zone are mainly due to the components  $\sigma_{\phi\phi}(z)$  and  $\sigma_{zz}(z)$  (Fig. 3.12). The values of the components  $\sigma_{rr}$  and  $\sigma_{rz}$  are 10–20 times less and do not have a significant impact on the nature of the deformation of the reactors. Local extrema on the dependence  $\sigma_{zz}(z)$  correspond to the inflection points  $T(z)$ . Compressive  $\sigma_{ii} < 0$  and tensile  $\sigma_{ii} > 0$  nature of the stresses leads to the curvature of the reactor during the recovery process, that is, to the appearance of a bulge and concaveness of its wall.

Comparing the effective stresses with the conditional yield strength  $\sigma_{0.2}$ , it is possible to determine the width of the plastic deformation zones  $\Delta z^{pl}$  (the area on the  $z$  axis where  $\sigma_{eff} > \sigma_{0.2}$ ) and the

maximum values of plastic deformation  $\varepsilon_{\max}^{\text{pl}}$  in this area using the expression:

$$\varepsilon_{\max}^{\text{pl}} = \max \left( \frac{\sigma_{\text{eff}} - \sigma_{0,2}}{E_t} \right). \quad (3.13)$$

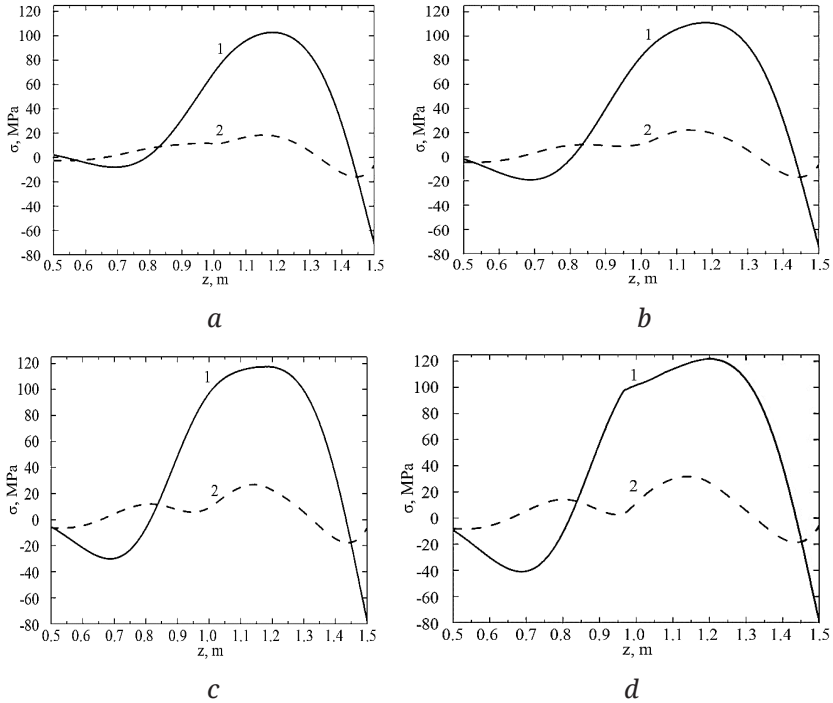


**Figure 3.12** – Distribution profiles of the stress tensor component  $\sigma_{zz}$  – curve 1 and  $\sigma_{\phi\phi}$  – curve 2 in the reduction reaction zone for different overheating temperatures  $\Delta T$ : *a* –  $\Delta T = 25^\circ\text{C}$ ; *b* –  $\Delta T = 50^\circ\text{C}$ ; *c* –  $\Delta T = 75^\circ\text{C}$ ; *d* –  $\Delta T = 100^\circ\text{C}$

There is a certain temperature range  $\Delta T$  for which the condition  $\sigma_{\text{eff}} < \sigma_{0,2}$  is met (the curve of effective stresses  $\sigma_{\text{eff}}$  lies below the curve  $\sigma_{0,2}$ ) and there is no plastic deformation (Fig. 3.13).

With a certain value  $\Delta T_{\text{crit}}$  in accordance with the criterion of plasticity of Mises  $\sigma_{\text{eff}} \geq \sigma_{0,2}$ , the appearance of plastic deformation is

likely. In addition, it follows from Fig. 3.13 that with an increase in the value of  $\Delta T - \Delta T_{crit}$ , the length of the zones of plastic deformation  $\Delta z^{pl}$  and deformation  $\varepsilon_{max}^{pl}$  increase (Fig. 3.14).

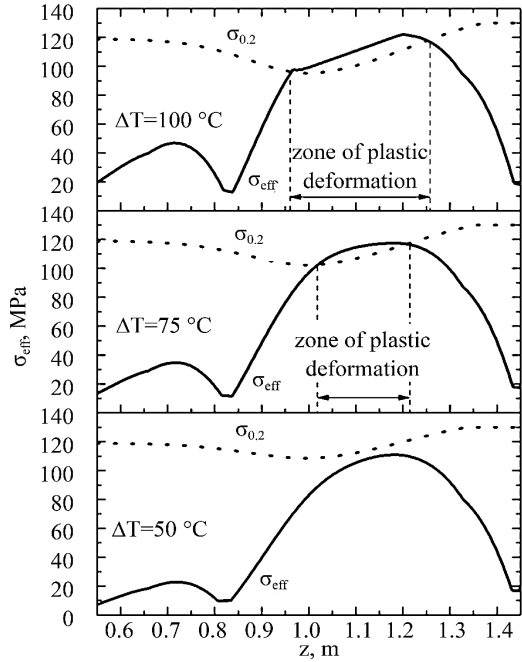


**Figure 3.13** – Distribution of effective stresses according to Mises  $\sigma_{eff}$  and conditional yield strength  $\sigma_{0.2}$  in the reaction zone at different  $\Delta T$

To determine the temperature of critical overheating  $\Delta T_{crit}$ ,  $\sigma_{eff}(z)$  were calculated in the temperature range  $\Delta T=50 - 100\text{ }^{\circ}\text{C}$  in increments of  $5\text{ }^{\circ}\text{C}$  and compared with the corresponding dependences  $\Delta\sigma_{0.2}(z)$ . The resulting dependences  $\Delta z^{pl}(\Delta T)$  and are shown in Fig. 3.14.

Based on the dependences (Fig. 3.14), it follows that when  $\Delta T > \Delta T_{crit} = 60\text{ }^{\circ}\text{C}$ , the walls of a 10-ton reactor in the process of reducing titanium tetrachloride with magnesium perceive plastic deformation. Its maximum value can reach  $\varepsilon_{max}^{pl} = 5.5\%$ .

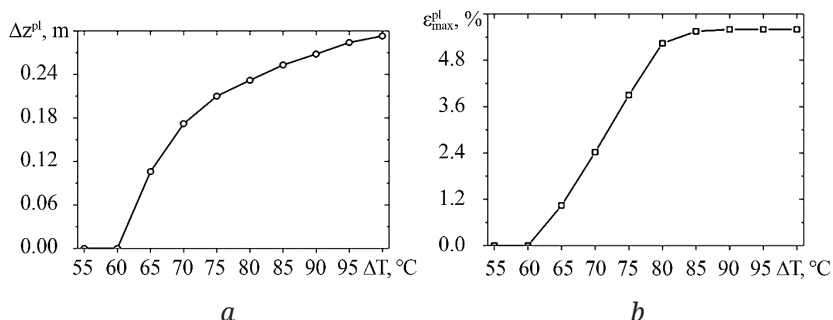


**Figure 3.14** – The dependence of the width of the plastic deformation zone  $\Delta z^{pl}$ : *a* – on the maximum plastic deformation; *b* – on the overheating temperature  $\Delta T$  in the reaction zone

Analytical review showed that the main proposal to solve the problem of thermoplastic deformation of the reactor is to install a refrigerator in the reaction zone, which greatly complicates the structure of the reactor and the technological process of restoring sponge titanium.

Unlike the world's existing reactors, whose performance is 1, 4, and 5 tons per cycle, 10-ton reactors will be subject to more significant temperature drops and corresponding hot deformations. They are just beginning to be introduced into production in the world.

Modeling the process of thermoplastic deformation of the reactor under the conditions of obtaining a titanium sponge made it possible to determine the temperature gradient in the upper part of the reactor wall, which leads to its local plastic deformation. The solution to the problem of increasing the service life of the reactor would be to prevent overheating of the reactor wall within the operating temperature. The physical and mechanical parameters of the reactor wall material, which are necessary to prevent the formation of an annular strip of plastic deformation, have also been determined.

The results of this work allow us to put forward requirements for the use or development of materials and to develop a progressive technology for the reduction of sponge titanium by the magnesium thermal method in high-performance reactors.

The system of equations (3.9) makes it possible to establish the dependence of the deformation tensor coefficients on the temperature gradient  $\partial T/\partial z$ . By controlling the temperature gradient, it is possible to influence the plastic deformation of the reactor walls.

The corresponding requirements for the material of reactors have been established, which prevent the appearance of plastic deformation at an operating temperature of 950 °C: the coefficient of linear expansion  $\alpha \leq 20 \times 10^{-6} \text{ K}^{-1}$ , the conditional yield strength  $\sigma_{0.2} = 120 \text{ MPa}$ .

Practical use of maintaining temperature restrictions  $\Delta T_{crit} = 60 \text{ °C}$  makes it possible to increase the life of 10-ton reactors.

The disadvantage of the study is that it does not have a very sensitive temperature control and control system in the reaction zone.

The development of this work is to design a new material that would meet the requirements and create a new temperature control and control system.

The minimum overheating temperature of the reactor walls in the reaction zone, which leads to the appearance of plastic deformation,  $\Delta T_{crit} = 60 \text{ °C}$ , has been determined.

### **3.6 Metallurgical aspects of production of chromium – nickel steels with low carbon contents**

The mechanism of deterioration of chromonickel stainless steels been studied under real industrial conditions of the titanium sponge production.

At present time the metallurgical industry of CIS and Ukraine has developed and is mastering some low-carbon and chromium-nickel-manganese steels of the austenitic ferrite and austenitic classes of 02X17H2Г8ФДч, 04X18H10, 05X18H10T and other grades. These steels are melted in open electric furnaces with further fining of the intermediate product in a gas-oxygen converter, where the high-chromium melt is decarbonized and alloyed, and the metal is reduced to a set chemical composition and a necessary temperature. The experimental-industrial testing of the new grades of steels was

carried out by the san plan with the reflection of the peculiarities of the technologies in specially developed TY.

The intermediate product of the steels mentioned above was burdened and smelted with an additive of ferrochrome of  $\Phi X$  800... $\Phi X$  950 grades first, and before pouring of the intermediate product into the converter some high-carbon ferrochrome was added up to 12% of the mass of the metal. At this moment it is possible to add some other ferroalloys or a metal discard. For low-carbon steels ( $\leq 0,03\%$  C) some especially pure additives were used – nickel HKC or H-O, and alloying with manganese was carried out with the addition of metal manganese of MP1, MP2 grades.

The fining and the heat finishing of the chemical composition in the converter were carried out in three periods [233]. The adjustment of the chemical composition of every grade of the low-carbon stainless steel was carried out with the doping of high-clean alloys into the melt – metal chromium, electrotechnical nickel and others. The metal was poured into slab moulds, the duration of the filling was 180–310 seconds receive an ingot of 9–16 tons.

In practice, the reduction of carbon contents in chromium-nickel steels of 18–10 sorts does not always influence positively upon their corrosion stability and sometimes promotes its reduction and deterioration of longevity of the parts and the units of the equipment.

It becomes especially apparent while exploitation of the products made of them under the conditions of high temperatures and corrosive medium.

For example, the following demands are made to the steel 12X18H10T, applied to produce reactor bodies (converters) in magnesium-thermal manufacture of titanium sponges:

- oxidation resistance to 1,100 °C temperature;
- mechanical strength and viscosity in atmospheric forcing;
- corrosion stability to the influence of moisture, molten magnesium, molten and gas magnesium and titanium chlorides;
- reasonable prices and manufacturability.

The numerous researches carried out by well-known native and foreign scientists have only confirmed the current opinion

that the steel 12X18H10T possesses the optimum combination of the properties mentioned above [234–237]. Following the general tendency to reduce carbon contents in stainless steels one of CIS enterprises made a decision in 2001 to use another grade of steel for this purpose – X6CrNiTi18-10 (1.4541) produced by Thyssen Krupp, Germany, the analogue of which is the steel 05X18H10T (all-Union State Standard) (Table 3.5).

The comparison of the chemical composition of the two steels has showed that they differ in their carbon contents, and in Germany steels X12CrNiTi18-10 and X6CrNiTi18-10 are their analogues correspondingly.

The investigation of the phase composition, carried out with the aid of calculations of equivalents by chromium and nickel, established that all the four melts of the steel X6CrNiTi18-10 (1.4541) are two-phase according to the well-known Sheffler diagram (Fig. 3.15, p. 1, 2, 3, 4).

The content of ferrite in these melts can come to 10–15% as against the steel X12CrNiTi18-10 (1.4878) – the analogue of the steel 12X18H10T which has a single-phase austenitic structure (see Fig. 3.15). Moreover, the metal of the steel X6CrNiTi18-10 of all the four melts was attracted with a magnet to a variable degree. This is the first confirmation of a two-phase – austenitic ferrite structure of the metal of the melts being investigated.

The interior surface of the mechanisms is in contact with the titanium sponge, the melt  $MgCl_2$ , molten Mg, molten and vaporous  $TiCl_4$  and lower titanium chlorides in different aggregative states at the temperature up to 1,000 °C. But the main source of the fracture is still the anoxic oxidant  $TiCl_4$  [238].

In the exploitation process of the reactors made of the two-phase steel, there were changes in the chemical composition of the interior surface. The iterative calculation of equivalents by chromium and nickel showed that the interior surface of the reactor metal after some cycles of exploitation could have either an austenite-martensite or an austenite-ferrite-martensite structure (see Fig. 3.15). This fact brought to the reduction of the durability of the mechanisms in 1.7 times and the contamination of the titanium sponge with nickel.

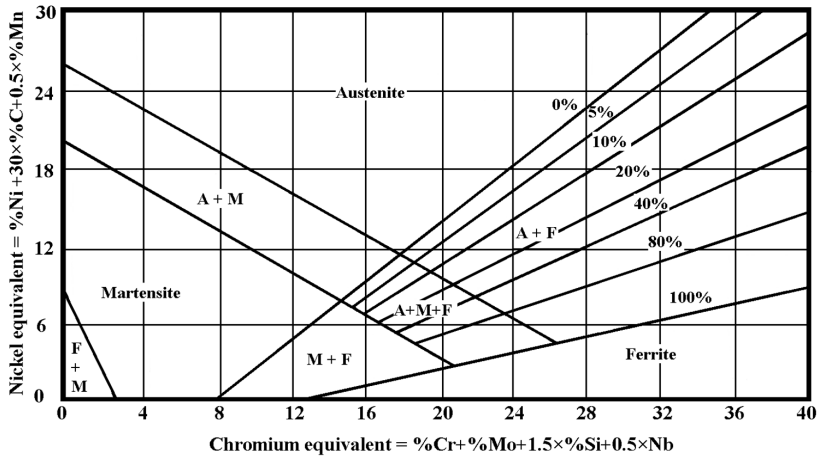


**Figure 3.15** – The structural diagram of stainless steels (Sheffler)

We have established a considerable amount ~15% of the second phase of ferrite, by means of a microstructural analysis of the sample of one of the melts of the steel X6CrNiTi18-10 in the reference state (Fig. 3.16, *a, b*).

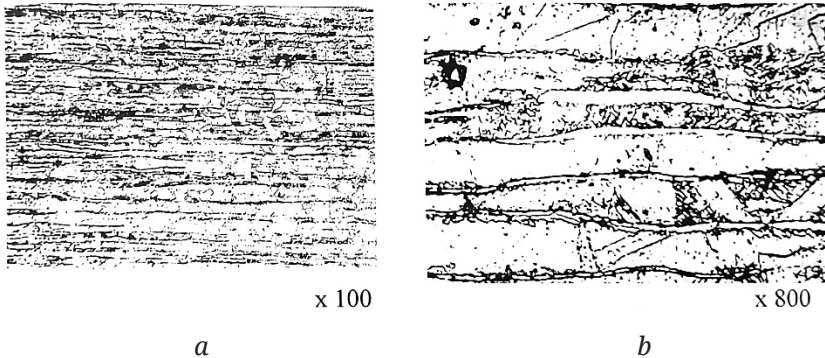


**Figure 3.16** – The microstructure of the steel 05X18H10T  
in the state of supply microhardness  
of the austenitic fields:  $H_{\mu}$  558)

In process of exploitation of the reactors, the chemical composition of the interior surface changes, and consequently the phase composition. The metal structure becomes three-phase – austenite-ferrite-martensite; the martensite is lath and low-carbon (Fig. 3.17). A certain amount of titanium is quite often entered into austenitic steel  $\sim(5 \times \% C)$  to reduce susceptibility to the grain-boundary corrosion. Titanium, already in molten steel, fixes carbon and nitrogen in a fast carbonitride phase and balks the appearance of chromium carbides and nitrides.

So, converting fast carbides into low-carbon steels, titanium reduces the stability of austenite and promotes formation of ferrite. Besides, it acts as an alpha-formative element and at its abundant content (more than the necessary amount for carbon fixation) it promotes ferrite formation. In its turn at higher temperatures, the alloying elements are redistributed intensively among the phase components. Susceptibility to electrochemical corrosion of the steels of 10–18 types is connected with the appearance of intercrystalline ferrite, which is formed of austenite under internal stresses connected with distortion of the borders of crystals. These internal stresses play the same role as a mechanical hardening, changing the austenite into a faster ferrite or low carbon martensite.



**Figure 3.17** – The microstructure of the steel 05X18H10T, the deformation martensite (microhardness  $H_{\mu}$  714)

Moreover, the dissolubility of carbon in ferrite is lower than in austenite, there is an eduction of dispersed ferric carbide or

other elements in the intercrystalline zone and they together with the ferrite form a structure that is similar to troostite of carbon steels that on account of great heterogeneity is easily exposed to electrochemical influence because of difference of the electrochemical potential of the phases.

In purely austenitic steel this does not bring to heterogeneity of the structure, and the alloys remains austenitic. However, there is an eduction of carbon in the form of ferric and chromium carbide or even in form free carbon in two-phase and three phase steels in the heating interval of 400...800 °C. The great corrosion susceptibility of the marginal areas can be explained by the stresses, which are formed as a result of such an eduction.

In their turn the heterogeneous structures having different electrochemical potentials can be exposed to the intensive dissolution in the presence of the electrolyte.

From the premises it follows that chromonickel steel must be the material applied while producing reactors, with such a content of the austenite formers – Ni and C, which could provide the constancy of the austenite structure in the process of the whole service life of the reactors.

### **3.7 Optimization of chemical composition of Lou pearlitic steel of the special setting**

The prospect of increase of production of sheet rent of the worked out steel can be seen not only in necessities internal and external markets but also in optimal combination of her physico-mechanical properties and technology of production. Such must steel possess totality of enhanceable strength and plastic descriptions, that, largely, provided by the state of the weld-fabricated connections and thermal affected of difficult details zone. The decision of these tasks this work is sanctified to.

Research of descriptions of mechanical properties of low-alloy steel for motor industry at cold and hot treatment.

Low-alloy brands are known became [239], that allow in the process of treatment to improve strength descriptions of material. Well known low-alloy steel [239], in the complement of that enters: carbon, silicon, manganese, chrome, nickel, aluminium, copper, phosphorus, nitrogen, magnesium, REM other iron. The lack of this steel is a decline of mechanical descriptions of the weld-fabricated guy-sutures as a result of receipt of tempering structures. Introduction in the complement of steel of calcium, titan, tungsten, niobium assists the removal of negative influence of tempering structures, here the level of shock viscosity goes down in the thermal affected of the weld-fabricated guy-sutures zone.

For the wheeled production the high-strength brand of low-alloy steel is worked out, a carbon, manganese, silicon, titan, phosphorus, vanadium, niobium, chrome, is used in basis of that [240].

Applying the method of planning of experiment [241] an experiment is carried out and dependence of row of mechanical descriptions of the offered steel is certain depending on her chemical composition: tensile ( $\sigma_B$ ) of MPa, limit of fluidity ( $\sigma_T$ ) of MPa strength, to shock viscosity (KCU) MJ/m<sup>2</sup>, relative lengthening ( $\delta_5$ ) %.

Mechanical tests were conducted in the cold state at monaxonic tension of the tested model of MP-100, concordantly GOST 1497-84 (Table 3.6).

**Table 3.6** – Experimental mechanical description become

Offer steel	Mechanical descriptions			
	$\sigma_B$ , MPa	$\sigma_T$ , MPa	$\delta_5$ , %	KCU, MJ/m <sup>2</sup>
1	427	321	33	0,85
2	525	473	25	0,65
3	502	345	30,5	0,95
4	503	451	28	0,90
5	413	309	29,5	0,55
6	575	496	18	0,45
7	499	443	29,5	0,80
prototype	760	265	34	0,80

As independent variables were chosen: maintenance in steel of chrome ( $X_1$ ), maintenance in steel of vanadium ( $X_2$ ), maintenance

in steel of titan ( $X_3$ ). In the process of search of optimal composition of alloy, in an induction stove with a basic lining-up by a capacity 50 kg it was the laboratory melting is conducted became. The got founding forged on purveyances measuring a  $10 \times 80 \times 120$  mm, with subsequent rolling in the hot state.

Intervals and levels of change of factors are driven to the Table 3.7. For reduction of number of experiments supposing nonlinear character of functions of response in-process used a symmetric composition plan the second order [241].

**Table 3.7 – Research factors**

Description	Factors		
	Cr, % m.	V, % m.	Ti, % m.
Code	$X_1$	$X_2$	$X_3$
Basic level	0,15	0,15	0,15
Interval of varying	0,05	0,05	0,05
Bottom level	0,10	0,10	0,10
Top level	0,20	0,20	0,20

For all descriptions used equalization of regression of 2th order. Further processing of experimental data and optimization of chemical composition, conducted by means of application «Statistica», package that allowed to promote efficiency of researches in several times.

After determination of coefficients of equalizations of regression, the row of equalizations that show dependence of mechanical properties became from maintenance of alloying elements was got.

Numeral values of coefficients of regression and their meaningfulness, certain taking into account distinction of dispersions for every function of response, and also the t-test of meaningfulness and estimation of model adequacy on the criterion of Fisher are presented in a Table 3.8.

For the estimation of adequacy of equalizations a calculation was created on the got equalizations of regression for base-level of chemical composition became. The results of calculations were confronted with experimental data. An error between the calculation and experimental values of function of response does not exceed 2%.

Using the package of software's of MATLAB, three-dimensional models that simplify research of dependence between the group of factors and mechanical properties (Fig. 3.18–3.21) prospected in this work are built.

**Table 3.8** – Results of regressive analysis  
of alloying complex

Alloying complex	Equalization of regression	$\Delta b$	t-test	F-test
Cr-V-Ti	$\sigma_B = 824 - 7385Cr - 991V + 1627Ti + 23222Cr^2 - 9417Ti^2 + 4200CrV + 4200CrTi + 4200VTi$	2.55	2.78	$6.09 > 4.3$
Cr-V-Ti	$\sigma_T = 716 - 9636Cr + 162V + 2586Ti + 32983Cr^2 - 2153V^2 - 11033Ti^2 + 2900CrV + 2900CrTi + 2900VTi$	2.55	2.78	$6.26 > 5.61$
Cr-V-Ti	$KCU = 0,52 + 9,52Cr - 1,63V - 2,67Ti - 31,78Cr^2 + 12,22Ti^2 + 7,0CrV - 10,0CrTi$	0.015	2.78	$6.16 > 4.88$
Cr-V-Ti	$\delta_5 = 32 + 280Cr - 161V - 115Ti - 1206Cr^2 + 353Ti^2 + 735CrV - 215CrTi + 65VTi$	0.025	2.78	$6.26 > 4.79$

On Fig. 3.18, 3.19 it is shown that with the change of chemical composition mechanical descriptions change became. The tendencies of increase of tensile and fluidity strength are visible. For example, at maintenance of Ti and Cr 0,2% and 0,14% accordingly a maximal  $\sigma_B = 500$  MPa etc.

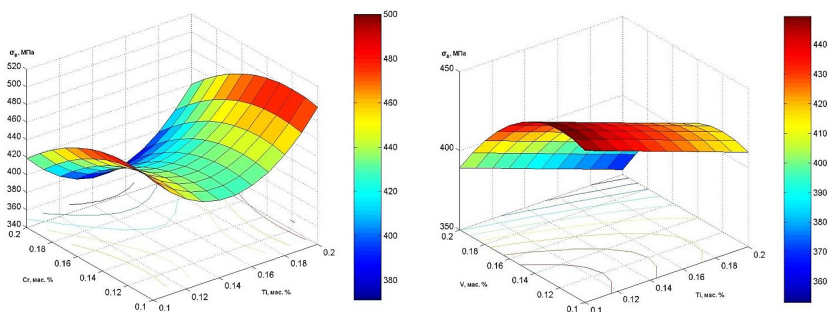


**Figure 3.18** – Optimization of chemical composition  
became on tensile strength ( $\sigma_B$ )

Physical and mechanical laws of metals structure formation  
in the processes of treatment and deformation

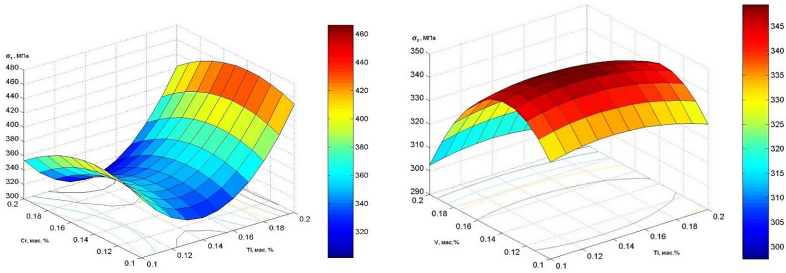


**Figure 3.19** – Optimization of chemical composition became on the limit of fluidity ( $\sigma_T$ )

On a Fig. 3.20, 3.21 the change of shock viscosity and relative lengthening is shown from the same chemical elements. At a value Ti and Cr 0,16% and 0,2%,  $KCU=0,8$  MJ/m<sup>2</sup>.

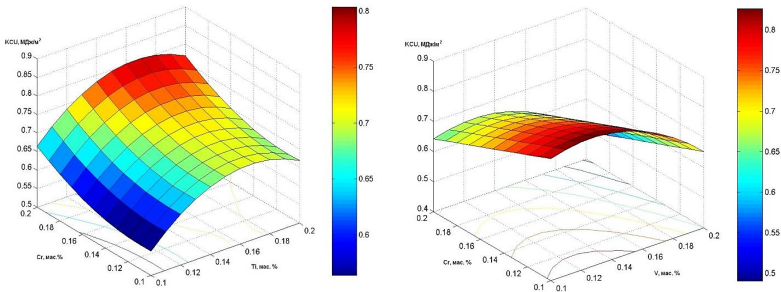


**Figure 3.20** – Optimization of chemical composition became with shock viscosity

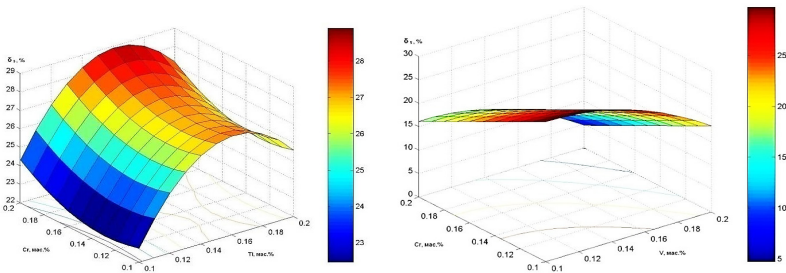


**Figure 3.21** – Optimization of chemical composition became from the relative lengthening

Chemical composition of steel is presented accordingly in a Table 3.9,  $\sigma_B=407$  MPa,  $\sigma_T=323$  MPa,  $KCU=0,78$  MJ/m<sup>2</sup>,  $\delta_5=27,5\%$ .

**Table 3.9** – Composition of alloying elements become, providing optimal properties

Cr, % m.	V, % m.	Ti, % m.
0.15	0.15	0.15

From the analysis of picture 1–4 evidently, that stronger than all mechanical properties of steel depend on maintenance in steel of chrome and titan. Notedly influences their correlations. Presentation of results of experiment appeared the polynomial of the second degree to justified – considerable part of nonlinear members here meaningfully differs from a zero. On results optimization optimal chemical composition of steel, the masses are recommended, %: carbon – 0,10, silicon – 0,31, chrome – 0,1, vanadium – 0,13, titan – 0,12 (Table 3.5).

**Table 3.10** – Optimal indexes of mechanical properties of the worked out low-alloy steel

<b>Mechanical properties</b>			
$\sigma_B$ , MPa	$\sigma_T$ , MPa	KCU, MJ/m <sup>2</sup>	$\delta_5$ , %
407	323	0,78	27,5

Tests became in the hot state conducted on the modern plastometer of Gleeble 3,800 and dilatometer. Operating parameters of plastometer:

- temperature  $t=20\dots1,700$  °C;
- rate of movement of puncheon to 2,000 mm/s;
- logarithm of deformation  $\epsilon_{com}=0.01-1.2$ ;  $\epsilon_{ten}=0.01-0.15$ .

For clarification of temperature condition of researches an experiment on determination of temperatures of transit of  $Ar_1$ , and  $Ar_3$  points was conducted for this brand became, that had corresponded 724 °C and 898,6 °C (Fig. 3.22). The sizes standards corresponded  $d \times h=5 \times 5$  mm [242].

At research on a plastometer, standards were measuring  $d \times h=10 \times 12$  mm chambered, into that air was pumped out and

created a vacuum for the exception of oxidization of metal. Management by a plastometer it was come by true by the special computer programs on a temperature, speed and degree of deformation. At stated intervals in the process of ladening tension of fluidity and logarithmic deformation was fixed. In a Table 3.11 the thermomechanical parameters of the deformed standards are presented.

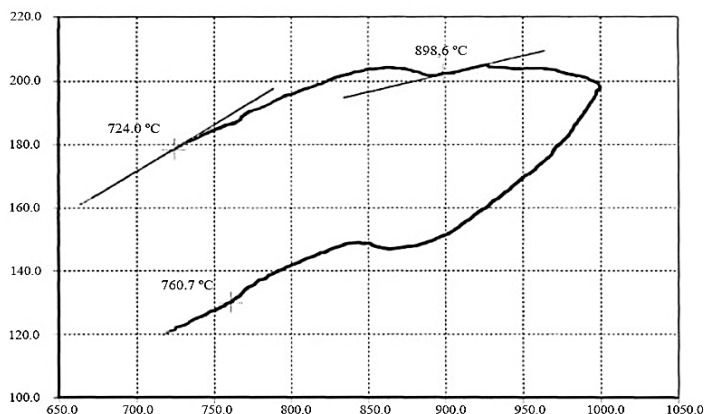


**Figure 3.22** – Dilatometer of standard

**Table 3.11** – Parameters of deformation

Standards	1	2	3	4	5
Temperature, °C	770	800	850	900	950
Speed of deformation, s <sup>-1</sup>	10				
Degree of deformation	0,01–1,2				

On Fig. 3.23 the diagrams of compression of standards are presented at different temperatures, showing dependence of tension of fluidity on logarithmic deformation of compression, on the different stages of forming. With the increase of degree of deformation  $\alpha$ , grows only at a temperature 850 °C and saves an index at 900 °C. It contingently flowing of  $\alpha - \gamma$  transformation (Fig. 3.23, curves 2, 3).

Resistance of deformation  $10X\Phi T\Gamma\check{c}$  became with the increase of temperature of deformation from 800 °C to 850 °C not considerably increases and only at high-rate of deformation remains almost

unchanging. It contingently the action of two opposite factors: temperature, that reduces resistance of deformation and structural, increasing resistance of deformation, as a result of increase of stake of austenite in steel (Fig. 3.24, *a, b*). As well as it was necessary to expect, with the increase of speed of deformation resistance of deformation rises, special at the increase of stake an austenitic constituent (Fig. 3.25, *a, b, c*).

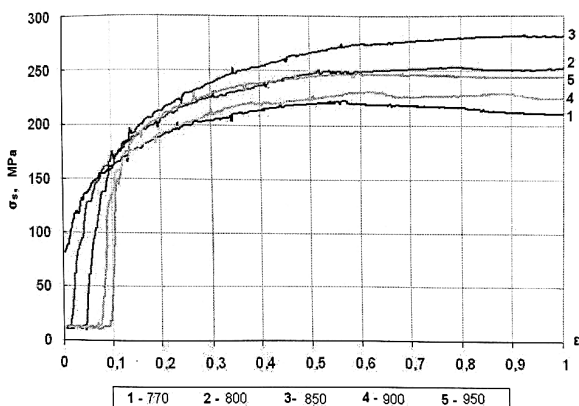


**Figure 3.23** – Dependence of tensions on the initial stage of deformation

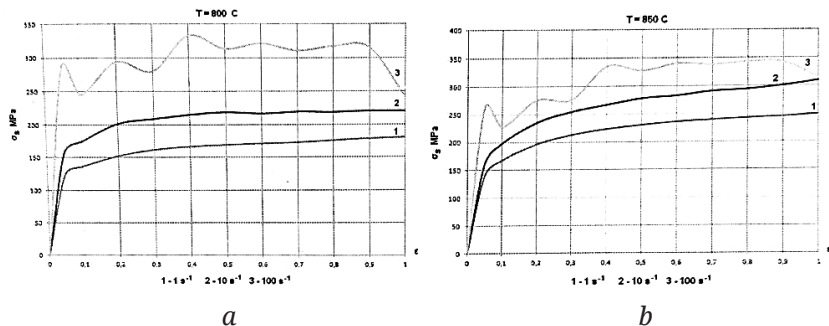


**Figure 3.24** – Dependence of resistance of deformation on the degree of deformation at different temperatures:  
*a* – 800 °C; *b* – 850 °C

Physical and mechanical laws of metals structure formation  
in the processes of treatment and deformation

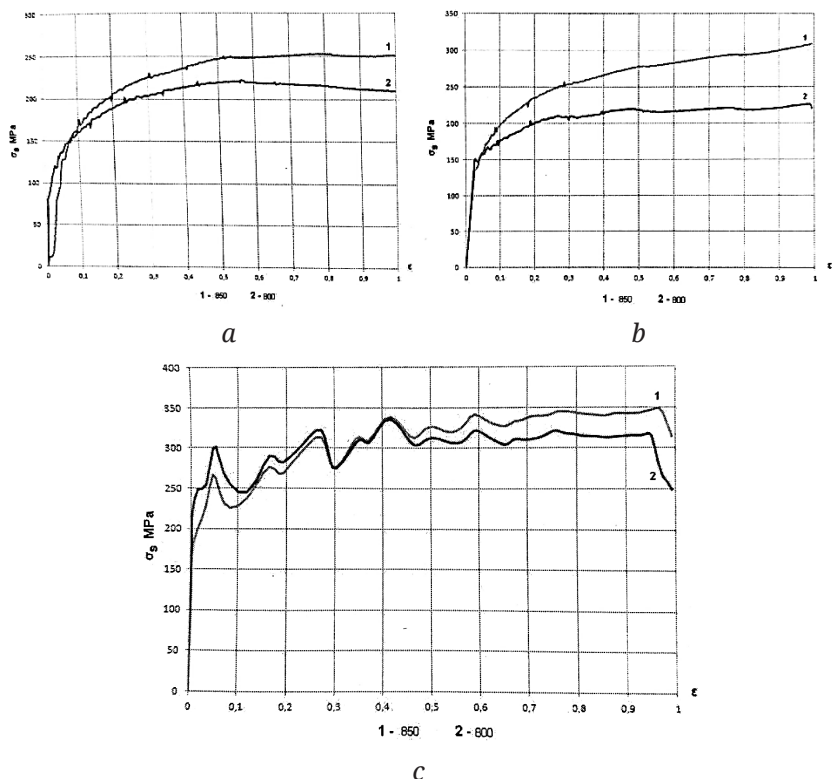


**Figure 3.25** – Dependence of resistance of deformation on speed of deformation: *a* –  $1 \text{ s}^{-1}$ ; *b* –  $10 \text{ s}^{-1}$ ; *c* –  $100 \text{ s}^{-1}$ .

1. New low-alloy steel of 10XΦТБч is worked out and investigational for the wheeled production.

2. Recommendable optimal chemical composition became, the masses, %: carbon – 0,10, silicon – 0,31, chrome – 0,1, vanadium – 0,13, titan – 0,12.

3. The features of plastic forming of new brand are educed became in the conditions of hot-working.

### 3.8 Structural changes of multiphase low-carbon steel in deformation and heat treatment

There are two main industrial methods of producing multiphase carbon steel.

(1) Heating of hot-or cold-rolled steel in the temperature range  $Ac_1$ - $Ac_3$ ; or somewhat above the critical point  $Ac_3$ , with subsequent regulated cooling. With the appropriate choice of steel composition and subsequent heat treatment, we may obtain ferrite-martensite structure with specified properties.

(2) Production of steel by hot rolling, which may be used to obtain steel sheet or coils subjected to regulated cooling after hot rolling [243]. Laboratory experiments and preliminary industrial trials show that this method is very promising (2–4).

In the production of two-phase steel by any method, the factors determining the final structure are the composition, deformation conditions, cooling rate, and final temperature in hot deformation. The influence of the rolling parameters on the structural and phase transformations and on the mechanical properties of the steel is of considerable interest. The influence of the rolling parameters and cooling conditions on the structural and phase transformations in low-alloy steel was considered in [244–247].

#### ***INFLUENCE OF DEFORMATION***

For each steel, we need the appropriate combination of temperature, strain, and strain rate so as to obtain fine-grain austenite structure with highly developed polygonal substructure. With increase in deformation temperature, the subgrains grow and the subboundaries migrate, with greater stability of the substructure. However, on reaching the critical temperatures, there is a risk of dynamic grain growth. The strength of the steel increases as the deformation temperature falls and approaches the point  $A_3$ . Therefore, hot rolling is conducted from 1,150...1,250 °C to temperatures 20...30 °C above  $A_3$ . In that case, the final rolling temperature  $t_{fr}$  is the quenching temperature of the steel.

At the end of rolling, strengthened ferrite may be formed in the two-phase region, and laminar ferrite-martensite structure may appear, with sharp decrease in plasticity and increase in strength of the steel. It makes sense to end the rolling of the steel a little above the critical point  $Ar_3$ , in order to utilize the accelerated ferrite deposition under the influence of the accumulated strain and maintain the decrease in austenite grain size.

Deformation of the austenite shifts the onset of ferrite deposition to the left by 2.5 orders of magnitude while the isolines of  $\gamma$ -phase conversion (corresponding to the formation of an equal quantity of ferrite) are shifted upward, according to the hypothesis in [248]. That yields 85% ferrite in steel with 0.3–0.5% Mo after 10-s residence of the steel strip on the exit roller conveyor, without pearlite formation.

The strain rate must be optimal, since dynamic recrystallization is activated when the strain rate is too high, with loss of thermal stability of the steel structure, and the required strengthening is not attained when the strain rate is too low. The optimal strain (20–40%) will depend on the temperature and strain rate. The use of stepwise deformation as the steel passes through several cells, with total reduction of 20–40%, facilitates deformation, results in more uniform reduction, and promotes dynamic polygonization of the grains. The interval between the cells must be less than the incubation period for recrystallization. In other words, only static recovery must occur in the interval between the cells [249].

### ***INFLUENCE OF COOLING***

After hot deformation, the steel must be sharply cooled so as to retain the substructure and the small grains obtained on deformation. The steel is quenched to martensite, which inherits the structure of the high temperature cold-worked austenite. Low-carbon martensite is fragmented (with developed cellular sub structure) and consists of small grains. The inheritance of the structure of hot-deformed austenite by the martensite may be attributed to the shear processes martensitic transformation, in which one of the close packed planes  $(111)_A$ , is converted to the plane  $(110)_M$ , while the direction  $[110]_A$ , is converted to the

direction  $[111]_M$ . Dislocations that belong to the family  $(111)[110]_A$  in austenite become slip dislocations of the bcc lattice in the  $(110)[111]_M$  family, according to [247]. The dislocation density in the martensite is somewhat greater than after ordinary quenching.

In controlled rolling, the martensitic plates become considerably smaller; their mean width is approximately half that observed after rolling. That leads additional grain boundaries and subboundaries capable of preventing dislocational motion and facilitating stress relaxation, with consequent increase in the resistance to brittle failure. In martensitic transformation, the geometry of the martensitic plates changes. As they grow, the plates encounter numerous structural defects in the austenite crystal, with consequent change in the direction and rate of growth. That reduces the probability that the martensitic plates will reach the grain boundaries, thereby preventing the development of high stress in the boundary regions. That ensures better properties of the steel than quenching.

Various recommendations have been made regarding steel cooling to produce hot-rolled ferrite-martensite steel. Besides the accelerated deposition of 80–85% ferrite, the duration of relatively slow cooling of the steel (at 5...10 °C/s) may be increased to 40 s, and then the two-phase ferrite-austenite structure obtained is subjected to fast cooling, ensuring partial  $\gamma \rightarrow \alpha$  transformation.

In the production of such steel, higher cooling rates ( $V_{co}$ ) of the ferrite may be used (without impairment of the properties) than in heat treatment from the two-phase region, according to [245]. The explanation offered was that the high density of dislocations and other  $d$  [244–247] effects in the hot-rolled steel increases the diffusion rate, with the faster removal of interstitial atoms from the ferrite matrix and their redistribution in the remaining  $\gamma$  phase.

### ***INFLUENCE OF THE WINDING TEMPERATURE***

If the winding temperature  $t_{wi}$  is reduced below the final temperature of pearlite transformation, the quantity of martensite obtained will be equal to the quantity (volume fraction) of residual austenite. For steel with 0.07 wt % C, 1.10 wt % Mn, 0.8 wt % Si, 0.5 wt % Cr, 0.4 wt % Mo, and 0.045 wt % Al, the optimal winding

temperature is  $t_{wi}=500\text{ }^{\circ}\text{C}$ , as shown in [250]. At  $600\text{ }^{\circ}\text{C}$  two-phase ferrite-martensite steel is not obtained. At  $550\text{ }^{\circ}\text{C}$ , it is only obtained in 2.3 mm sheets. Reducing  $t_{wi}$  also prevents bainitic transformation in the absence of molybdenum. For example, on reducing the winding temperature to  $200\text{ }^{\circ}\text{C}$ , such structure is obtained in steel containing 0.15 wt % C, 0.5 wt % Si, and 1.5 wt % Mn (after 50% reduction close to  $Ar_3$ , at a cooling rate of  $40\text{ }^{\circ}\text{C/s}$ ).

Hot-rolled high-performance ferrite-martensite steel containing 0.06 wt % C and 1.4 wt % Mn or 0.06 wt % C, 14 wt % Mn, and 0.7 wt % Si may be produced with  $t_{fr}=700\text{ }^{\circ}\text{C}$  and  $V_{co}=30\text{--}70\text{ }^{\circ}\text{C/s}$  (including direct quenching in oil) if  $t_{wi}\leq 200\text{ }^{\circ}\text{C}$ , as shown in [251, 251]. However, if  $M_r < t_{wi} < t_r$ , accelerated cooling may lead to the partial replacement of ferrite by bainite. Good properties are also observed for steel containing 0.05 wt % C, 2.1 wt % Si, and 2.4 wt % Mn (with  $t_{fr}$  close to  $Ar_3$ , and  $t_{wi} < 600\text{ }^{\circ}\text{C}$ ) [245].

For steel containing 0.05 wt % C, 1.5 wt % Mn, 1 wt % Si, and 1 wt % Cr, we find that the upper critical value of  $t_{wi}$  in order to obtain two-phase structure is  $540\text{ }^{\circ}\text{C}$ . With  $t_{fr}=600\text{--}830\text{ }^{\circ}\text{C}$ , fast cooling ( $V_{co}\ 60\text{ }^{\circ}\text{C/s}$ ) begins. The mechanical properties of 2.9 mm steel sheet containing 0.05 wt % C, 0.8 wt % Mn, 1.5 wt % Si, and 1.4 wt % Cr ( $\sigma_u=620\text{--}650\text{ N/mm}^2$ ,  $\sigma_{0.2}/\sigma_u < 0.6$ ,  $\delta_2 > 30\%$ ) are insensitive to the winding temperature in the range  $t_{wi}=350\text{--}500\text{ }^{\circ}\text{C}$  and to the type of cooling (directly after rolling from  $860\text{ }^{\circ}\text{C}$ ). With increase in manganese content, the initial cooling temperature must approach  $t_{wi}$ . For steel containing 0.09 wt % C, 1–1.5 wt % Si, and 0.8 wt % Mn, the recommended conditions are  $t_{fr}=800\text{--}850\text{ }^{\circ}\text{C}$ ,  $t_{in.co}=750\text{ }^{\circ}\text{C}$ ,  $V_{co}=80\text{ }^{\circ}\text{C/s}$ , and  $t_{wi}=500\text{ }^{\circ}\text{C}$ .

### 3.9 Formation of polygonized structures and nuclear recrystallization under controlled rolling of low carbon steels

Formation of the fine structure of alloys is an actual problem of modern materials science that the industrial production of various products of wide use face. Most of these products are made by hot and cold rolling, forging, stretching and drawing. This raises

questions from related areas of knowledge solid-state physics, metal physics and mathematics, namely, where the first nuclei of new phases originate in this material, which physical parameters are most significant when the grain boundaries appear and interact. Such (and many other) questions materials scientists have while developing the new advanced technologies [252, 253].

One of the objectives of the presented work was to study the mechanisms of the influence of the block structure formation during hot plastic deformation of low carbon 10XФТБЧ type steels to increase the strength and ductility of rolled steel.

Structure research methods. Transmission diffraction electron microscopy and microdiffraction were used to study the structural state of steel. These methods allow obtaining quantitative data on the lattice defects and the nature of its development with increasing degree of deformation. Light quantitative and high-quality metallography were used as well. These methods capable of providing overall picture of structure formation over large areas microsections that is not available for electron microscopy of foils with its ultra-high locality.

Light metallography was performed on the Neophot-2 microscope with the “H-100×0.95” immersion objective lens and the “Olimpus-C-350Z” camera. Metallographic sections were prepared according to the scheme: cutting – grinding – mechanical polishing – electrolytic polishing.

The study of the location interaction of low-angle (polygonal) and high-angle special borders in the concept of coincidence site lattice (CSL) was carried out in direct and oblique illumination, since under direct illumination not all elements of the grain-boundary network are clearly identified. In the photographs shown in Figure 3.26, taken under direct (*a*) and oblique (*b*) illumination, some special boundaries are visible only in one of them (Fig. 3.26, *b*, shown by arrows). Therefore, the responsible plots of grain-boundary ensembles, the decoding of which requires the visualization of all links of the grain-boundary network, were photographed under four lighting conditions: in one direct and in three oblique – 120° from each other. This technique makes it possible to record the manifestations during the subsequent

processing of the footage more fully – all satisfactorily etched boundaries [3, 4, 5].

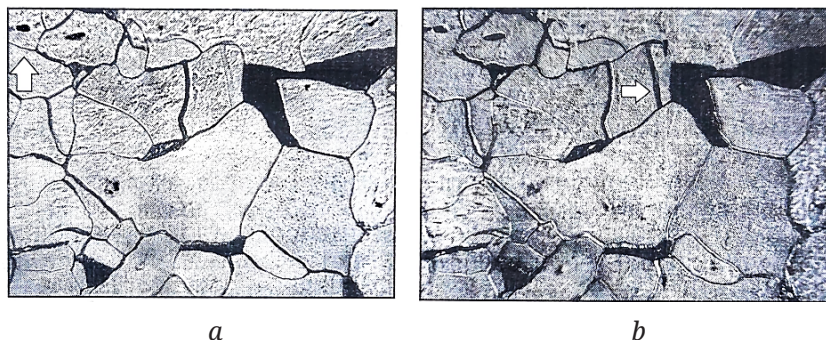


**Figure 3.26** – The influence of the direction of illumination on the identification of some large-angle grain boundaries in steel:  
*a* – direct illumination; *b* – oblique illumination  $\times 360$

Electron microscopic studies were performed on the EM-125 device with the accelerating voltage of 100 kV, the chamber length was 510 mm, the selector diaphragm was 1.5  $\mu\text{m}$  in diameter in the scale of the sample.

Thin foils were prepared according to the following scheme: cutting along the rolling direction – rod with the diameter of 3.2 mm – disc section with the thickness  $\delta=0.25$  mm – leveling on thin abrasive paper – chemical thinning in aqueous hydrogen peroxide solution to the thickness of 0.1 mm electrolytic thinning in chrome-acetic electrolyte, in an open magnetic micro suspension – mounting on the “duble-greed” – storage in gelatin capsules with a diameter of 4 mm.

Thermomechanical treatment was carried out under industrial conditions on a sheet-rolling reversing mill in line with the following mode: heating the billet to 1,200  $^{\circ}\text{C}$   $\rightarrow$  time exposure for 5 hours  $\rightarrow$  rough rolling at the decreasing temperature to 950  $^{\circ}\text{C}$   $\rightarrow$  cooling (subcooling) on the roller table to the selected intercritical interval temperature (ICI): 900...700  $^{\circ}\text{C}$   $\rightarrow$  finish rolling (7–12 cycles of 5–10%) for grinding the grain of proeutectoid ferrite and forming a dispersed grain-sub-grain structure  $\rightarrow$  air cooling. An alternative

option is accelerated cooling (quenching) from ICI temperatures for substantial metal hardening. Under production conditions, there is a need for careful selection of hot deformation modes for each new steel grade or even for different melting options or casting methods, since the temperature range of critical points and the redistribution of carbon leads to significant fluctuations in mechanical properties, in particular, impact strength at lower temperatures [6, 7, 8].

Microstructure samples were taken for research as the total strain rate accumulated at the points  $\varepsilon=9.4, 21.2, 29.5$  and  $39.0\%$  at final deformation temperature of  $750, 770, 800$  and  $900\text{ }^{\circ}\text{C}$ .

***The results of the study of the dislocation, grain-boundary and polygonised***

In this work, the focus was on samples, the deformation of which ended at temperatures of  $750$  and  $850\text{ }^{\circ}\text{C}$ , since they correspond to the lower part of ICI, when up to  $40\text{--}65\%$  of ferrite is separated and subjected to deformation) from the structure. Then, the strain hardening of the low-strength steel component (ferrite) is realized. Therefore, it is important to obtain the true mechanisms of structure formation in the period when dislocation inflow ends and polygonization and recrystallization of ferrite begins (or rather continues), and  $\gamma \rightarrow \alpha$  transformation of residual austenite proceeds.



*a*



*b*

**Figure 3.27** – Structure of hot-rolled steel 10XФТБЧ.  
Final deformation temperature ( $^{\circ}\text{C}$ ): *a* –  $750$ ; *b* –  $770$ ,  $\times 360$

Figure 3.27 shows the structures formed in the final “tongue” of the strip 3 seconds after the end of the last deformation cycle

and accelerated cooling of its surface to 600 °C. It is established that a large part of the ferrite has a polygonised structure, but in a quantitative sense, it is much less (after deformation), than it follows from the iron carbon diagram (Fig. 3.27, *a*). The balance is off by numerous ferrite grains free from polygonal structures, partially or completely surrounding the pearlite colonies (Fig. 3.27, *a, b*). This means that they are:

- formed after deformation (internal volumes are free from substructure);
- not the result of short-term subcooling down to 600 °C (they have an equiaxial, not Widmannstätt form);
- are not recrystallization nuclei, since, according to von Neumann Mullins criterion, the number of sides of an embryo grain capable of free growth should be more than six.

Both von Neumann and Mullins proceeded from the assumption that all boundaries are the same, that is, they are uniform in their atomic structure, physical and mechanical properties. Although this is not always the case, we will assume that polygonal (subgrain) boundaries exhibit the same properties and obey the von Neumann-Mullins criterion [9, 10, 11].

Three special cases attract attention, when on one border of ferritic grains from one joint to another, both positive curvature and negative are observed (marked in Fig. 3.28). Such boundaries also indicate a gradual transition of the embryo to the high-angle grain boundaries category.

If we imagine the embryo as circles equal in area to the corresponding polygons and sub-grains as circles with diameters  $d_{\text{sub}}$ , then we get a clear idea of the nature of the development of recrystallization nuclei in a polygonized hot-deformed matrix (Fig. 3.29).

Such conventional representations of recrystallization nuclei look even clearer if they are placed in the form of concentric circles.

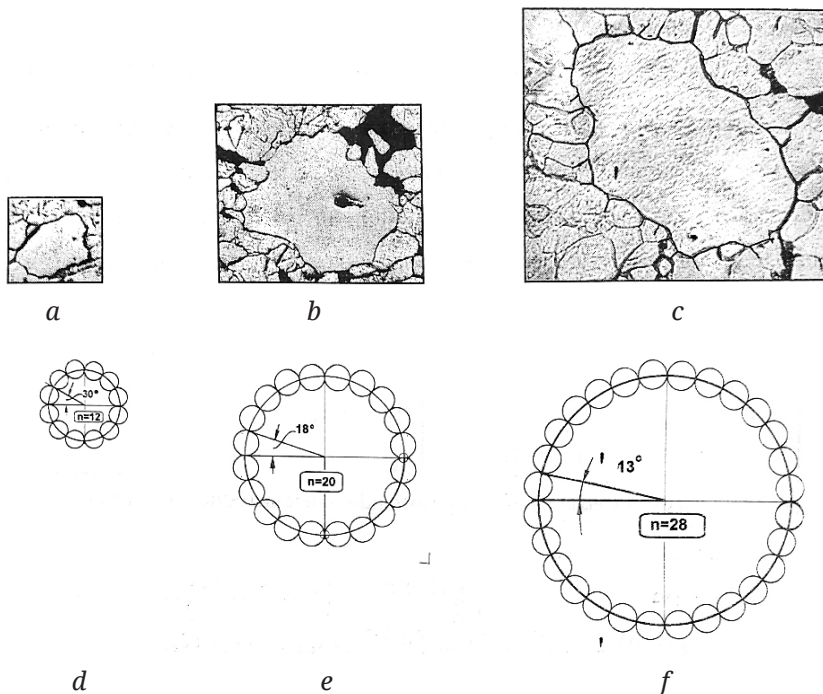


**Figure 3.28** – Comparison of the real structural situation in the area of recrystallization nuclei in polygonized hot rolled 10XΦТБЧ steel with idealized models for spherical polygons and nuclei with different numbers of sides ( $n$ ): *a, d* – 12; *b, e* – 20; *c, f* – 28; *a, b, c* – photographs reduced to the same scale; *d, e, f* – conventional representations of the interaction of spherical nuclei with the spherical subgrains boundaries

While the embryos grow in size, sub-grains also grow in diameter, although their angular size is conventionally reduced.

1. Comparisons have been made of the real structural situation in the area of recrystallization of hot rolled 10XΦТБЧ steel with idealized models for spherical polygons and embryos with different numbers of sides.

2. It has been shown the role of special grain boundaries in the proeutectoid ferrite of low carbon steels on the formation of their structure and properties.

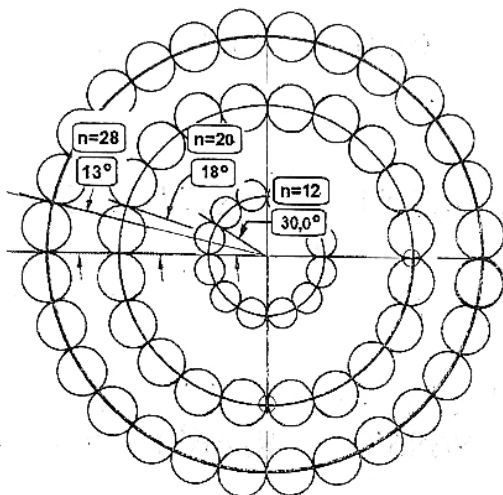


**Figure 3.29** – The combined image of the embryos development and surrounding polygons in the process of recrystallization of hot-deformed ferrite steel

### 3.10 Formation of the grain boundary structure of low-alloyed steels in the process of plastic deformation

Modern material science solves many technological problems facing the industrial production of a variety of products for a wide range of purposes, most of which are manufactured by hot and cold rolling, forging, extrusion, drawing, etc. At the same time questions arise from related fields of knowledge such as solid-state physics, mathematics namely, where the first nuclei of new phases appear in a given material, what physical parameters are most significant in the manufacture of products by hot deformation. In particular when improving the technology of controlled rolling with the aim of improving the strength and plastic parameters of

rolled metal, it is important not only to obtain fine grain of ferrite in the structure, but also to trace its development from the initial to the final stage of deformation under different temperature and time conditions.

The task of the present work was to refine the available data as well as to obtain the new data on the formation of a block (polygonal) structure under controlled rolling of low-carbon steels 10Г2ФБ and 10ХФТБч (Standard of Ukraine) to increase the strength and ductility of rolled products.

Deformation-thermal treatment was carried out under industrial conditions on the double-stand rolling mill according to the experimental controlled rolling regime; heating of the billet to 1,200 °C → homogenization for 5 hours → rough rolling ( $\epsilon \approx 40\text{--}50\%$ ) with a temperature dropping to 950 °C → technological cooling (subcooling) in air up to the chosen temperature of the intercritical interval (ICI): 900...700 °C → finish rolling (7–12 cycles of 5–10%) for grain grinding of the precipitated eutectoid ferrite and formation of dispersed grain-subgrain structure → cooling in air.

A fine structure was studied on a transmission electron microscope – EM-125 with an accelerating voltage of 100 kV, a camera length of 510 mm, a selector diaphragm with a diameter of 2.5  $\mu\text{m}$  on a sample scale. Thin foils were prepared by cutting the bar across in the direction of rolling and recessing the rod with a diameter of 3.2 mm from it according to the disk technique.

The light metallography is made on a Neofot-2 microscope with an immersion objective “H-100 $\times$ 0.95” and a digital camera “Olimpus-C-350Z”. Sections were prepared according to the traditional technology, but with mandatory electropolishing (removal of a layer of work-hardened metal 10–20 microns thick).

In the work, the main attention was paid to samples whose deformation ended at temperatures of 750 and 770 °C, since they correspond to the lower part of the ICI, when up to 80–85% of ferrite is precipitated (and deformed) in the structure and the deformation hardening of the ferrite – the low-strength component of steel, is implemented. That is why it is important to obtain the details of the structure formation during the period when the incoming of dislocations is over and the polygonization and recrystallization

of ferrite begins (or rather continues), as well as the  $\gamma \rightarrow \alpha$  transformation of the residual austenite.

The method of microdiffraction [252] allows obtaining approximate information about next quantities:

- $\phi$  – the angle of azimuthal blurring of reflexes in a certain area. In our case, it is  $2.5 \mu\text{m}$  – the diameter of the selector diaphragm;

- $\phi'$  – the misalignment angle on one medium subboundary  $\phi_{\text{sub}}$ ; the result of dividing the total blur angle ( $\phi$ ) by the number of subreflexes  $k$  in one full reflex,  $\phi' = \frac{\phi}{k} = \phi_{\text{sub}}$ ;

- $d_{\text{sub}}$  – the size of subgrains (the average chord) located in the analyzed area.

The results for the samples deformed at  $770^\circ\text{C}$  and cooled in air are shown in Fig. 3.30.

The structure of the strip, which received the maximum degree of deformation ( $\varepsilon=42\%$ ), was fixed by quenching in parts: the first in 3 seconds, the second after 30 seconds, the third after 300 seconds of time-exposure.

The data shown in the diagrams (Fig. 3.30) show that with increasing of  $\varepsilon$ :

- the azimuthal disorientation angle is increased, and, as a result, the partial angle  $\phi_{\text{sub}}$  on a single subboundary is increased as well;

- subgrains are reduced to  $3 \mu\text{m}$ .

During the time-exposure:

- the azimuthal disorientation angle  $\phi$  is decreased, the post-deformation polygonization process begins;

- the azimuthal disorientation angle on a single subboarder  $\phi' = \phi_{\text{sub}}$  is decreased;

- the sizes of subgrains are increased to  $6 \mu\text{m}$  and their quantity is decreased.

The results of the study of grain-boundary and polygonized structure and nucleation in hot-deformed ferrite. Fig. 3.31 shows the general structure formed in steel after 300 sec after the end of deformation and cooling in air.

SECTION 3  
Structural changes during deformation and heat treatment of metals

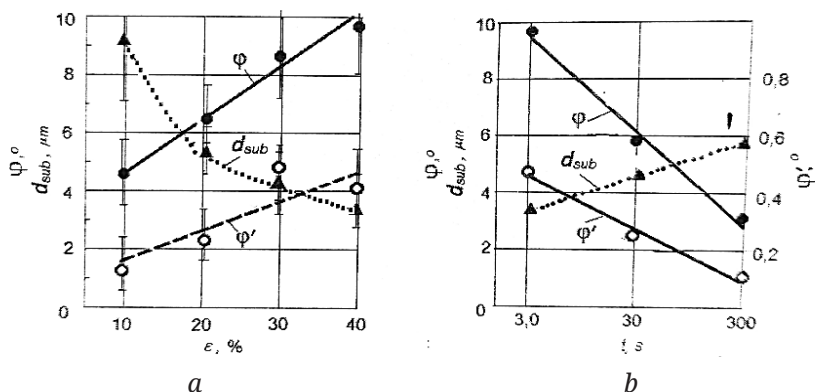


**Figure 3.30** – Characteristics of the subgrain structure of the hot-deformed ferrite after rolling at 770 °C and cooling in air: *a* – changing of  $\varphi$ ,  $\varphi'$  and  $d_{sub}$  from the degree of hot deformation; *b* – the same parameters in the post-deformation period

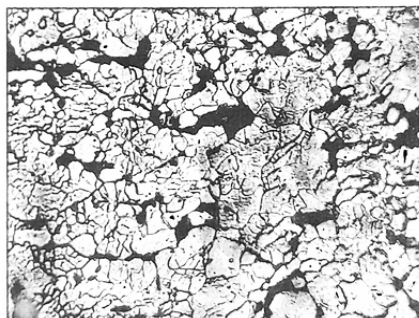


**Figure 3.31** – The structure of the hot-rolled steel 10XΦТБч (Standard of Ukraine)

The end-of-deformation temperature is 750 °C, the time-exposure is 300 sec [253, 254]. It is noteworthy that the biggest part of ferrite has polygonized structure, but some larger subgrains are free from dislocations, that is, they are potential nuclei of recrystallization. In the structural sense, this phenomenon has not been completely investigated [255]. From the von Neman-Mullins concept, such grains are capable of growth if the number of sides  $n$

is more than six. In their reasonings, both von Neumann [256] and Mullins [257] proceeded from the assumption that all the large-angle boundaries are the same, that is, there is uniformity in terms of atomic structure, energy intensity and tension forces. Although this is not always true, we assume in this case that the polygonal (subgraine) boundaries exhibit similar properties and also obey the von Neumann-Mullins criterion based on the equilibrium of tension forces in triple junctions lying on the perimeter of  $n$  sides. Such approach is successfully used by researchers in their works [7], studying the interactions of the large-angle and subgrain boundaries.

In Figure 3.32, *a*, a subgrain with a number of sides of at least 12 is observed in the central part.

The internal angles between tangents to the boundary lines in triple junctions of polyhedral formations (nuclei) with the number of sides  $n=12$  (No. 49);  $n=20$  (No. 44) and  $n=28$  (No. 52) in 10XΦТБч steel (Standard of Ukraine) after hot rolling at 770 °C and cooling in calm air for 300 seconds were investigated (detected and measured).

At the same scale, these grains are shown in Fig. 3.32, *a, c, e*. The corresponding schematic maps are shown in Fig. 3.32, *b, d, f*. Next to the diagrams are tables of angles located on the numbered joints of the inner side of the growing grain (Fig. 3.33, *b, d*). The curvature of the boundaries between the junctions was also considered, the arrows indicate the direction to the center of the curvature of the boundary, that is, the direction of its migration at a given moment.

Some morphological features of these subgrains-nuclei are revealed as the number of sides in them increases.

Grain No. 49 grows, the curvature centers of most segments are directed outwards, therefore the area increases in size, although on the sections A, B and C the boundaries are fixed by relatively large particles of special carbides. It can be assumed that these particles are not random, since they tend to repeat the bends of the growing polygon, and the film morphology, increased etching confirm that the carbides precipitate at the forming boundaries, and not the boundaries are stopped by the already formed particles. In addition, it should be taken into account that Suzuki's carbon atmospheres exist on the subgrain boundaries, and the growing grain, while

SECTION 3  
Structural changes during deformation and heat treatment of metals

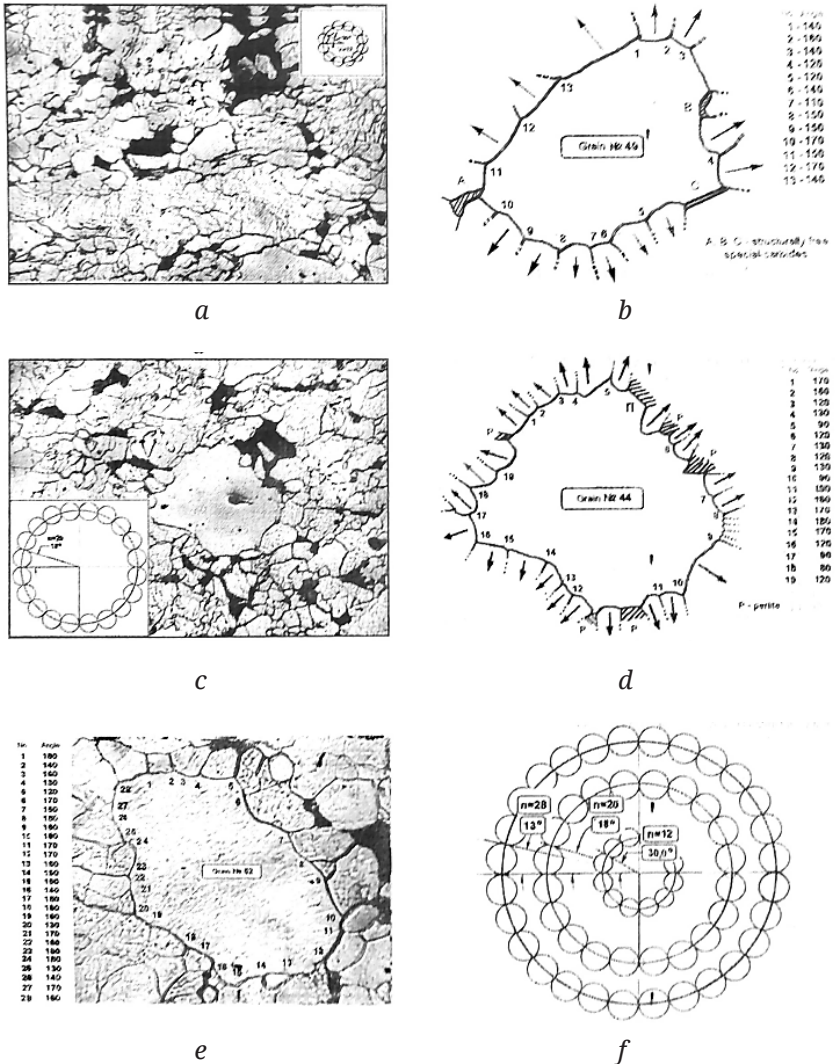


**Figure 3.32** – Enlargement of individual subgrains with an increased number of sides and the results of measurements of internal angles in triple junctions: *a, c, e* – images of polyhedral nuclei; *b, d, f* – schematic map of nuclei

absorbing polygonal boundaries, releases carbon and displaces it to the outside of the nuclei. Therefore, in the initial hot-deformed ferrite, near the perimeter of the nuclei, local microinhomogeneities supersaturated by carbon commensurate with the size of the polygons appear. As the “non-carbon” nucleus grows, the migrating nucleus-matrix border is enriched with carbon and at some point a cementite particle nucleates that rapidly grows along the most large-angle segment of the boundary until all excess carbon is spent on building a cementite single particle [8].

A similar phenomenon accompanies practically all growing nuclei, they can be seen in the figures containing nuclei, but they are almost not observed in the final, completely recrystallized ferrite-pearlite mixture.

The measurements showed that there are only two equilibrium 120-degree joints (see the table in Fig. 3.32, *b*). This means that the inner boundaries of the nucleus in the majority already differ from the small-angle subgrain boundaries, by their greater tension, as their misalignment angles have already been increased by “inheriting” misalignments of the surrounding outer (already absorbed) polygon subboundaries.

Grain No. 44 (Fig. 3.32, *c, d*) contains 20 border segments that tend to move to the outside increasing the size of the subgrain nucleus, although along the inner perimeter there are five more segments belonging to pearlite colonies, which, as is known, do not move under the effect of the tension of external intraphase subboundaries or large-angle boundaries. The center of curvature of the segment 8–9 is located (at first glance!) inside the grain, but with a larger magnification, it is revealed that the segment 8–9 consists of five smaller segments that are turned by the centers of curvature to the outside. When analyzing 20 triple junctions it turned out that the number of 120-degree joints increased to 5, in addition, one 180-degree joint appeared (No. 14). Its appearance indicates the presence of two large-angle high-energy boundaries on the section 13–14–15 (Fig. 3.32, *c, d*), which confirms the validity of coalescence mechanisms of the subgrains rotations during the formation and growth of nuclei of recrystallization of hot-deformed metals [9].

Grain no. 52 is the largest (Fig. 3.32, *e, f*), 28 triple joints were analyzed in it, which do not contain inner angles of less than 120 degrees, but contain 180 degrees angles (five cases). This means that the number of boundaries with an extremely high tension (with a large specific surface energy) increased, and the grain is a full member of the network of large-angle boundaries. Both positive and negative curvature were observed. Such boundaries also indicate a gradual transition of the nucleus to the category of large-angle grain boundaries.

The development of nuclei can be traced on the histograms of the distribution of inner corners opposing the outer small-angle subgrain boundaries (Fig. 3.33). They are constructed on the basis of the analysis of a small number of cases in each individual experiment, as the number of sides is limited by the very nature of nucleation. Despite this, the nuclei contain interesting information about the nuances of migration and the interaction of small-angle and large-angle boundaries during the recrystallization of hot-deformed materials.

The lower limit of cases is limited to 7, that is, the number that is theoretically required by the Neumann-Mullins concept for a growing nucleus. It is obvious that the theoretical diagram for a 6-sided "nucleus" will have a peak (mode) of 120°, (Fig. 3.34, curve 1).

The histogram of grain No. 49 (Fig. 3.34, curve 2) shows that the angles are distributed uniformly within 100...170 °C, and the peak is located at 140 °C, which shows a significant increase in misorientation at the boundaries of the nucleus, but their tension is not much different from tension of polygonal boundaries.

It should be recognized that even at this early stage the nucleus already has an individuality, almost all its boundaries are distinguished by more significant misalignment angles and generating capacity.

On the assumption of the larger the nucleus, the longer was its existence, it can be seen that the early formed grain No. 44 containing 20 sides exhibits a somewhat unexpected distribution of internal angles with two modes at 120 and 170 °C (Fig. 3.34, curve 3). If we take into account that the peak is observed at around 160 °C for grain No. 52 (Fig. 3.34, curve 4), while 120 degree joints are not even

observed, it becomes clear that the large nucleus has practically reached the limiting state, contains only large-angle boundaries, it is surrounded only by small polygons, so if it grows, it happens very slow, while nucleus No. 44 is at the intermediate stage of development, when full-scale large-angle boundaries have already appeared (170-degree peak), and low-energy segments of boundaries (120-degree peak) are still encountered.

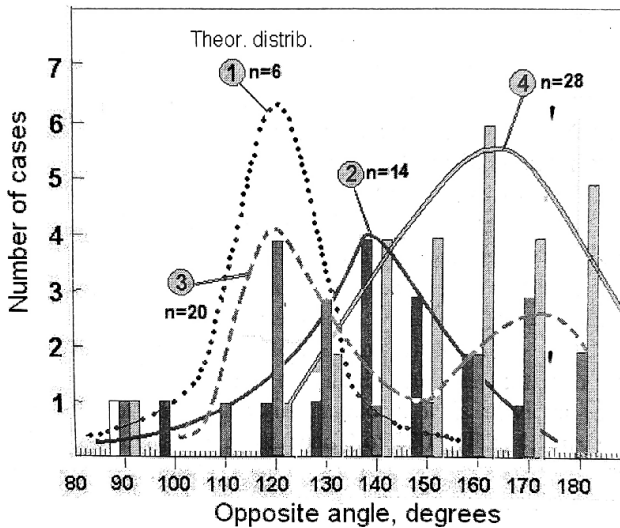


**Figure 3.33** – Development of the nucleus of recrystallization in hot deformed ferrite after deformation. Each grain is represented by its histogram

If the nuclei are represented by circles that are equal in area to the corresponding polygons and the subgrains are also circles with a diameter  $d_{sub}$ , (see the insets in Fig. 3.33, a and 3.33, c), we get a clear idea of the nature of the development of the recrystallization nuclei in the polygonized hot-deformed matrix (Fig. 3.33, f).

1. Based on theoretical and experimental studies, a methodology and a scheme for the formation and growth of nuclei of the recrystallization of ferrite grains in a polygonized structure of ferrite-perlite steels after controlled rolling are proposed.

2. New data was obtained on the dependence of the parameters (misalignment angles and sizes of subgrains) of the block (polygonal) structure on the degree of deformation during hot rolling of 10Г2ФБ and 10ХФТБч steels, as well as their behavior during time-exposure after the end of deformation.

3. The development allows us to predict the processes of recrystallization and the formation of mechanical properties at the hot deformation of ferrite-pearlitic steels.

4. It is shown that the hardening of the rolled stock of ferrite-pearlite steels can also be achieved by forming a rational grain-boundary structure, by forming special grain boundaries during thermoplastic treatment.

### **3.11 Structural changes in corrosion-resistant steel**

Recently, plates made of corrosion-resistant chrome steels are more often being used in the construction of articles whose manufacture is associated with a high degree of cold working. However, anisotropic deformation occurs and the steel has little stampability which limits its applications. This makes it necessary to use the more expensive chrome-nickel or chrome-manganese steels of the austenitic class. It was established during detailed studies on the cold working of corrosion-resistant steels that the austenitic steels have several advantages over other types during dual and single axial extension. Anisotropic deformation causes increased surface roughness of articles with decorative finishes. This requires additional labor in order to remove these defects.

Anisotropic deformation in steels of the ferritic and martensitic-ferritic class is significant and arises at lower levels of deformation than in the austenitic steels.

It is known that the appearance of anisotropic deformation depends, not only on the nature of the metal, but also on its structural state. Consequently, in order to increase plasticity and decrease anisotropic deformation of steel 06Kh18ch one can increase the uniformity of its structural state.

An analysis of test results carried out using traditional technology of metallurgical processing showed that changing the ingot rolling regime, and then of the slabs, has little effect on the properties of the metal. The formation of the structure and basic properties of steel 06Kh18ch occurs at a later stage in the technological processing: hot-rolling of the plate (semifinished rolled products) and its further processing.

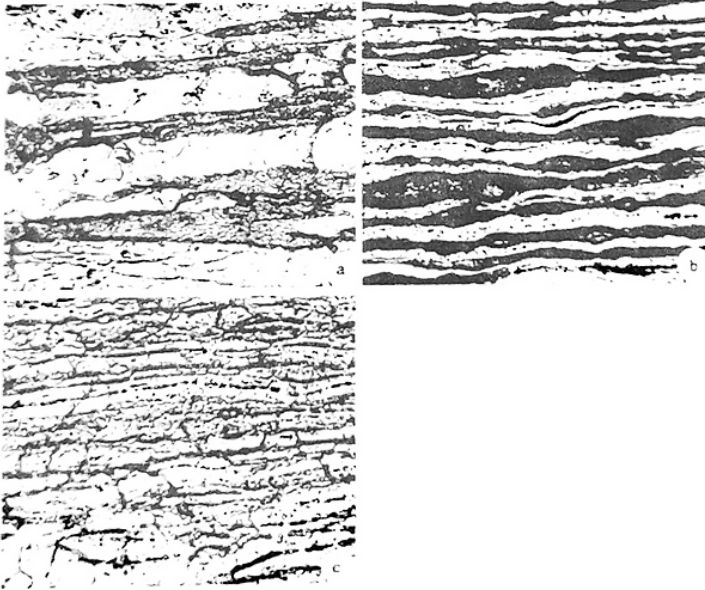
It was established that the temperature of the final rolling 850...950 °C does not always ensure that there will be complete recrystallization of the rolled products as a result of its rapid cooling before reeling in the rollers. And independent of the fact that the temperature of the metal in the rollers remains high for a substantial period of time (500...700 °C), its structure shows little change.

Therefore, the structure of steel before cold rolling is nonuniform and consists of structurally free ferrite and small amounts of low-carbon martensite, or the decomposition products of the austenite (Fig. 3.34, *a*).

The hardness of hot-rolled bands is 85–92 HRB and is determined by the temperature of the final roll1 (Fig. 3.36) and the chemical composition of the steel within the limits of the technological conditions (mainly the concentration of carbon). The final cold-rolling of the semifinished product with a nonuniform structure often leads to the formation of torn edges and rips in the cold-rolled bands.

Form changes in the metal during rolling are to a large degree a result of plastic deformation in the ferritic component (see Fig. 3.34, *b*). Such inhomogeneity in the deformation during rolling causes a nonuniform crystallographic orientation of the crystals in the cold-worked metal after the recrystallization heat treatment. In order to decrease the hardness of the semifinished rolling and to improve its structure before cold-working, various preliminary heat treatment regimes were tried: anneal at 760...780 °C or harden in a transition furnace in the temperature interval from 820...970 °C for 2–3 min. The holding time is chosen to approximate the working conditions of the hardening unit of the cold-rolling department of the “Zaporozhstal” complex.

SECTION 3  
Structural changes during deformation and heat treatment of metals



- 1) hot rolled; 2) the same as 1 followed by cold-working to  $\epsilon=60\%$ ;
- 3) the same as 2 followed by a final recrystallization anneal; 4) the same as 1 followed by a preliminary (before heat treatment) cold-working to  $\epsilon=20\%$ ;
- 5) the same as 4 followed by cold-working to  $\epsilon=40\%$ ;
- 6) the same as 5 followed by a recrystallization anneal

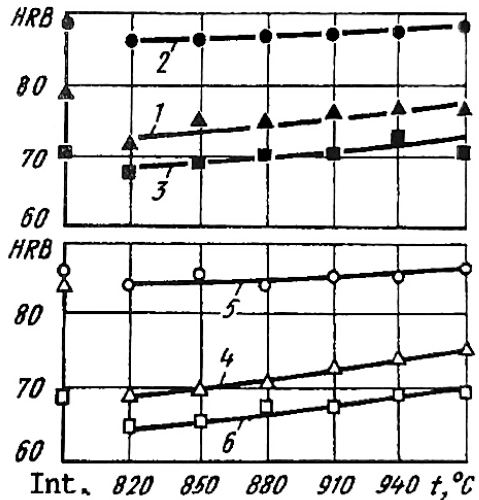


**Figure 3.34** – The hardness of metal-lurgically processed steel 06Kh18ch as a function as a function of the temperature of pre liminary heat treatment

As a result of the studies, it was established that the optimum heat treatment regime for the semifinished rolled products is the hardening treatment at 820...850 °C (holding for 2–3 min) or annealing at 760...780 °C in the bell furnaces. However, annealing worsens the etchability of the bands. The hardness of the semifinished rolled products was from 79 HRB to 70–71 HRB (Fig. 3.35). The structure consisted of grains of recrystallized structurally free ferrite (light-field component) and isolated finely dispersed ferrite-cementite mixtures (dark-field component) (Fig. 3.36, *a*). With increase in temperature to 880 and 970 °C, the hardness of the metal increases to 74 HRB and 77 HRB respectively, and the structure becomes similar to the initial since the partial  $\alpha \rightarrow \gamma$  transformation in this steel occurs at 870 °C (see Fig. 3.34, *a* and Fig. 3.34, *d*). The cold-rolling which follows, both with and without a preliminary heat treatment, occurs as a result of plastic deformation of the ferritic component. The structure consists of structurally free ferrite grains which are extended along the rolling direction. These are alternated with wavelike regions of low-carbon martensite (Fig. 3.36, *e*).

The structure of the steel which has undergone preliminary heat treatment over the optimum regime followed by cold-working consists of grains of structurally free ferrite extended along the rolling direction. This ferrite forms as a result of separation of the decomposition products and alternates with the carbides (see Fig. 3.36, *b*).

In order to determine the optimum process regime, an intermediate rolling of the semi-finished products was carried out to a thickness of 3.0 mm with a preliminary heat treatment over the optimum regime. Judging from the hardness and the structural state of the steel, such a treatment is the most preferred (see Fig. 3.34). However, an additional alkaline-acid etching process is required which complicates and increases the expense of cold-rolling plates.

The structure of the steel after cold-rolling of the semifinished products to a given thickness followed by a final recrystallization anneal (without any intermediate treatment) consists of relatively fine-grained recrystallized ferrite with a segregation of the coarse carbide inclusions primarily to the grain boundaries (see Fig. 3.34, *c*

and Fig. 3.36). A similar structure is seen in steels that have the intermediate treatment in the interval from 880...970 °C (see Fig. 3.35, *f*).

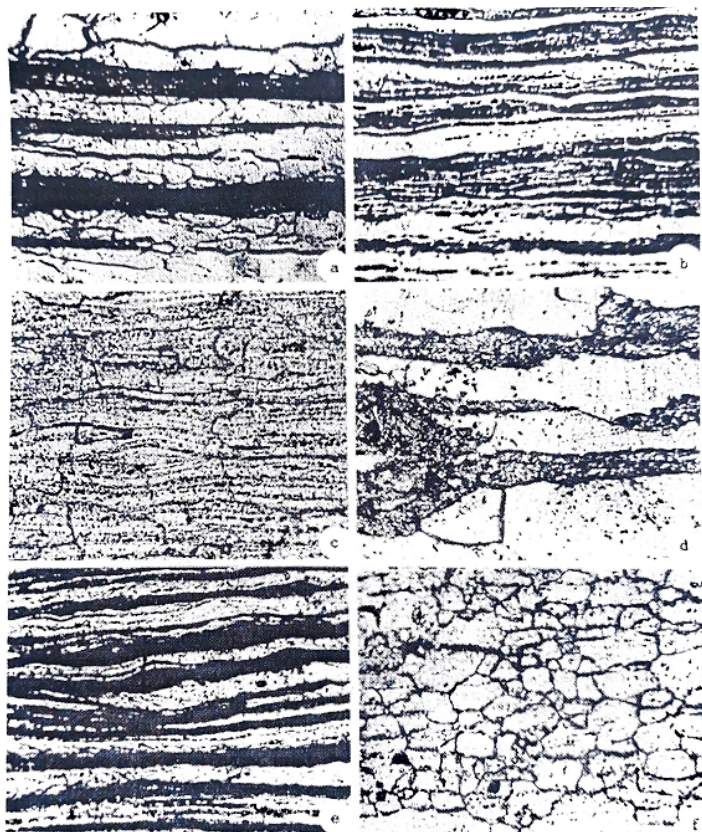


**Figure 3.35** – The microstructure of steel 06Kh18ch at various stages of the treatment with preliminary heat treatment over the optimum regimes (*a–c*), and at higher temperatures (*d–f*).  $\times 800$

The preliminary heat treatment of the semifinished products over the optimum regime ( $t=820$  °C) facilitates a decrease in the hardness in the cold-rolled state to 65 HRB, and forms a fine-grained structure of ferrite with a uniform distribution of the carbides

(see Fig. 3.35, c). The final recrystallization anneal of the cold-rolled plates was carried out in accordance with the diagram given in Fig. 3.36 [258].

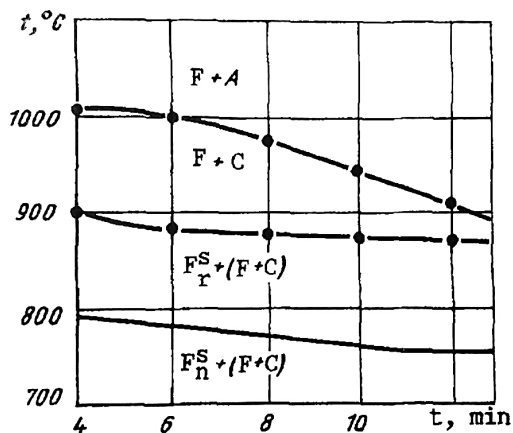


**Figure 3.36** – Diagram of the structural components of steel 06Kh18ch used to choose the recrystallization heat treatment regimes of the cold-worked metal: F + A) ferrite and austenite; F + C) ferrite and carbide; F<sub>r</sub><sup>S</sup> structurally free recrystallized ferrite; F<sub>n</sub><sup>S</sup> nonrecrystallized ferrite

The application of a preliminary heat treatment to the plates of corrosion-resistant steel 06Kh18ch significantly improved their mechanical properties. For example, the ductility increased from 35 to 40–50%, and the hardness decreased to 65 HRB.

The increased ductility of the steel has a beneficial effect on its stampability. Also, the appearance of anisotropy in the deformation only occurs at intense levels of deformation  $\epsilon=0.22$  as opposed to  $\epsilon=0.175$  (without a preliminary heat treatment of the product).

The elimination of anisotropic deformation, which arises in steel 06Kh18ch during the preparation of table instruments, permits us to recommend it in industrial production.

### 3.12 Structure and properties of the corrosion-resistant sheet steel 06Kh18ch alloyed with rare-earth metals and calcium

The nickel-free, ferritic, corrosion-resistant steels 08Kh18T1, 08Kh17T, and 08Kh18F2T alloyed with titanium possess high corrosion resistance and good mechanical properties. However, titanium oxides and carbonitrides in their structure decrease their formability, and especially their response to polishing.

As was stated in works [259–261], rare-earth metals (REM) influence the ferrite formation in steels. The present work studies the influence of rare-earth metals and calcium additions on the structure and properties of corrosion-resistant, high-chromium steel 08Kh13. Ferrocerium FTsM-5 and silicocalcium SK30 were used for alloying. Laboratory melts were produced in an induction furnace of 4–8 kg capacity, and cast into ceramic molds at 1,620 °C. Rare-earth metals and calcium were introduced into the steel before casting. Castings were heated to 1,000 °C and forged with a pneumatic hammer into sheet bars 150 mm thick, which were then rolled in a laboratory rolling mill at 1,250 °C into sheets 3.8 mm thick. After etching with alkali and acid, the hot-rolled sheets were cold rolled in a laboratory rolling mill to sheets 0.8 and 1.0 mm thick, using the deformation rates customary for the “Zaporozhstal” works. The sheets were then normalized at 920 °C, followed by etching with acid and alkali.

To study the metallographic structure of the castings, the optical microscope MIM-8M was used. gent. type. Cross sections were first mechanically polished, then etched with Vilella’s reagent. Mechanical properties were determined with a tensile testing machine of the “Avery” type. Erichsen cupping tests were made with a machine of the “Erichsen” type on 0.80-mm-thick sheet specimens. To assess the polishing properties quantitatively, nonmetallic inclusions and carbide particles were counted using a linear intercept method [262]. Inclusions were counted using the metallographic microscope MIM-7, equipped with an eyepiece micrometer with cross-hair graticules and 100 scale divisions. After measuring the number and size of inclusions, the index of the metal

impurity content was calculated as the sum of the inclusion lengths divided by the total length spanned in the counting

$$I = \sum \frac{m_i a_i b}{l}, \quad (3.14)$$

where  $m_i$  is the average size of inclusions of a certain size group measured in divisions of the micrometer;  $a_i$ , number of counted inclusions of that size group;  $b$ , length of one micrometer division,  $\mu\text{m}$ ; and  $l$ , total length of counting,  $\mu\text{m}$ .

Resistance of the steel to intercrystalline corrosion was measured by the recommended method of AM GOST 6032-58. Microhardness was measured with a PMT-3 tester, using a load of 0.02 N. Distribution of the carbide phase was studied with the electron microscope UEMV-100A, using carbon replicas.

Metallographic studies of the as-cast 08Kh13 steel with different additions of ferrocerium FTsM-5 detected nucleation and growth of the ferrite phase along the martensite grain boundaries (Table 3.12).

Alloying with rare-earth metals causes an increase in the elongation of steel 08Kh13 due to formation of ferrite in the structure, mainly along the grain boundaries (Fig. 3.37). Microhardness tests on the dark and light phases of 08Kh13 steel alloyed with rare-earth metals confirmed the presence of ferrite along martensite grain boundaries (Fig. 3.37, c). The ferrite phase was not detected if calcium alone was used as an alloying element for 08Kh13 steel. However, the introduction of calcium in proportions 1.0–1.5 to the rare-earth metals improves the fluidity and deoxidation of the steel, thus assisting the absorption of rare-earth metals in the steel. The optimum alloying addition of rare-earth metals (by calculation) is considered to be 0.4–0.6%. Taking into account some technological aspects of manufacture, in particular, “pulling-in” of the steel stream during the casting process, it was necessary to reduce the alloying addition of rare-earth metals to 0.3–0.4% (by calculation).

SECTION 3  
Structural changes during deformation and heat treatment of metals

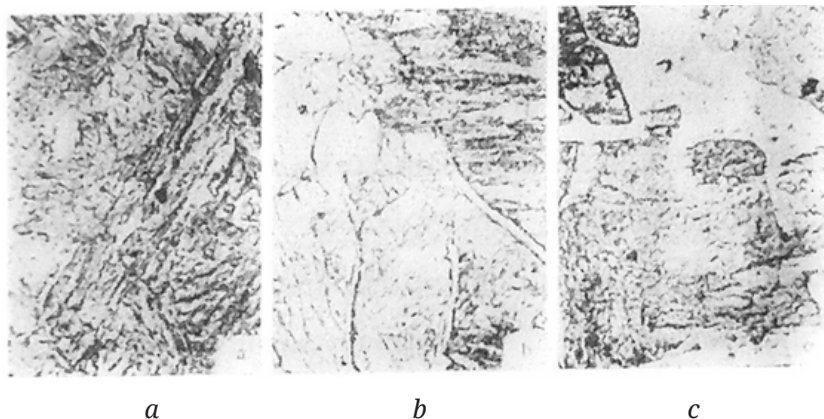


**Figure 3.37** – Microstructure of 08Kh13 steel,  $\times 1,000$ :  
*a*) not alloyed with rare-earth metal; *b*) alloyed with 0.2% of rare earth metals; *c*) alloyed with 0.4% of rare-earth metals

**Table 3.12**

Steel	REM content, %	$\delta_s$ , %	Structure
08Kh13	—	15.3	Martensite
08KH13Ch	0.2	17.8	Martensite + ferrite (traces)
	0.3	23.2	Martensite + ferrite 9%
	0.4	24.4	Martensite + ferrite 12%
	0.6	25.2	Martensite + ferrite 13%

**Table 3.13**

Chromium content, mass%	Erichsen cupping test penetration, mm	$\delta_s$ , %	HRB	Susceptibility to intercrystalline corrosion
13.01	—	24	—	Susceptible
14.16	6	32	100	Not susceptible
15.3	10	36	93	
16.05	11	38	84	
17.05	12	40	78	
18.04	12	41	79	Immune
19.1	11	40	80	

In order to identify the lowest chromium content which would ensure the characteristics required in nickel-free stainless steels containing 0.3% rare-earth metals and 0.2% Ca, a series of laboratory melts was produced (Table 3.13). Steel 08Kh13 was used as the matrix metal. Studies were carried out on sheet specimens 0.8 mm thick, quenched from 920 °C.

The optimum contents of rare-earth metals, calcium, and chromium were identified using the data in Tables 3.12, 3.13. Using the results of the laboratory studies, and taking industrial conditions into account, a corrosion-resistant steel 06Kh18Ch (DI79) alloyed with rare-earth metals and calcium was produced.

To study the technological processes of melting and cold-rolled sheet production, as used by “Dneprospetsstal” works, one industrial melt of 06Kh18Ch steel was produced. The chemical composition of the melt was: C – 0.06%, Mn – 0.02%, Si – 0.20%, P – 0.035%, S – 0.009%, Cr – 18.45%, Ni – 0.41%, Cu – 0.15%, V – 0.05%, and W – 0.12%. Into this melt 0.38% of ferrocerium FTsM-5, 0.2% of Ca, and 0.005% of Mg were introduced (calculated contents).

The steel was melted in a 40-ton capacity arc furnace of the open type, using the technological method applied for remelting of rejects with oxygen. Metal was cast by the bottom pouring method into X-shape molds giving 11.8-ton ingots. Exothermic mixture No. 4 was used in the process. The temperature of metal in the ladle was 1,590 °C. Further working of the ingots into cold-rolled sheets 0.8 mm thick was carried out by the “Zaporozhstal” works, using their conventional technology for corrosion-resistant steels.

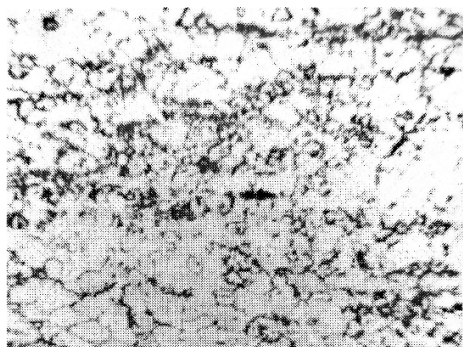


**Figure 3.38** –  
Microstructure of a cold-  
rolled 06Kh18Ch steel  
sheet manufactured  
from the experimental-  
industrial melt  
of that steel,  $\times 200$

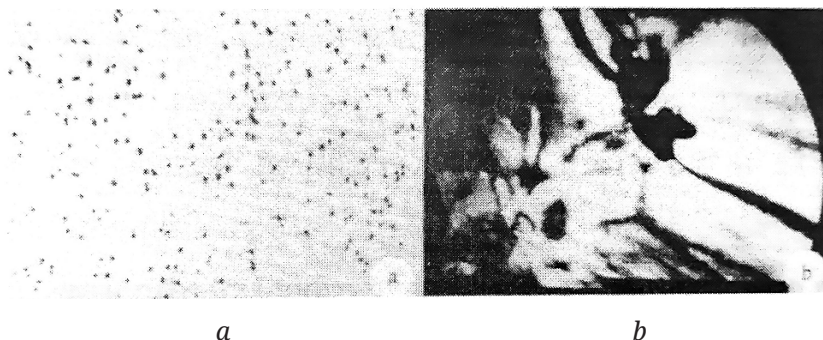


**Figure 3.39** – *a)* distribution and shape of nonmetallic inclusions,  $\times 115$ ; *b)* nonmetallic inclusion in a metal matrix, 5,000. Both in 08Kh18T1 steel



**Figure 3.40** – Distribution and shape of nonmetallic inclusions in an industrial melt of 06Kh18Ch steel,  $\times 115$

The microstructure of a cold-rolled sheet of 06Kh18Ch steel is shown in Fig. 3.38. Mechanical properties of that steel were as follows:  $\sigma_v=550$  MPa,  $\sigma_t=360$  MPa,  $\delta_5=41\%$ , Erichsen penetration 11.5 mm.

Tests by GAS proved that 06Kh18Ch steel has corrosion resistance equal to that of 12Kh18N9, provided the same technological process is used for their manufacture. Steel produced for articles with decorated surfaces must possess the ability to take a high-quality polish. Because of this, and aiming to replace nickel-chromium steel 12Kh18N9 with chromium steel 06Kh18Ch, their polishing properties have been studied.

Stainless steels, because of their low hardness and their sensitivity to surface damage, are very difficult to polish. Nonmetallic inclusions of various types, acting as internal abrasives, cause polishing defects. In titanium-containing stainless steels of the austenitic and ferritic types, a large number of angular nonmetallic inclusions of complex composition are present, including titanium carbonitride. During the polishing process these inclusions cause damage to the metal surface. In the final polishing stages these inclusions tend to fall out, leaving deep pits in the metal surface. Nonmetallic inclusions found in titanium-free steels are of completely different type and shape. Introduction of rare-earth metals into steels promotes the formation of favorable rounded-shape inclusions, while the absence of titanium carbides and nitrides makes them softer.

To quantitatively assess the polishing properties of sheets of 06Kh18Ch, 12Kh18N9, and 08Kh18Tl steels, nonmetallic inclusions and carbide particles were counted linearly. It was found in this way that inclusion counts for 06Kh18Ch were  $4.61 \times 10^{-3}$ ; for 12Kh18N9 steel,  $4.36 \times 10^{-3}$ ; and for 08Kh18Tl,  $3.58 \times 10^{-3}$ . Apart from this, some of the nonmetallic inclusions in 08Kh18Tl steel were as large as 20–40  $\mu\text{m}$ , while in steels 12Kh18N9 and 06Kh18Ch they were not larger than 10  $\mu\text{m}$ . Thus, it was confirmed that steel 06Kh18Ch can be used for manufacture of decorative components for cars. The consequent economy of nickel will comprise 90 kg per ton of steel.

1. Introduction of rare-earth metals and calcium into chromium stainless steels considerably increases their ductility and resistance to intercrystalline corrosion, at the same time preserving their polishing properties.

2. A new economically alloyed, nickel-free stainless steel 06Kh18Ch, containing, as calculated, 0.3–0.4% rare-earth metals and 0.2% Ca, was developed.

3. Industrial tests on chromium steel 06Kh18Ch proved that this steel is suitable for manufacturing car components with decorative surfaces, and is in no way inferior to chromium-nickel steels of the 12Kh18N9 type.

### 3.13 Structure formation during recrystallization of cold-rolled sheet steel

Economically alloyed stainless steel 06Kh18ch (DI79) is intended for manufacturing articles by stamping followed by polishing their surface. Compared with steels of the ferritic class stabilized with titanium, this steel has better polishability as a result of the fact that its structure does not contain coarse or brittle oxide and carbonitride precipitates which are contained in excess in steels with titanium [263].

However, steel 06Kh18ch relates to steels of the semiferritic class, and with rapid cooling from high temperature in air or in water it is partly quenched to martensite, as a result of which it is embrittled. The aim of the present study is determination of the optimum recrystallization heat-treatment schedule for cold-rolled steel 96Kh18ch in order to obtain an equilibrium structure.

The study was carried out on steel from an industrial melt (0.06% C; 0.02% Mn; 0.20% Si; 0.035% P; 0.09% S; 18.45% Cr; 0.41% Ni; 0.15% Cu; 0.05% V; 0.12% W) and factory reduction.

To the steel was added (by calculation) 0.38% ferrocerium FTSM5, 0.2% Ca and 0.005 Mg.

Specimens were cut from strip 0.76 mm thick rolled in the cold condition under factory conditions, heated to 850...1,200 °C (through each 50 °C) and soaked for 1, 2, 3, 4, 5, and 30 min, and then water cooled, simulating cooling conditions during heat treatment of strips in a continuous furnace under production conditions.

Steel microstructure was studied in an MIM-8 microscope. Microhardness was determined in PMT-3 equipment with a load of 0.2 N. X-ray diffraction analysis of specimens with determination of the solid solution lattice parameter was carried out in a DRON-1 diffractometer in copper radiation with monochromatization of diffracted beams. The depth of Erichsen cupping was determined in MTL10G equipment according to GOST 10510-63.

In the first stage of the work a study was made of the structure of hot-rolled steel (original condition before cold rolling).

As a result of the study it was established that the temperature at the end of hot rolling at 850...950 °C does not provide recrystallization of the structure. After soaking at these temperatures the steel structure is not uniform, and it is characterized by alternating light and dark components (Fig. 3.41, *a*). It may be assumed that the phase with high etchability is low-carbon martensite. The hardness of steel after hot rolling is HRB 87. Steel with this structure rolls comparatively well in the cold condition.

Then a study was made of the microstructure of cold-rolled steel after heat treatment in the laboratory by the schedules indicated above (Fig. 3.41, *b–e*).

It was established that on heating cold-rolled strip in the temperature range 850...950 °C there is recrystallization of ferrite grains and decomposition of martensite areas (inherited from hot-rolled metal) into a ferrite-carbide mixture.

On heating to a temperature above 950 °C there is carbide phase dissolution and solid solution saturation with carbon, and during subsequent rapid cooling martensite forms in the structure of steel 06Kh18ch. The commencement and degree of carbide dissolution depend not only on temperature, but also on soaking time at the given temperature (Fig. 3.41, *b–f*). With an increase in recrystallization-treatment temperature for cold-rolled steel, microhardness increases both for the martensitic and ferritic components of the structure obtained as a result of water cooling (Fig. 3.42).

It should be noted that after heating in the temperature range 900...950 °C microhardness is reduced a little, which is caused by decomposition of martensite inherited by the cold-rolled metal from hot-rolled material. There is precipitation of carbide phase from solid solution and a reduction in its lattice parameter (Fig. 3.41).

Starting from 1,000 °C there is an intense increase in cold-rolled steel microhardness, caused by carbide dissolution and formation of martensite in areas of high carbide concentration. With an increase in heating temperature there is also a change in the ratio of structural components; the amount of ferrite increases,

but for martensite it decreases. The increase in microhardness for martensite as a result of a preferential concentration of carbon in it proceeds more intensely than for the microhardness of ferrite. This process is also accompanied by an increase in the solid solution lattice parameters, which is connected with an increase in martensite tetragonality (Fig. 3.42).

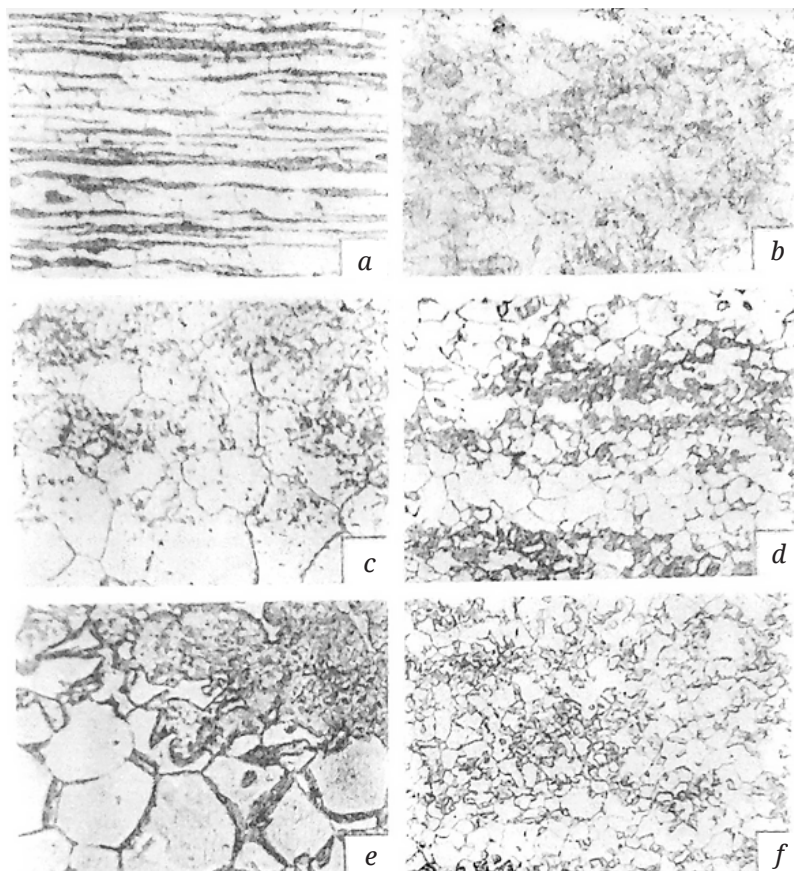


**Figure 3.41** – Microstructure of steel 06Kh18ch after hot rolling (*a*) and recrystallization treatment at different temperatures (water cooling); *b, c*) 950 °C for 3 min; *d, e*) 1,050 °C for 3 min; *f*) 950 °C for 5 min: *a*)  $\times 115$ ; *b, d, f*)  $\times 200$ ; *c, e*)  $\times 1,000$

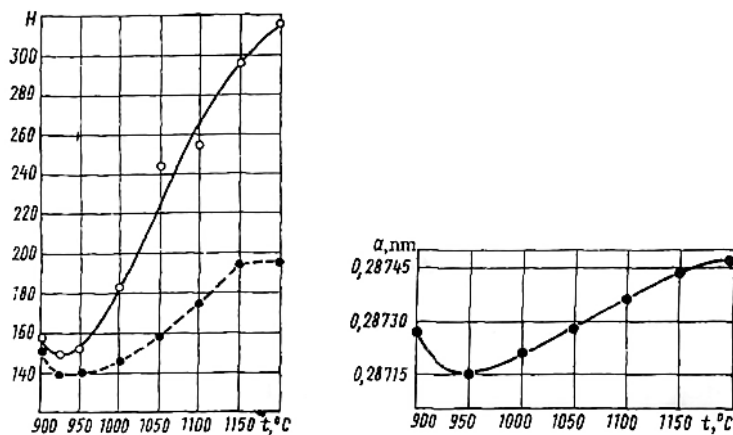


**Figure 3.42** – Dependence of microhardness (solid line is martensite decomposition products; broken line is structurally free ferrite) and solid solution lattice parameter for steel 06Kh18ch on recrystallization-treatment temperature

On the basis of the results of metallographic studies of the structure, microhardness measurements and x-ray diffraction analysis, the structural state diagram was plotted for steel 06Kh18ch on coordinates of heating temperature-soaking time at the given temperature (Fig. 3.42). It was established from this diagram that the temperature-time interval (region 2) corresponding to the structural state of steel 06Kh18ch is close to equilibrium for conditions of rapid cooling (in water or in air). The existence of this range is connected apparently with the presence of REM in the steel, which by reducing carbon diffusion hinder the occurrence of carbide formation and dissolution [259]. This effect may be used in order to select the recrystallization heat-treatment schedule for cold-rolled sheet with the aim of obtaining metal with the optimum structure and properties during its treatment in a high-productivity continuous furnace under production conditions.

In view of the fact that there are high requirements for steel 06Kh18ch stamp ability, an evaluation was made of its process ductility after treatment by different schedules. The highest

ductility indices in Erichsen tests are possessed by steel 06Kh18ch heat treated in the range for existence of an equilibrium structure (Fig. 3.42, region 2). The results of determining process ductility for cold-rolled steel 06Kh18ch sheet after different heat treatment are given in Table 3.14.

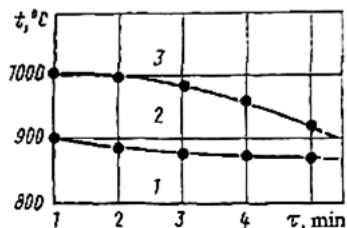


**Figure 3.43** – Structural state diagram for steel 06Kh18ch:  
1) ferrite + ferrite-carbide mixture; 2) ferrite + carbides;  
3) ferrite + martensite

**Table 3.14**

Heat-treatment schedule	Erichsen test, mm	Structure
Annealing at 800 deg C for 5 h	10.0–11.5	Ferrite + carbides
Recrystallization treatment for 3 min at temps., deg C*	9.5–11.0	
	800	Ferrite + ferrite – carbide mixture
	1,050	Ferrite + martensite

\* Water cooling.

On the basis of the results of studies carried out it is possible to conclude that heating to 920...950 °C (heating time 2 min/mm) followed by rapid cooling provides the maximum ductility for cold-rolled steel 06Kh18ch sheet ( $\delta_5 = 40\text{--}42\%$ ).

### 3.14 The effect of plastic deformation on the structure formation of low-alloy steel

Hot plastic deformation is still considered as one of the most promising ways of obtaining a fine-grained structure of metals, which is capable of providing a high level of mechanical properties. In this study, the influence of selected deformation parameters at variable temperature on the structure and properties of low-alloy steel 10XΦТБч (Standard of Ukraine) is investigated [264–266]. The chemical composition of the studied low-alloy steel, wt %: C – 0,08–0,12; Si – 0,10–0,50; Mn – 0,15–0,50; Cr – 0,14–0,16; V – 0,10–0,15; Ti – 0,12–0,15; Nb – 0,07–0,15; barium – 0,0005–0,0015; rare earth elements – 0,001–0,010; while the content of sulfur and phosphorus in the steel does not exceed 0,035%.

Tests of the hot steel were carried out with a modern plastometer “Gleeble 3800” and a dilatometer. Working parameters of the plastometer were:

- test temperature – 20...950 °C;
- speed of the punch – up to 2,000 mm/sec;
- degree of logarithmic deformation –  $\varepsilon_{comp}=0,01-1,2$ ;

$\varepsilon_{dist}=0,01-0,15$ .

When tested on the plastometer, samples with a ratio of  $d \times h = 10 \times 12$  mm were placed in a chamber in which air was evacuated and a vacuum was created to prevent oxidation of the metal. Special computer programs carried out control over the plastometer by temperature, speed and degree of deformation. At certain intervals during the loading process, the yield stress and the logarithmic deformation were recorded. Table 3.15 shows the thermomechanical parameters of the deformed samples.

**Table 3.15** – Deformation parameters

Samples	1	2	3	4	5
Temperature, °C	770	800	850	900	950
Deformation rate, sec <sup>-1</sup>	100	100	100	100	100
Degree of deformation, ln ε	1.2	1.2	1.2	1.2	1.2

The size of the actual grain and the ratio of the structural components of the ferrite perlite samples were determined using a software-hardware complex which includes the “AXIOVERT 200 MAT” light inverted microscope. To quantify the microstructure, the “Sigmaplot” computer program that process digital images of structural components by constructing histograms of the distribution of the brightness level, corresponding to different details of the structures was used. The confidence interval was 0.95. As a result of processing, the ratios of the areas, occupied by the corresponding structural components were determined.

Fig. 3.44 presents diagrams of sample compression at different temperatures, showing the dependence of the yield stress on the compression deformation logarithm at different stages of shaping. The Hensel-Spittel mathematical model was used to describe the change in the yield stress, depending on the logarithmic deformation, temperature and deformation rate.

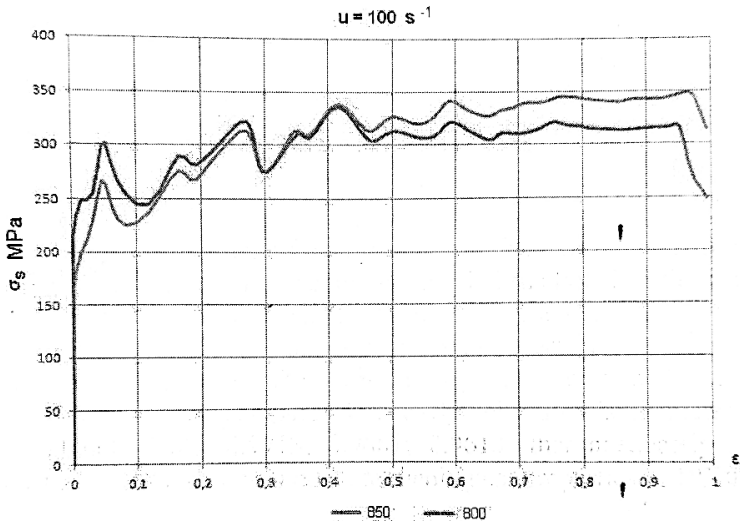


**Figure 3.44** – Dependence of the deformation resistance on the degree of deformation at various temperatures at a speed of  $100 \text{ s}^{-1}$

To calculate the correlation coefficient, the corresponding function in the “Excel” program was used. It is established that the computed Hensel-Spittel model is characterized by the following correlation coefficients: 0.9713, 0.9661, 0.9613, that adequately reflects the existing interrelations and can be used to model the rheological properties of 10XΦТБч steel.

To develop plastic deformation modes that provide the maximum possible grinding of the structure of low-carbon low-alloy steels, detailed information on the effect of austenite deformation regimes on formation of optimal structure of the steel in the state of delivery is needed. To determine the critical degrees of deformation, which provide formation of recrystallized austenite grains, studies of the effect of the degree and temperature of deformation on the structure of low-alloyed low-carbon steel were made. The deformation temperature was varied from 770 °C to 950 °C, the degree and rate of deformation were kept constant ( $\ln \varepsilon = 1.2$ , deformation rate – 100 s<sup>-1</sup>). Microstructures and distribution diagrams by the grain-size number are shown in Fig. 3.45 and Fig. 3.46.

After deformation at the temperature of 770 °C, a ferrite-pearlite structure with a main grain-size number of 9–11, 2.42% – grain-size number of 14, and 28.34% with a grain size number of 10 (Fig. 3.46, *a*) is formed in the steel. There are 81.5% of ferrite and 18.5% of pearlite formed in the steel. This is because the deformation takes place in a two-phase region with formation of a significant fraction of ferrite (Fig. 3.46, *b*).

After the deformation at the temperature of 850 °C, a structure with the main grain-size number of 11–12 is formed. There are 33.35% of grains with grain-size number of 11 and 31.09% with grain-size number of 12 in the structure (Fig. 3.47, *a*). At the same time 62.04% of ferrite and 37.95% of pearlite are formed in the structure (Fig. 3.47, *b*). This indicates grinding of the  $\gamma$ -phase as a result of recrystallization and formation of a subgrain structure inside the grain.

SECTION 3  
Structural changes during deformation and heat treatment of metals

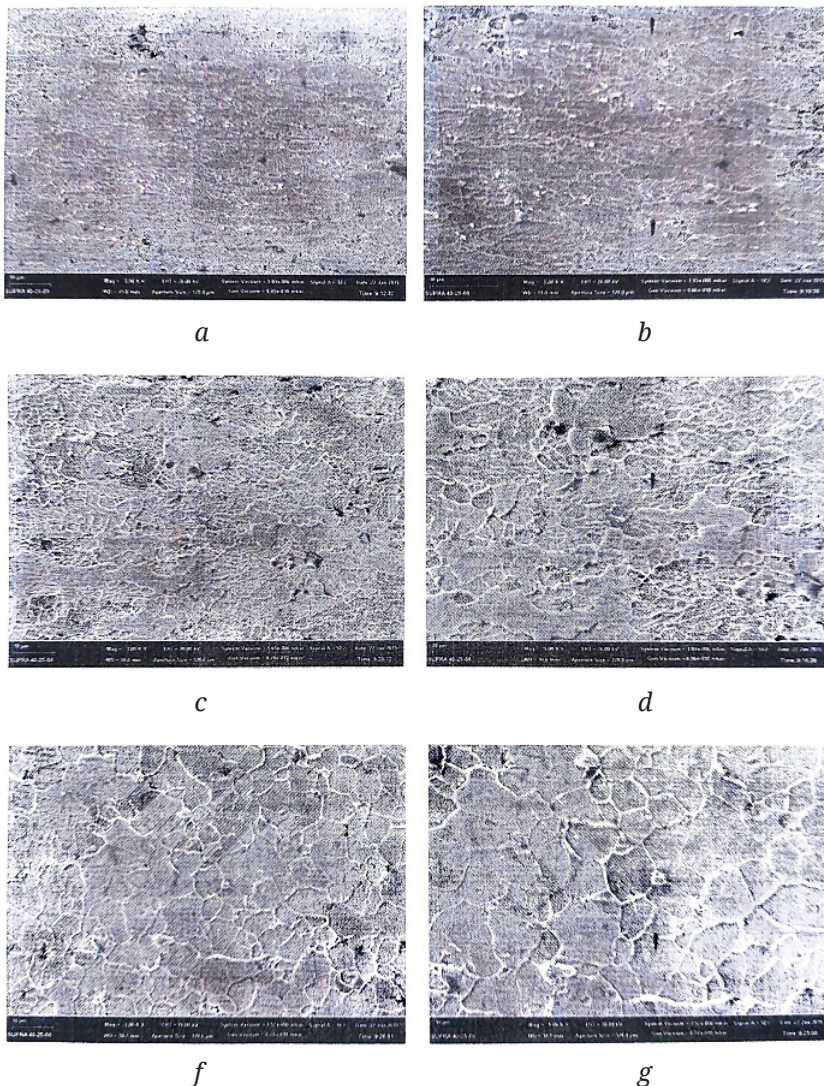


**Figure 3.45** – Microstructures of low-alloy steel 10XTBy after deformation: *a, b* – 770 °C; *c, d* – 800 °C; *f, g* – 850 °C; *a, c, f* –  $\times 3,000$ ; *b, d, g* –  $\times 5,000$ ; Degree of deformation is  $\ln \epsilon = 1.2$  and deformation rate is  $100 \text{ s}^{-1}$

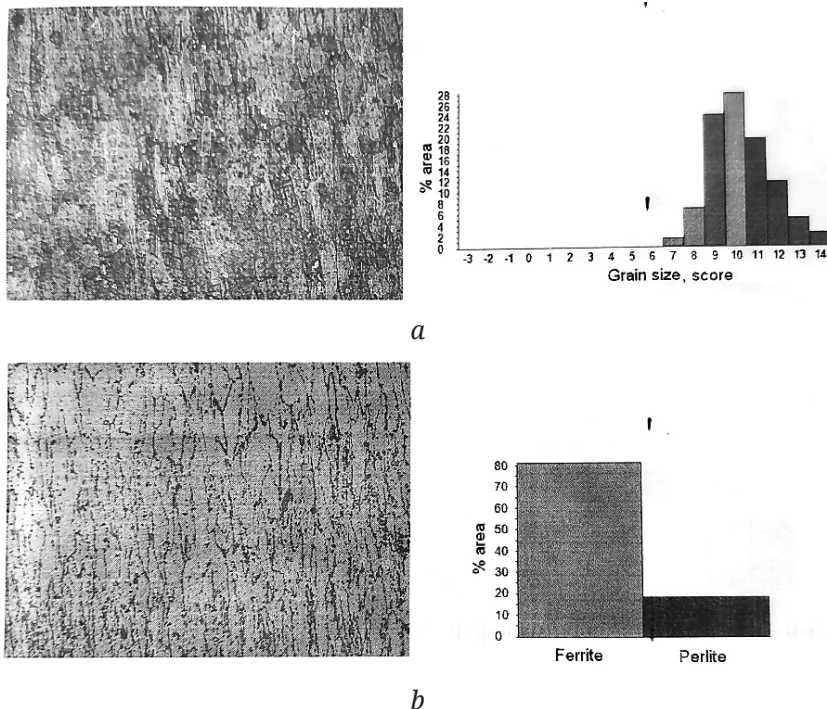
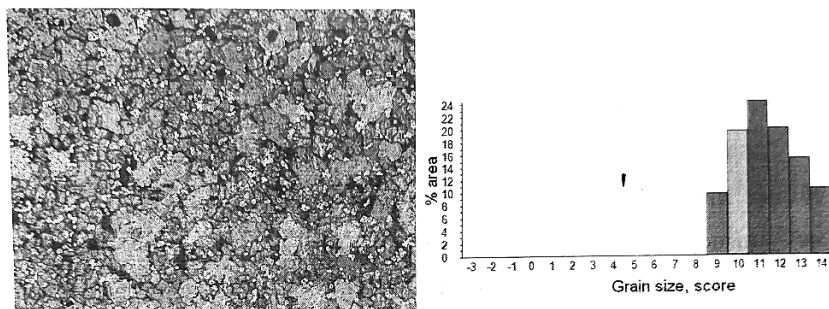


**Figure 3.46** – Results of a study of the microstructure of steel,  $\times 250$ :  
*a* – distribution by the grain-size number, *b* – phase distribution;  
after deformation  $\ln \varepsilon = 1.2$  at the temperature of  $770\text{ }^{\circ}\text{C}$   
and deformation rate of  $100\text{ s}^{-1}$

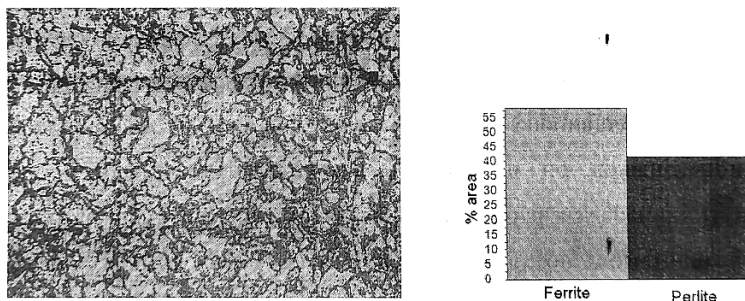
A further increase in temperature to  $950\text{ }^{\circ}\text{C}$  leads to an insignificant increase in the average size of the structural element after deformation  $\ln \varepsilon = 1.2$ . The structure consists of 24.52% of grains with the grain-size number of 11 and 20.16% of grains with the grain-size number of 12. The highest grain-size number of 14 is 10.50%. At the same time, 58.46% of ferrite and 41.53% of perlite are formed in the structure.

When looking at the grain size distribution histograms, it can be seen that the distribution pattern is similar at different deformation temperatures. Analysis of the phase distribution

histograms established the differences between them. At the deformation temperature of 770 °C, the distribution peak is the share of ferrite, which is more than 80%. At higher temperatures the share of ferrite decreases and lies within the range of 58–62%, which indicates a change in the ratio of the structural constituents of ferrite (with predominantly large-angle disorientations between grains) [216].



*a*



*b*

**Figure 3.47** – Results of a study of the microstructure of steel,  $\times 250$ :  
*a* – distribution by the grain-size number; *b* – phase distribution;  
 after deformation  $\ln \varepsilon = 1.2$  at the temperature of 950 °C  
 and deformation rate of 100 s<sup>-1</sup>

Microhardness was measured on the studied samples. Dependences of the change in microhardness and average grain size on the deformation temperature was established. Microhardness of

the sample deformed with the degree of deformation  $\ln \varepsilon = 1.2$  at the temperature of 770 °C, is the lowest and amounts to 260 HV. Increase in temperature to 850 °C leads to increase in hardness up to 320 HV. Further increase temperature does not affect the microhardness.

The minimal microhardness was obtained on samples deformed at the temperature of 770 °C. The most fine-grained structure is observed in these samples. This is due to the fact that plastic deformation occurs in the two-phase region and the share of ferrite is the greatest – 80% of ferrite and 20% of pearlite.

The obtained data is in line with modern concepts of the structure formation mechanisms depending on the deformation temperature of steel. According to these concepts, fragmentation is the dominant mechanism of the structure grinding at the deformation temperature of 770 °C. The effect of this mechanism is partial recrystallization of ferrite and change of the initial orientation to disoriented subgrains (fragments) with small-angle dislocation boundaries of deformation origin.

At higher temperatures, two competing mechanisms are implemented: fragmentation and initial processes of dynamic austenite recrystallization. Due to formation of ferrite at the temperature of 770 °C, minimal hardness is observed, while maximal hardness in combination with small grain size is observed after deformation at 850 °C with the deformation degree  $\ln \varepsilon = 1.2$ .

Thus, the appropriate choice of modes for the 10XΦТБч type steel allows obtaining higher strength and plastic properties. This makes it possible to control obtaining of a given set of properties, and in the future – steel with the same chemical composition for producing after sheet rolling of different categories of strength with increased plastic properties.

The obtained test results for the studied steel with different grain size and calculated stress  $\sigma_i$  can be used later to construct the dependence of  $\sigma_T$  on  $d$  using the Petch-Hall model. It is known that this dependence follows a well-known relationship:

$$\sigma_T = \sigma_i + k \times d^{-\frac{1}{2}}, \quad (3.15)$$

where  $\sigma_T$  – is the tensile yield strength or the flow stress;  $d$  – grain size;  $\sigma_i$  and  $k$  – parameters characterizing given material.

Thus, an experimental-theoretical method has been developed for determining the interrelations between the stress-strain state of a metal, the grain size  $d$ , and the yield strength  $\sigma_T$ . To get a full picture of the effect of plastic deformation on the changes in structural-phase transformations in the new 10XΦТБч steel grade, more comprehensive studies with using of modern plastometric methods of testing the stress-strain flow of a metal and its mathematical description are required.

The study of experimental 10XΦТБч type steel on a plastometer using special computer programs made it possible to establish critical points of phase transitions and optimal energy parameters of hot deformation that allows choosing a hot deformation temperature in the range of 850...950 °C.

## REFERENCES

1. Методы анализа поверхности / под ред. А. Задерны. Пер. с англ. под ред. В. В. Кораблёва, Н. Н. Петрова. – М. : Мир, 1979. – 540 с.
2. Нефёдов В. И., Черепин В. Г. Физические методы исследования поверхности твёрдых тел. – М. : Наука, 1983. – 296 с.
3. Антонов В. Н., Кобзарь Ю. М., Красовский Е. Е., Шаталов В. М. О возможностях определения степени деформации металла методом электронно-фотонной эмиссии // *ФХММ* 24, 112 (1988).
4. Swift A. J. Modern surface analysis in materials science. *Metals and Mater.* 4, 688 (1988).
5. Пашаев Э. А., Абдулаев М. Выход оже-электронов в условиях дифракции рентгеновских лучей // *Кристаллография* 34, 263–265 (1989).
6. Рыбакова Л. М., Куксенова Л. И., Босов С. В. Рентгенографический метод исследования структурных изменений в тонком поверхностном слое металла при трении // *Заводская лаборатория*. – 1973. – № 3. С. 293–296.
7. Shulakov A. S. Application of ultra-soft X-ray emission spectroscopy for solid surface studies // *Crust. Rev. and Technol.* – 1988. – 23, № 6. – P. 835–838.
8. Alonso M., Soria F. May Auger electron spectroscopy provide surface structural information // *Surface. Sci.* – 1986. – 178, № 1-3. – P. 509–518.
9. Вудраф Д., Делчар Т. Современные методы исследования поверхности: пер. с англ. – М. : Мир. – 1989. – 564 с. : ил.
10. Васильев Д. М., Трофимов В. В. Рентгеновская тензометрия как метод исследования напряжённого состояния поверхностных слоёв // *Физика и технология обработки поверхности металлов. Материалы темат. сб.* – Л., 1984. – С. 58–72.
11. Васильев Д. М., Трофимов В. В. Современное состояние рентгеновского способа измерения макронапряжений. Обзор // *Заводская лаборатория*. – 1984. – 50, № 7. – С. 20–29.
12. Жебынев Д. А., Шоршоров М. Х., Любовь Б. Я., Алёхин В. П. Влияние скорости пластической деформации на кинетику релаксации экзоелектронной эмиссии с поверхности алюминия // *Известия АН СССР. Металлы*. – 1976. – № 1. – С. 64–69.
13. Алёхин В. П. Физика прочности и пластичности поверхностных слоёв материалов. – М. : Наука, 1983. – 280 с.

14. Крылова И. В. Физико-химическая природа экзоэмиссии и её применение в исследованиях поверхности твёрдых тел // *Журнал физической химии*. – 1981. – LV, № 11. – С. 2721–2733.
15. Минц Р. И., Кортвов В. С., Александров В. Л., Крюк В. И. Экзоэлектронная эмиссия при циклическом нагружении аустенитных сталей // *Физика металлов и металловедение*. – 1968. – 26, № 4. – С. 681–687.
16. Кортвов В. С., Слесарев А. И., Рогов В. В. Экзоэмиссионный контроль поверхности деталей после обработки. Киев : Наукова думка, 1986.
17. Кортвов В. С., Минц Р. И., Мясников И. Е. Влияние условий деформации на энергетический спектр экзоэлектронной эмиссии металлов // *Известия вузов. Физика*. – 1971. – 9. – С. 83–87.
18. Мясников И. Е., Кортвов В. С. Влияние нагрева на интенсивность и энергию экзоэлектронов деформированного алюминия // *Известия вузов. Цветная металлургия*. – 1972. – 6. – С. 136–140.
19. 12th Annual Meeting: Advances in Surface and Interface Physics, Modena, 14–16 Dec., 1987 *Vuoto: Sci. and Technol.* – 19 // 88. – 18, № 1. – P. 3–49.
20. Мальшев В. С., Косачёв М. А., Ломаев Г. В. Контроль параметров поверхностных слоёв стали 13X12H2B2MФ после пластического деформирования поверхности выглаживанием // *Дефектоскопия*. – 1987. – № 9. – С. 85–87.
21. Царёв Б. М. Контактная разность потенциалов. – М. : Госмехтеориздат, 1955. – 280 с.
22. Савицкий Е. М., Буров И. В., Корольков В. А., Иващенко Е. В., Литвак Л. Н., Кузнецов В. А. Работа выхода электрона элементов, измеренная методами контактной разности потенциалов и термоэлектронной эмиссии // *Физика и химия обработки материалов*. – 1985. – № 2. – С. 121–123.
23. Андреев Л. А. Усовершенствование метода вибрирующей струны для изменений контактной разности потенциалов. Завод. лаб. 28, 962–965 (1962).
24. Алейников Н. М., Грибков С. П. О некоторых особенностях метода динамического конденсатора // *Поверхность*. 70–76 (1985).
25. Юнда Н. Т. Измеритель распределения поверхностного потенциала. *ПТЭ* 201–204 (1984).
26. Алейников Н. М., Грибков С. П. Автоматизированный измеритель поверхностного потенциала // *ПТЭ*. – 1984. – 2. – С. 213–216.

27. Литовченко В. Г., Лысенко В. С., Новоминский В. А., Турчанинов В. И. Комбинированный метод измерения контактной разности потенциалов и поверхностной проводимости // *Приборы и техника эксперимента*. – 1976. – № 1. – С. 217–220.
28. Бачински Я., Малэцки Х., Стемпиньски М. Установка для измерений работы выхода электронов из металла методом динамического конденсатора // *ПТЭ*. – 1979. – № 4. – С. 205–206.
29. Фонов В. Н., Глазунов Н. Н., Калинин Б. А., Заярный А. П. Установка для измерения контактной разности потенциалов // *ПТЭ*. – 1981. – № 6. – С. 183–184.
30. Алейников Н. М., Алейников Н. М. О наблюдении релаксационных колебаний поверхностных зарядов методом динамического конденсатора // *Поверхность*. – 1987. – № 9. – С. 31–36.
31. Сакалаускас С. Ю., Добровольскис А. Т. Измеритель распределения поверхностного электрического потенциала // *ПТЭ*. – 1978. – № 3. – С. 165–168.
32. Алсаханов Ю. И., Иванов К. Н., Ширапова Д. Ц. Установка для исследования зависимости контактной разности потенциалов твердых тел от толщины адсорбированного слоя на их поверхности // *ПТЭ*. – 1991. – № 1. – С. 167–170.
33. Surplice N. A., D'Arcy R. J. A critique of the Kelvin method of measuring work functions // *J. of Physics E: Sci. Ins.* – 1970. – Vol. 3, p. 477–482.
34. Коваль В. Ф., Борюденюк И. В. Прибор для измерения работы выхода // *ПТЭ*. – 1992. – № 2. – С. 251–254.
35. Жарин А. А., Шпеньков Г. П. Измеритель контактной разности потенциалов // *ПТЭ*. – 1978. – № 2. – С. 267.
36. Белов А. К., Крячко В. В., Мажулин А. В. Вибратор для измерителя контактной разности потенциалов с зондом малого диаметра // *ПТЭ*. – 1978. – № 1. – С. 204–205.
37. Лысенко В. С., Турчаников В. И. Измерение термостимулированных изменений контактной разности потенциалов // *ПТЭ*. – 1980. – № 3. – С. 240–243.
38. Островский А. А., Баш В. Я. Термоэлектрический метод изучения напряжённо-деформированного состояния материалов. Киев. Технол. ин-т пищ. пром-ти. Киев, 1988, 8 с. – Деп. в УкрНИИТИ, N712-Ук 88 от 23.03.88.
39. Кунин Н. Ф., Меламед И. З. Изменение термосилы металлов подгруппы меди под действием пластической

- деформации при разных температурах // Физика металлов и металловедение. – 1956. – 2, № 3. – С. 423–427.
40. Кунин Н. Ф. Изменение термоэлектродвижущей силы металлов при пластической деформации // Физика металлов и металловедение. – 1956. – 2, № 2. – С. 237–243.
  41. Мурашов Р. Р., Боровский С. М., Паскудский Е. А., Линников В. М., Смыслов А. М. О взаимосвязи пластической и упругой деформации с излучательными характеристиками авиационных материалов. – Уфа, 1988. – С. 120–126.
  42. Shabel Barric S., Young Robert F. A new procedur for the rapid determination of yield and tensile strength from hardness test // Nondestact. Charact. Mater.: Proc. and Int. Symp., Montred, July 21–23, 1986. – 1987. – P. 335–343.
  43. Ishibashi Tatsuya, Shimoda Shigeru. The Correlation Between Hardness (Mean Contact Pressure by a Spherical Indentet) and Flow Stress // ISME International Journal. – 1988. – 31, № 1. – P. 117–125.
  44. Черменский О. Н., Спицына И. Н. Определение напряжения текучести металлов и сплавов при статической предельной нагрузке. Методика ГСССД МЭ 34-85. М. : ГСССД, 1985. – 27 с.
  45. Vitovec Franz H. Stress and Load Dependence of Microindentation Hardness // 15–18 July, 1984. Philadelphia, Pa.
  46. Лоскутов С. В. О применении методики контактного электросопротивления при испытаниях материалов на кинетическое индентирование // 3-я Международная научно-техническая конференция. ОТТОМ-3, Украина, Харьков : ННЦ ХФТИ, «Контраст», 2002. 9–13 сентября 2002. – С. 32–34.
  47. Шабанов В. М. К вопросу об оценке степени пластической деформации при вдавливании // Высокоэффективные технологии обработки материалов в энергетике : сб. науч. трудов. № 207. – М. : Моск. энерг. ин-т, 1989. – С. 128–132.
  48. Маслов В. П., Новиков В. Н., Цицилиано А. Д. Определение характеристик упругости и пластичности переходных металлов вдавливанием индентора // Завод. лаб. – 1988. – 54, № 8. – С. 90–92.
  49. Леонов В. В., Брюханов А. В. Взаимосвязь поверхностной энергии вещества с его микротвёрдостью // Физ. и химия обраб. матер. – 1987. – № 5. – С. 151–152.
  50. Дрозд М. С. Определение механических свойств металла без разрушения. – М. : Металлургия, 1963. – 171 с.
  51. Дрозд М. С., Матлин М. М. Определение модуля нормальной упругости по глубине остаточного отпечатка индентора // Завод. лаб. – 1988. – 54, № 12. – С. 85–89.

52. Исхакова Г. А., Рахимьянов Х. М. Определение механических характеристик термоупрочнённого слоя по новому числу твёрдости // Завод. лаб. – 1987. – 53, № 8. – С. 77–78.
53. Tirupataiah Y., Sundararajan G. A. Comprehensive Analysis of the Static Indentation Process // Materials Science and Engineering. – 1987. – 91. – Р. 169–180.
54. Ланков А. А., Рогозин Г. И. Кривая твёрдости. Метод оценки предельной твёрдости упруго-пластических материалов // Механика и физика контактного взаимодействия. – Калинин : КГУ, 1985. – С. 15–20.
55. Ланков А. А. Предельная твёрдость и пластичность упруго-пластических материалов // Контактное взаимодействие твёрдых тел : сб. научн. тр. – Калинин : КГУ, 1986. – С. 9–22.
56. Бульчѐв С. И., Алѐхин В. П. Метод кинетической твёрдости и микротвёрдости в испытании вдавливанием индентора // Завод. лаб. – 1987. – 53, № 11. – С. 76–80.
57. Бульчѐв С. И., Алѐхин В. П., Шоршоров М. Х. Исследование физико-механических свойств материалов в приповерхностном слое и в микрообъѐмах методом непрерывного вдавливания индентора (обзор) // Физика и химия обработки материалов. – 1979. – № 5. – С. 69–82.
58. Галанов Б. А., Григорьев О. Н., Мильман Ю. В., Рагозин И. П., Трефилов В. И. Определение твёрдости и модуля Юнга при упруго-пластическом внедрении инденторов в материалы // ДАН СССР. – 1984. – 274, № 5. – С. 815–817.
59. Хольм Р. Электрические контакты. Пер. с англ. под ред. Д. Э. Брусина, А. А. Рудницкого (Иностранная литература, 1961).
60. Pashley M. D., Pethica I. B., Tabor D. Adhesion and micromechanical properties of metal surfaces // Wear. – 1984. – № 100. – Р. 7–31.
61. Lee Anthony, Mamrick M. S. Fretting corrosion of thin – plated copper alloy // Iece transactions on components, hybrids and manufacturing technology. V. CHMT-10, № 1, 1987. P. 63–67.
62. Braunovic M., Braunovic M. Effect of fretting on the contact resistance of copper, aluminum and nickel-coated aluminum wire connections // Wear. – 1986. – 112, № 2. – Р. 181–197.
63. Кончиц В. В., Мешков В. В., Мышкин Н. К. Триботехника электрических контактов. Под ред. академика АН БССР В. А. Белого. – Минск : Наука и Техника, 1986. – 255 с.
64. Lanchon H., Макара В., Murgaux A., Saint Jean Paulin I. A mathematical study to obtain quantitativ effects of roughness in tehcnical problems // Wear. – 1985. – 109. – Р. 99–111.

65. Степанов А. В., Милькоманович Е. А. Влияние растворения на искусственное сдвигообразование // ЖЭТФ 21, 409–412 (1951).
66. Степанов А. В. Основы прочности кристаллов (Наука, 1974).
67. Hryniewicz T, Skubala W. Surface Effects in Micromachining of Metals and Alloys, SCT 38, 281–287 (1989).
68. Ровинский Б. М., Баранов Ю. В., Костюкова Е. П. Влияние полирующей среды на характер субструктуры при деформации монокристаллов вольфрама // ФТТ 16, 3207–3211 (1974).
69. Baxter W. J. Measurement of surface fatigue damage by exoelectron emission // Met. Trans. – Vol. 6A. – № 4. – 1975. – P. 749–754.
70. Жукин У. Д., Савенко В. И., Кочанова Л. А. Роль поверхности и среды в переходах упругость-пластичность-хрупкость в металлических кристаллах // *Поверхность*. – 1985. – 7. – С. 105–114.
71. Kramer I. R. Influence of the surface layer on the plastic flow deformation of aluminium single crystals, Trans. Met. Soc. AIME 233, 1462–1467 (1965).
72. Kramer I. R. Surface layer effects on the plastic deformation of iron and molybdenum // Trans. Met. Soc. AIME 520–528 (1967).
73. Kramer I. R. Surface layer effects on the mechanical behaviour of metals // Adv. Mech. and Phys. Surfaces 3, 109–120 (1986).
74. Duguet D. J. The role of free surface in the deformation of metal single crystals // Scr. Met. 3, 513–516 (1969).
75. Степанов Э. Н., Алехин В. П., Гуров К. П. Релаксационные процессы при циклическом нагружении образца и наличии объемных источников и стоков вакансий // ФММ 200-203 (1991).
76. Криштал М. А., Мерсон Д. Л., Алехин В. П., Зайцев В. А. Распространение пластической деформации по сечению образца и акустическая эмиссия при одноосном растяжении меди // Физика металлов и металловедение 63, 1011–1016 (1987).
77. Горицкий В. М., Иванова В. С., Орлов Л. Г. О различии пластической деформации поверхностных и внутренних слоев поликристаллического железа при усталостном нагружении // ДАН СССР. – 205, № 4. – 1972. – С. 812–814.
78. Алехин В. П., Рагуля А. В., Ерёмченко В. И., Шоршоров М. Х., Алехин О. В. О кинетической модели «вакансионного насоса» при циклическом сжатии кристалла // Физ. мет. и металловед. 65, 190–197 (1988).
79. Алехин В. П., Иванов В. Д., Красулин Ю. Л., Тимофеев В. Н., Углов А. А., Харланова З. И. Источник дислокаций

- в полупроводнике при сварке полупроводников с металлами // Физика и химия обработки материалов, 98–105 (1967).
80. Алёхин В. П., Зайцев В. А., Куликаускас В. С. Исследование поверхностной микропластичности монокристаллов молибдена методом обратного рассеивания // Физ. и химия обраб. матер., 112–115 (1988).
  81. Степанов Э. Н., Алехин В. П., Гуров К. П. Релаксационные процессы при циклическом нагружении образца и наличии объемных источников и стоков вакансий // Физика металлов и металловедение. – 1991. – № 5. – С. 200–203.
  82. Strained Metallic Surfaces: Theory, Nanostructuring and Fatigue Strength (2009), by Valim Levitin and Stephan Loskutov.
  83. Гликман Е. Э., Сальман В. Р., Кузнецов В. А. Влияние поверхностной энергии на зернограничное проскальзывание в свинце // *Поверхность*, 134–146 (1984).
  84. Орлов В. Г. Влияние поверхностного натяжения на гетерогенное зарождение дислокаций в кристаллах // ФТТ 14, 3691–3693 (1972).
  85. Алексеев А. А., Горячев С. Б., Струнин Б. М. Скопление дислокаций у поверхности кристалла // ФТТ 16, 3549–3553 (1974).
  86. Гегузин Я. И., Овчаренко Н. Н., Парицкая Л. Н. Исследование некоторых физических процессов, происходящих на поверхности кристаллических тел при высокой температуре // ФММ 12, 42–46 (1961).
  87. Бекренев А. Н., Миркин Л. И. Малоугловая рентгенография деформации разрушения материалов (Моск. университет, 1991).
  88. Буйнов Н. Н. Структура следов скольжения по поверхности деформированных алюминиевых сплавов // ФММ 2, 477–483 (1956).
  89. Гегузин Я. Е., Овчаренко Н. Н. Поверхностная энергия и процессы на поверхности // УФН 76, 283–328 (1962).
  90. Гурьев А. В., Кукса Л. В. Исследование границы раздела упругой и пластической деформации в стали // ФММ 21, 116–124 (1966).
  91. Вдовин Е. Е. Прямое наблюдение электропереноса дислокаций в металлах // ФТТ 30, 311–314 (1988).
  92. Балашов Б. Ф., Петухов А. Н., Архипов А. Н. Влияние остаточных напряжений на сопротивление усталости сплава ВТ-9 // Проблемы прочности. – 33–37 (1981).
  93. Биргер И. А., Мавлютов Р. Р. Сопротивление материалов (Наука, 1956).

## REFERENCES

94. Вишняков Н. А., Грингауз Г. Д., Рудзей Г. Ф. Влияние остаточных напряжений на выносливость образцов при программном нагружении. Проблемы прочности. – 34–37 (1981).
95. Павлов В. Ф. Влияние характера распределения остаточных напряжений по толщине поверхностного слоя детали на сопротивление усталости // Известия вузов. Машиностроение, 3–6 (1987).
96. Сулима А. М., Евстигнеев М. И. Качество поверхностного слоя и усталостная прочность. – Машиностроение, 1974.
97. Вишняков Я. Д., Писарев В. Д. Управление остаточными напряжениями в металлах и сплавах (Машиностроение, 1989).
98. Технологические остаточные напряжения. Под ред. А. В. Подзея (Машиностроение, 1973).
99. Трофимов В. В., Радеева Е. Н. Об изменении напряжений в упрочнённых приповерхностных слоях изделий при усталости // Проблемы прочности. – 30–33 (1979).
100. Дёмкин Н. Б., Рыжов Э. В. Качество поверхности и контакт деталей машин (Машиностроение, 1981).
101. Крагельский И. В. Трение и износ (Машиностроение, 1968).
102. Комбалов В. С. Влияние шероховатости твёрдых тел на трение и износ (Наука, 1974).
103. Дёмкин Н. В. Контактное шероховатых поверхностей (Наука, 1970).
104. Vitovec Franz H. Stress and Load Dependence of Microindentation Hardness // Microindent. Techn. Mater. Sci. and Eng. Symp., Philadelphia, Pa, 15–18 July, 1984. – 1985. – P. 175–185.
105. Oliver W. C., Hutchings R., Pethica I. B. Measurement of Hardness at Indentation Depths as Low as 20 Nanometres // Microindent. Techn. Mater. Sci. and Eng. Symp., Philadelphia, Pa, 15–18 July, 1984–1985. – P. 47–71.
106. Hsu Tung and Peng Hian-Mao. Experimental studies of atomic step contrast in reflection electron microscopy // J. Metals 38, 30 (1986).
107. Osakabe Nobuyuki, Matsuda Tsuyoshi, Endo Junji, and Tonomura Akira, Observation of atomic steps by reflection electron holography // Jap. J. Appl. Phys. Pt. 2 27, 1772–1774 (1988).
108. Kumar Vijay. Defects on surfaces // Bull. Mater. Sci. 10, 161–172.
109. Henzler Martin. Atomic steps on surfaces // Angew. Chem 101, 539 (1989).
110. Van der Merwe J. H. Interplay of surface misfit and monoatomic steps on crystal surfaces. 1. Basic theory // Phys. Rev. B: Condens. Matter. 37, 2892–2901 (1988).

111. Van der Merwe J. H. and Kunert Herbert. Interplay of surface misfit and monoatomic steps on crystal surfaces. 2. Dependens of energy of formation on step orientation // Phys. Rev. B: Condens. Matter 37, 2902–2910 (1988).
112. Van der Merwe J. H. and Kunert Herbert. Interplay of surface misfit and monoatomic steps on crystal surfaces. 3. Model for the {110} of an anisotropic BCC cristal // Phys. Rev. B: Condens. Matter. 39, 5017–5024 (1989).
113. Van der Merwe J. H. and Shiflet G. J. The elastostatics of atomic steps on crystal surfaces. 1. A pair of steps of opposite sign enclosing a lower terrace // Surface Sci. 256, 171–186 (1991).
114. Shiflet G. J. and Van der Merwe J. H. The elastostatics of atomic steps on crystal surfaces. 2. Two identical island platean terraces // Surface Sci. 256, 187–194 (1991).
115. Redfield A. C., Zangwill A. Attractive interaction between steps // Phys. Rev. B. 46, 4289–4291 (1992).
116. Webb M. B., Men F. K., Swartzentruber B. S. Surface step configuration under strain: kinetics and step-step interaction // Surface Sci. 242, 23–31 (1991).
117. Jiang P., Jona F., Marcus P. M. Step profiles predicted with modified point-ion model for eight face-centered- and body-centered-cubic surfaces // Phys. Rev. B: Condens. Matter. 35, 7952–7958 (1987).
118. Srolovitz D. J., Hirth J. P. Elastic analysis of the energy and relaxation of stepped surfaces // Surface Sci. 255, 111–119 (1991).
119. Ройх И. Л., Болотич И. П. О соотношении между выделяющейся  $H_2O_2$  и количеством образующихся молекул окисла при атмосферной коррозии Mg и Al // Доклады Академии наук СССР 137, 126–129 (1961).
120. Ройх И. Л., Ордынская В. В., Болотич И. П. О влиянии механической обработки на величину поверхности металлов. Доклады Академии наук СССР 146, 1316–1317 (1962).
121. Gilman J. J. Debris mechanism of strain-hardening // J. Appl. Phus. 33, 2703–2709 (1962).
122. Гольдинер М. Г. Образование дислокаций вблизи поверхности кристалла // ФТТ 17, 625–626 (1975).
123. Гольдинер М. Г. Об упругом взаимодействии точечных и линейных дефектов со свободной поверхностью кристалла // Физика метаталлов и металловедение 4, 867–868 (1974).
124. Фридель Ж. Дислокации (Мир, 1967).
125. Набарро Ф. Р., Бадзинский Э. С., Холт Д. Б. Пластичность чистых монокристаллов (Металлургия, 1967).

## REFERENCES

126. Алёхин В. П., Иванов В. Д., Красулин Ю. Л., Тимофеев В. Н., Углов А. А., Харланова З. И. Источник дислокаций в полупроводнике при сварке полупроводников с металлами // ФХОМ, 98–105 (1967).
127. Барахтин Б. К., Владимиров В. И., Иванов С. А., Овидько И. А., Романов А. Е. Эффект периодического изменения дефектной структуры при пластической деформации // ФТТ 28, 2250–2252 (1986).
128. Владимиров В. И., Клявин О. В., Кусов А. А. Распределение дислокаций вблизи поверхности кристалла при пластической деформации // ФТТ 27, 2926–2930 (1985).
129. Лихтман В. И., Ребиндер П. А. Влияние адсорбционно-активных сред на механические свойства металлов // Известия АН СССР 17, 313–332 (1953).
130. Чаевский М. И. Применение расплавов Sn и эвтектики Pb – Sn для упрочнения циклически деформируемых деталей машин // ФММ 10, 604–608 (1960).
131. Третьяк И. Ю., Слипченко Т. В., Мещерякова Т. Н. Влияние воздуха и вакуума на длительную прочность сплава ЭИ868 // ФХММ 24, 13–15 (1988).
132. Кальшпенко И. Ф., Юдин В. Д., Колеров О. К., Букова Г. З. Рентгеноструктурное исследование влияния внешней среды на усталостную долговечность алюминиевых сплавов. Прикладная рентгенография металлов (ЛГТУ, 1990), р. 84.
133. Кальшпенко И. Ф., Юдин В. Д., Колеров О. К., Букова Г. З. Рентгеноструктурное исследование влияния внешней среды на усталостную долговечность алюминиевых сплавов. (ЛГТУ, 1990). С. 84.
134. Урбах М. И., Бродский А. М. О зависимости характеристик адсорбции на металлах от степени покрытия поверхности // *Поверхность*, 27–36 (1984).
135. Миндюк А. К. К вопросу о связи работы выхода электрона с электронным строением металлов // Физико-химическая механика материалов 7, 97–98 (1971).
136. Кортгов В. С., Слесарев А. И., Рогов В. В. Экзоэмиссионный контроль поверхности деталей после обработки (Наукова думка, 1986).
137. Levitin V. V., Loskutov S. V., Pravda M. I., Serpetzky B. A. Influence of cyclic stresses upon the electronic work function for the metal surface // *Solid State Communications*. – 1994. – Vol. 92. – N 12. – P. 973–976.
138. Lagowski I. Local Changes of the Work Function of Germanium and Silicon due to Dislocations // *Phys. solids state* 5, 555–561 (1964).

139. Bachmann G., Berthold W., Oechsner H. Work Function Spectroscopy as a tool for Thin Film Analysis // *Thin Solid Films*, 149–154 (1989).
140. Craig P. P. Direct Observation of Stress-Induced Shifts in Contact Potentials // *Physical Review Letters* 22, 700–703 (1969).
141. Besocke K., Krahl-Urban, Wagner H. Dipole moments associated with edge atoms: a comparative study on stepped Pt, Au and W surfaces // *Surface Science*, 39–46 (1977).
142. Дигилов Р. М., Созаев В. А., Хоконов Х. Б. Анизотропия поверхностной энергии и работы выхода в присутствии адсорбата // *Поверхность*, 138–139 (1987).
143. Дигилов Р. М., Созаев В. А., Хоконов Х. Б. Анизотропия поверхностной энергии и работы выхода щелочных металлов // *Поверхность*, 13–18 (1987).
144. Андреев Л. А., Палигэ Я. Влияние деформации на работу выхода монокристаллических молибденовых нитей // *ФТТ* 3, 3076–3082.
145. Андреев Л. А., Палигэ Я. Изменение работы выхода электрона при холодной деформации молибдена и тантала в условиях сверхвысокого вакуума // *Доклады АН СССР* 152, 1086–1088 (1963).
146. Минц Р. И., Мелехин В. П., Кортов В. С., Семко Ю. Д. Изменение работы выхода электронов и экзоелектронная эмиссия при растяжении меди и алюминия // *Известия вузов. Цветная металлургия*, 113–116 (1969).
147. Кортов В. С., Минц Р. И., Мясников И. Е. Влияние условий деформации на энергетический спектр экзоелектронной эмиссии металлов // *Известия вузов. Физика*. 83–87 (1971).
148. Мясников И. Е., Кортов В. С. Влияние нагрева на интенсивность и энергию экзоелектронов деформированного алюминия // *Известия вузов. Цветная металлургия*, 136–140.
149. Кочегаров Г. Г. Неупругость твердых тел при малых деформациях // *Письма в ЖТФ* 25, 29–36 (1999).
150. Beams I. W. Potentials on Rotor Surfaces // *Physical Review Letters* 21, 1093–1096 (1968).
151. Миндюк А. К. К вопросу о связи работы выхода электрона с электронным строением металлов // *Физико-химическая механика материалов*. – 1971. – 7, № 5. – С. 97–98.
152. Девяткин Е. А. О возможности использования изменения потенциала электрического поля, возникающего при деформации металла для оценки внутренних напряжений // *Материалы III Всесоюзного симпозиума «Технологические остаточные напряжения»*. М., 1988. – С. 142–146.

153. Коган Ш. М. Падает ли электрон в металлической трубе? // УФН 105, 158–161 (1971).
154. Bachmann G., Berthold W., Oechsner H. Work Function Spectroscopy as a tool for Thin Film Analysis // Thin Solid Films. – 1989. – 174. – P. 149–154.
155. Нестеренко Б. А., Сороковых А. И., Ляпин В. Г. Изменение поверхностной структуры Si (111) –  $3 \times 3$  – Al в условиях деформации изгибом // *Поверхность*. – 59–65 (1991).
156. Вишняков Я. Д. Современные методы исследования структуры деформированных кристаллов (Металлургия, 1975).
157. Минц Р. И., Мелехин В. П., Партенский М. Б. Деформационное изменение работы выхода электрона // ФТТ 16, 3584–3586 (1974).
158. Костецкий Б. И., Шульга О. В. Электросопротивление поверхностных слоёв металлов и механизм схватывания // Доклады Академии наук СССР, 188, 80–82 (1969).
159. Муха И. М., Штепан Я. Г., Вальчук Г. И. Субатомный механизм изнашивания трущихся поверхностей деталей // ФХММ 7, 111–113 (1971).
160. Жуховицкий А. А., Андреев Л. А. О влиянии диспергирования на работу выхода электрона // Доклады Академии наук СССР 142, 1319–1322 (1962).
161. Гохштейн А. Я. Поверхностное натяжение твёрдых тел и адсорбция (Наука, 1976).
162. Шпеньков Г. П. Физикохимия трения (применительно к избирательному переносу и водородному износу. БГУ, 1978).
163. Loskutov S. V. Work function for the deformed metal surface // Surface science. – 2005 – V. 585 / 1–2. – P. L166–L170.
164. Минц Р. И., Мелехин В. П., Сегаль В. М., Иевлев И. Ю. Изменение работы выхода электрона при термоупругой мартенситной реакции // Физика твёрдого тела. – 1972. – 14, № 8. – С. 2481–2483.
165. Тишин Е. А. К расчёту температурной зависимости работы выхода электронов плёночной системы W – Th // ЖТФ 46, 1057–1059 (1976).
166. Козьма А. А., Мальхин С. В., Рощенко С. Т. Стимулированное рентгеновским излучением изменение субструктуры, напряжённого состояния и периода решётки плёнок Al и Ti (ЛГТУ, 1990), Vol. 228, p. 84.
167. Городецкий Д. А., Мельник Ю. П. О корреляции между работой выхода и структурой мономолекулярных плёнок // Физика твёрдого тела. – 1974. – 16, № 9. – С. 2781–2783.

168. Lang N. D., Kohn W. Theory of Metal Surfaces: Charge Density and Surface Energy. Phys. Rev. B 1, 4555 – Published 15 June 1970.
169. Савицкий Е. М., Буров И. В., Литвак Л. Н. Работа выхода элементов // Доклады АН СССР. – 1974. – 218, № 4. – С. 818–820.
170. Hasegawa Y., Jia J. F., Inoue K., Sakai A., Sakurai T. Elemental contrast of local work function studied by scanning tunneling microscopy // Surface Science (386) 1–3 (1997), pp. 328–334.
171. Shaikhutdinov S. K., Schaak A., Imbihl R. Formation of low work function patches in the NO+H<sub>2</sub> reaction on a roughened Rh(110) surface // Surface Science (391) 1–3 (1997), pp. L1172–L1177.
172. Levitin V. V., Loskutov S. V., Pogosov V. V. Влияние деформации и остаточных напряжений в металлах на работу выхода электронов // Физика металлов и металловедение. – 1990. – № 9. – С. 73–79.
173. Koide Yasuo, Ishikawa H., Kobayashi S., Yamasaki S., Nagai S., Umezaki J., Koike M., Murakami Masanori. Dependence of electrical properties on work functions of metals contacting to p-type GaN // Applied Surface Science (117–118) 1–4 (1997), pp. 373–379.
174. Woodruff D. P. and Delchar T. A. Modern Techniques of Surface Science (Cambridge University Press, 1986).
175. Лоскутов С. В., Левитин В. В., Погосов В. В. Об измерении работы выхода электронов методом динамического конденсатора // Поверхность. – 1992. – № 8. – С. 121–123.
176. Zangwill A. Physics at Surfaces (Cambridge University Press).
177. Warren B. E. Progress in Metal Physics (Pergamon Press, 1959). Vol. 8.
178. Friedel J. Dislocations (Pergamon Press, 1964).
179. Levitin V. V., Garin O. L., Yatsenko V. K., Loskutov S. V. On structural sensibility of work function // Vacuum. – 2001. – 63, № 1-2. – P. 367–370.
180. Johnston W. G. and Gilman J. J. Dislocation velocities, dislocation densities, and plastic flow in lithium fluoride crystals // Journal of Applied Physics, 30:2 (1959), 129–144.
181. Matohnyuk L. Uskorennye Ustalostnyye Ispytanya (Naukova Dumka, 1988).
182. Минц Р. И., Мелехин В. П., Партенский М. Б. Деформационное изменение работы выхода электрона // Физика твёрдого тела. – 1974. – 16, № 12. – С. 3584–3586.
183. Levitin V. V., Loskutov S. V., Pravda M. I., Serpetsky B. A. Work function for fatigue tested metals // Nondestructive Testing and Evaluation. Vol. 17, 79–89. – 2001.
184. Brajczewska M., Henriques C., Fiolhais C. Dependence of metal surface properties on the valence-electron density in the stabilized jellium model // Vacuum, Vol. 63 (1-2) (2001), pp. 355–360.

## REFERENCES

185. Gyftopoulos E. P. Quantum-thermodynamic definition of electronegativity // Proc Natl Acad Sci USA. 1968 Jul; 60 (3): 786–93.
186. Рудницкий Л. А. Работа выхода электрона неидеальной поверхности металла. II. Ступенчатая поверхность и поверхность микрогранул // Журнал технической физики. – 1980. – 50, № 2. – С. 355–361.
187. Kilian H. G., Vettegren V. I., Svetlov V. N. Hierarchy of defect ensembles on the surface of loaded copper // Phys. Solid State 43, 2199 (2001).
188. Лоскутов С. В., Левитин В. В., Гордиенко В. Н. Формирование энергетического рельефа металлических поверхностей в процессах трения и изнашивания // Трение и износ. – 2002. – 2, № 23. – С. 176–180.
189. Mišković Z. L., Davison S. G., Goodman F. O. Statistical properties of local work function on stepped surfaces // Phys. Rev. B 60, 2025 – Published 15 July 1999.
190. Fall C. J., Binggeli N., Baldereschi A. Work functions and surface charges at metallic facet edges // Phys. Rev. B 66, 075405 – Published 6 August 2002.
191. Ivor Brodie. Uncertainty, topography, and work function // Phys. Rev. B 51, 13660. – Published 15 May 1995.
192. Davydov S. Yu. Effect of adsorption of group VI atoms on the silicon work function // *Physics of the Solid State*. Volume 47, pages 1779–1783 (2005).
193. Килиан Х. Г., Веттерген В. И., Светлов В. Н. Иерархия ансамблей дефектов на поверхности нагруженной меди // Физика твёрдого тела. – 2001. – 43, № 11. – С. 2107–2111.
194. Fomenko V. S. Emission Properties of Materials (Naukova Dumka, 1981).
195. Минц Р. И., Мелехин В. П., Кортов В. С., Семко Э. Д. Измерение работы выхода электронов и экзоэлектронной эмиссии при растяжении меди и алюминия // Известия вузов. Цвет. металлургия. – 1969. – № 2. – С. 113–116.
196. Craig Paul P. Direct Observation of Stress-Induced Shifts in Contact Potentials // Physical Review Letters 700 (1969).
197. Loskutov S. V., Levitin V. V., Man'ko V. K., Serpetsky V. A., and Pavlyutkin Y. S. Установка и методика испытаний образцов на усталость с одновременным измерением работы выхода электрона. Заводская лаборатория. – 1999. – № 7. – С. 43–45.
198. Kulemin A. V., Kononov V. V., Stebelkov I. A. Enhancement in fatigue strength of details by ultrasonic surface treatment // Strength Mater. 1981. (1): 70.

199. Green M. Solid State Surface Science (Zenith Radio Research Corporation, 1969), Vol. 1.
200. Пат. 105734 Україна, МПК G01N25 / 16, G01N25 / 48, G01B5 / 02. Диференційний дилатометр / Міщенко В. Г.; заявник і патентовласник Запорізький національний університет. – № а201308274; заявл. 01.07.2013; опубл. 10.06.2014, Бюл. № 11.
201. Пат. 94552 Україна, МПК C23C8 / 00, G01N13 / 00, G01B5 / 02, G01B21 / 02. Спосіб визначення параметрів дифузійного шару при хіміко-термічній обробці / Міщенко В. Г.; заявник і патентовласник Запорізький національний університет. – № а201007915; заявл. 24.06.2010; опубл. 10.05.2011, Бюл. № 9.
202. Пат. 94867 Україна, МПК G01N25 / 16, G01N25 / 48, G01B5 / 02, G01B7 / 16 . Диференційний дилатометр / Міщенко В. Г.; заявник і патентовласник Запорізький національний університет. – № а201007916; заявл. 24.06.2010 опубл. 10.06.2011, Бюл. № 11.
203. Lazechny I. M., Lisica O. V., Mischenko V. G., Snignoy V. L., Snignoy G. V., The transformation of austenite in cemented steel 13H3NVM2F // Novi materiali i tehnologii v metalurgii ta mashinobuduvanni. – 2011. – № 2. P. 47–52.
204. Lazechny I. N. and Banas I. P. Formation at TCT structure and properties of carburized steels of different heat re-sistance during TT process // Novi materiali. Novi materiali i tehnologii v metalurgii ta mashinobuduvanni. – 2005. – № 1 – P. 37–44.
205. Ervin V. Zaretsky. Rolling Bearing Steels – A Technical and Historical Perspective / Ervin V. Zaretsky – National Aeronautics and Space Administration, Glenn Research Center, Cleveland, 2012. – 16 s.
206. Лахтин Ю. М., Арзамасов Б. Н. Химико-термическая обработка металлов Ю. М. Лахтин. – М. : Металлургия, 1985. – 216 с.
207. Mishchenko V. G. et al. Method of regulation of decarbonization details at their thermal processing, (Patent of Ukraine № 108280, declared 01.07.2013, published 04.10.2015).
208. Basdirev S., Ivanov V. I., Nesterenko T. M., and Sereda B. P. Reduction of calibrated steel decarburization in thermal furnaces. Metaloznavstvo ta obrobka metaliv. – 2002. – №2. – P. 31–34.
209. Краснокутський П. Г. Теплотехнічні процеси і конструкції нагрівальних печей : навч. посібник / П. Г. Краснокутський, Ф. І. Колесник. – К. : ІСДО, 1995. – 248 с.
210. Jurgen Cappel, Matthias Weinberg and Rheinhold Flender. The metallurgy of roller-bearing steels. Steel Grips. – 2004, 2. – № 4. – P. 267–274.

## REFERENCES

211. Mishchenko V. G. et al. Cemented steel (Ukraine Patent of Ukraine № 108582, declared 12.05.2014, published 12.05.2015).
212. Chigirinskiy S. P., Shejko H. Dyja and Knapinski M. Experimental and theoretical analysis of stress state of plastic medium influence on structural transformations in low-alloy steels *Metallurgical and Mining Industry*, 11 (2015), 188–195.
213. Mishchenko V. G. and Sheyko S. P. “Structural changes of multiphase low-carbon steel in deformation and heat treatment”, *Steel in Translation*, 44 (2014), 928–930.
214. Adler Y. P., Markov E. V. and Hranovskyy Y. Planning experiment while searching optimal conditions (M. : Science, 1976), 93–191.
215. Spiridonov A. A. Planning the Experiment in the Study Technological Processes (M. : Engineering, 1981, 22–27).
216. Sereda B., Belokon Y., Sheyko S. and Sereda D. “The research of influence alloying elements on processes structure formation in stamp steel”. *AIST Steel Properties and Applications Conference Proceedings – Combined with MS and T’12, Materials Science and Technology 2012*, Pittsburgh, (2012), 453–456.
217. Sereda B., Sheyko S., Belokon Y. and Sereda D. “The influence of modification on structure and properties of rapid steel”. *Materials Science and Technology Conference and Exhibition 2011*, Columbus, (2011), Vol. 1, 713–716.
218. Eliseev Y. S. et al. Production of Gears Turbine Engines (M. : Higher School, 2001, 95–101).
219. Mishchenko V. G. and Yevsieieva N. O. Vplyv povzuchosti metalu na termin ekspluatatsii reaktoriv mahnietermichnoho vyrobnytstva tytanu // *FHMM*, 119–122 (2012).
220. Mamutova A. T., Ultarakova A. A., Kuldeev E. I., and Esengaziev A. M. Modern condition and proposed solutions for processing chloride waste of titani-um-magnesium production. Complex Use of Mineral Resources. *Mineraldik Shikisattardy Keshendi Paidalanu* 307, 173–180 (2018).
221. Tankeev V. P., Riaposov Iu. A., and Rymkevich D. A. Stanovlenie i razvitie proizvodstva gubchatogo titana v gorode Berezniki // *Titan* 2, 4–7 (2009).
222. Myshchenko V. G., Tverdokhlebskiy S. V., and Omelchenko O. S. Razvytye razrusheniya apparatov vosstanovleniya y prymesy v hubchatom tytane // *Visnyk dvyhunobuduvannia*, 135–137 (2004).
223. Putina A. O., Kochergin V. P., and Nechaev N. P. Izmenenie svoistv stali 12Kh18N10T v protsesse ekspluatatsii v magnietermicheskom proizvodstve i ee zashchita // *Zashchita metallov* 20, 772–775 (1984).

224. Fuwa A. and Takaya S. Producing titanium by reducing  $TiCl_2$ - $MgCl_2$  mixed salt with magnesium in the molten state // JOM 57, 56–60 (2005).
225. Mishchenko V. G. and Evseeva N. A. Polzuchest kak opredeliaiushchii faktor uvelicheniia sroka eksploatacii reaktorov magnietermicheskogo proizvodstva titana. Fiziko-khimichna mekhanika materialiv 48, 119–122 (2012).
226. Shejko S., Sukhomlin G, Mishchenko V., Shalomeev V., Tretiak V. Formation of the Grain Boundary Structure of Low-Alloyed Steels in the Process of Plastic Deformatio. (2018), pp. 746–753.
227. Sidorenko S. A. About the complex processing of chloride waste from the titanium tetrachloride production. Intellectual potential of the xxi century. Intellectual potential of the XXI century 2017. Available at: <https://www.sworld.education/konferu7-317/74.pdf>
228. Lunov V. V., Bielikov S. B., Ulitenko O. M., Yevsieieva N. O. (2011). Fizyko-matematychna model ta alhorytm rozrakhunku teplofizychnykh protsesiv tverdinnia zlyvka u vylyvnytsi. Teoryia y praktyka metallurhyy, 1–2, 26–32.
229. Kobayashi S., Oh S., Altan T. (1989). Metalforming and the Finite-Element Method. Oxford University Press, 377. doi: <http://doi.org/10.1093/oso/9780195044027.001.0001>
230. Jiang Z., Xie H. (2018). Application of Finite Element Analysis in Multiscale Metal Forming Process. Finite Element Method -Simulation, Numerical Analysis and Solution Techniques. doi: <https://doi.org/10.5772/intechopen.71880>
231. Golovanov A. P., Tiuleneva O. N., Shigabutdinov A. F. (2006). Metod konechnykh elementov v statike i dinamike tonkostennykh konstruktsii. Moscow : Mir, 392.
232. Rumiantcev A. V. Metod konechnykh elementov v zadachakh teploprovodnosti (Kaliningradskii Gosudarstvennyi Universitet, 1995).
233. Мищенко В. Г. Внепечное рафинирование коррозионно-стойких сталей XXII – Konferencia odlewnikow stali. – Krakow, 2000. – С. 33–39.
234. Путина О. А., Путин А. А. Повышение герметичности и надежности аппаратов в магниетермическом производстве губчатого титана // Доклады I научно-технической конференции по титану стран СНГ. М. : 1994. С. 176–189.
235. Диаграммы состояния двойных металлических систем : справочник: В 3 т. Под общ ред. Н. П. Лякишева (Mashinostroenie, 2001), Vol. 3.
236. Гармата В. А., Петрунько А. Н., Галицкий Н. В., Олесов Ю. Г., Сандлер Р. А. Титан (Metallurgiya, 1983).

## REFERENCES

237. Fontana M. G. Corrosion engineering. Mc Graw – Hill Book Company, Third Edition, 1986, 556 p.
238. Капитан А. В., Твердохлеб С. В., Мищенко В. Г. Механизмы разрушения материалов реторт в магнетермическом производстве губчатого титана. (НИЦХФТИ, ИПЦ «Контраст», 2003), pp. 51–58.
239. Гривняк М. Свариваемость стали (Mashinostroenie, 1984).
240. Пат. № 1404544, СССР. МПК4С22С 38 /42, Сталь / Фонштейн Н. М., Голованенко С. А. и др. – заявл. 15.11.1986; опубл. 23.06.1988.
241. Новик Ф. С., Арсов Я. Б. Оптимизация процессов технологии металлов методами планирования экспериментов (Mashinostroenie, 1980).
242. Потапов А. И., Мазунин В. П., Двойников Д. А., Коковихин Е. А. Методика исследования сопротивления деформации на пластометрическом комплексе. 59–63 (2010).
243. Minaev A. A. Sovmeshennye Metallurgicheskie Protsessy (Integrated Metallurgical Processes) (Tekhnopark DonGTU-UNITEKh, 2008).
244. Matrosov Yu. I. Controlled rolling: Multistage thermal and mechanical treatment of low-alloy steel, *Stal*, 1987, no. 7, pp. 75–80.
245. Bol'shakow V. I., Dolzhenko I. E., Dolzhenkov V. I. Termicheskaya Obrabotka Stali I Metalloprokata : Ucheb. Dlva Yuzoy (Heat Treatment of Steel and Rolled Products: A University Textbook) (Gaudeamus, 2002).
246. Spivakov V. I., Orlov E. A., Ganoshenko I. V., Volodarskii V. V. Influence of chemical composition and controlled-rolling temperature on the properties of pipe-steel sheet. *Fundamental'nye i prikladnye problem chermoi metallurgii* (Fundamental and Applied Problems of Nonferrous Metallurgy), 2005, no. 10, pp. 180–186.
247. Bernshtein M. L. Termomekhanicheskaya Obrabotka Metallov i Splavov (Thermomechanical Treatment of Metals and Alloys) (Metallurgiya, 1968).
248. Pogorzhel'skii V. I. Kontroliruemaya. Prokatka Nepre Ryvnolitogo Metalla (Controlled Rolling of ConTinuuous Cast Metal) (Metallurgiya, 1979).
249. Bel'chenko G. I. and Gubenko S. I. Osnovy Metallografii i Plasticheskoi Deformatsii Stali (Fundamentals of the Metallography and Plastic Deformation of Steel) (Vysshava Shkola, 1987).
250. Ivanchenko V. G., Tilik V.T, and Shtekhno O. N. Trends in the production of superthin hot-rolled strip, *Fundamentalnye*

- i prikladnye problemy chermoi metalurgii. Fundamental and Applied Problems of Nonferrous Metallurgy, 233–239 (2004).
251. Production of superthin hot-rolled strip at Zaporozhstal. Metallurg. Gornorud. Prom. 11–14 (2002).
252. Hirsch P. B., Howie A., Nicholson R. B., Pashley D. W., Whelan M. J. Electron Microscopy of Thin Crystals (Butterworth, 1965).
253. Shejko S., Shalomeev V., Mishchenko V. The effect of plastic deformation on the structure formation of low-Alloy steel. (2017), pp. 238–244.
254. Mishchenko V. G., Shejko S. P. Structural changes of multiphase low-carbon steel in deformation and heat treatment // Steel in Translation 44, 928–930 (2014).
255. Rios P. R. and Zöllner D. Grain growth – unresolved issues. 6, 629–638 (2018).
256. J. von Neumann: *Metal Interfaces*. (Cleveland, OH: American Society for Metals, 1952) 108–110.
257. Mullins W. W. Two-dimensional motion of idealized grain boundaries. Journal of Applied Physics 8, 900–904 (1956).
258. Babitskaya A. N., Mishchenko V. G., Movshovich V. S. Structural changes during re crystallization of cold-rolled plates of steel O6Kh18ch // Term. Obrab. Met. 42–43 (1985).
259. Zav'yalov A. S. and Sandomirskii M. M. Engineering Steels Alloyed with Rare Earth Metals (Mashinostroenie, 1969).
260. Averin V. V. Application of Rare Earth Metals in Microalloying of Steels. Steel and Nonmetallic Inclusions (Metallurgiya, 1978).
261. Savitskii E. N., Terekhova V. F. Physical Metallurgy of Rare Earth Metals (Metallurgiya, 1978).
262. Tsivirko E. I. Information Letter No. 10. Control of nonmetallic inclusions in cast and worked steels using the linear counting method. (1969).
263. Mishchenko V. G. and Natapov B. S. Structure and properties of corrosion-resistant steel O6Kh18ch alloyed with REM and calcium. Metalloved. Term. Obrab. Met. 32–34 (1983).
264. Мищенко В. Г., Булах А. И., Меняйло А. И., Шейко С. П., Кнапински М. Formation of the structural condition of the diffusive layer of stainless steel 06h18ch in the course of high-temperature cementation. *XVII international scientific conference new technologies and achievements in metallurgy, material engineering and production engineering*. Częstochowa, 2016. Nr. 56. P. 444–447.

#### REFERENCES

265. Mishchenko V., Ievsieva N., Lazechny I. The changes of chrome-nikel-manganese steels phase terms properties in course of operational heating. *Scientific Letters of Academic Society of Michal Baludansky*. 2014. V. 2, № 1. P. 89–94.
266. Mishchenko V. G., Menyaylo A. I. Control of carburization and decarburization processes of alloy steels at thermo-chemical and thermal treatment // *Metallurgical and Mining Industry* 244–249 (2015).

Izdevniecība “Baltija Publishing”  
Valdeķu iela 62 – 156, Rīga, LV-1058  
E-mail: office@baltijapublishing.lv

---

Iespiests tipogrāfijā SIA “Izdevniecība “Baltija Publishing”  
Parakstīts iespiešanai: 2023. gada 9. Janvāris  
Tirāža 300 eks.